Alma Mater Studiorum · University of Bologna

School of Science
Department of Physics and Astronomy
Master Degree in Physics

Many-Body Approach to the BCS-BEC Crossover for an Imbalanced Ultra-cold Fermi Gas

Supervisor:
Prof. Pierbiagio Pieri

Co-supervisor:
Dr. Michele Pini

Submitted by:
Marco Uguccioni

Academic Year 2021/2022

Abstract

The aim of this thesis is the study of the normal phase of a mass imbalanced and polarized ultra-cold Fermi gas in the context of the BCS-BEC crossover, using a diagrammatic approach known as t-matrix approximation. More specifically, the calculations are implemented using the fully self-consistent t-matrix (or Luttinger-Ward) approach, which is already experimentally and numerically validated for the balanced case.

An imbalance (polarization) between the two spin populations works against pairing and superfluidity. For sufficiently large polarization (and not too strong attraction) the system remains in the normal phase even at zero temperature. This phase is expected to be well described by the Landau's Fermi liquid theory. By reducing the spin polarization, a critical imbalance is reached where a quantum phase transition towards a superfluid phase occurs and the Fermi liquid description breaks down. Depending on the strength of the interaction, the exotic superfluid phase at the quantum critical point (QCP) can be either a FFLO phase (Fulde-Ferrell-Larkin-Ovchinnikov) or a Sarma phase. In this regard, the presence of mass imbalance can strongly influence the nature of the QCP, by favouring one of these two exotic types of pairing over the other, depending on whether the majority of the two species is heavier or lighter than the minority.

The analysis of the system is made by focusing on the temperature-coupling-polarization phase diagram for different mass ratios of the two components and on the study of different thermodynamic quantities at finite temperature. The evolution towards a non-Fermi liquid behavior at the QCP is investigated by calculating the fermionic quasi-particle residues, the effective masses and the self-energies at zero temperature.

Contents

Introduction

Superconductivity was discovered in 1911 by Onnes [1], who was studying the resistance of solid mercury at cryogenic temperatures. He observed that the resistance of the material abruptly vanished below a critical temperature, which corresponds to 4.2 K for mercury. Great efforts have been devoted to finding out how and why superconductivity works and the first theoretical model was conceived in 1935, summarized by the completely classical London constitutive equations [2]. In 1950, the phenomenological Ginzburg–Landau theory of superconductivity [3], which combined Landau's theory of second-order phase transitions with a Schrödinger-like wave equation, had great success in explaining the macroscopic properties of superconductors.

In 1957, Bardeen, Cooper and Schrieffer [4] proposed a complete microscopic theory of superconductivity, awarded with the Nobel prize in 1972. The BCS theory explained the superconducting current as a superfluid of Cooper pairs, pairs of electrons with size of order 10^3 times the typical inter-particle distance and formed through an effective attractive interaction due to the exchange of phonons. Two years later, Gor'kov showed that the BCS theory reduced to the Ginzburg-Landau theory close to the critical temperature [5].

In their work, the authors of the BCS superconductivity made a point to emphasize the differences between their theory, based on strongly-overlapping fermion pairs, and the one proposed by Schafroth, Butler and Blatt [6], based on the Bose-Einstein condensation (BEC) of non-overlapping composite bosons. Therefore, for some time, the interest in these two situations has been kept disjoint, until theoretical interest arose for unifying them. Interestingly, it turned out that Cooper pairs and composite bosons can be considered as two limiting (BCS and BEC) situations of the same theory where they share the same kind of broken symmetry. In this way, the Fermi system, in the crossover between the BCS and BEC regimes, smoothly passes through an intermediate region where the dimension of the pairs is comparable with the inter-particle spacing. This unified theory, known nowadays as BCS–BEC crossover, took shape initially through the work by Eagles [7] in 1969 in the context of superconducting semiconductors, and later through the works by Leggett [8] in 1980 and by Nozierès and Schmitt-Rink [9] in 1985, for an attractive Fermi gas respectively at $T = 0$ and in the normal phase above the critical temperature.

With the advent of high-temperature (cuprate) superconductors in 1987, in which the size of the pairs is comparable to the inter-particle spacing [10–17], the interest in the BCS–BEC crossover grew, also because of the possible applications in nuclear physics [18]. However, a real explosion of this activity started from 2003, with the

advent of the fully controlled experimental realization essentially of all aspects of the BCS–BEC crossover in ultra-cold Fermi gases [19]. Notice that, in this case, the fermions involved in pairing are neutral atoms (and not charged particles, as electrons in superconductors), so in this case the ordered phase is superfluid, rather then superconducting.

Some time ago, a theoretical and experimental research activity on ultra-cold polarized (i.e. spin imbalanced) attractive Fermi gases began [20, 21], mainly with the aim to understand the different nature of the superfluid phase. Quite generally, an imbalance between the two spin populations works against pairing and superfluidity and thus, for sufficiently large polarization (and not too strong attraction), the system remains in the normal phase even at zero temperature. Depending on the strength of the interaction, the superfluid phase can be either a Sarma phase, a homogeneous polarized superfluid predicted many years before by Sarma in the BCS limit at $T = 0$ [22], or a more exotic FFLO phase predicted by Fulde and Ferrell [23] and, independently, by Larkin and Ovchinnikov [24], characterized by a finite center-of-mass momentum of the pairs. Robust evidences of a FFLO phase have been reported in quasi-two-dimensional organic superconductors [25–27], as well in the iron-based multiband superconductor KFe_2As_2 [28]. For ultra-cold Fermi gases, indirect evidence for the occurrence of FFLO ordering has been reported so far only for one-dimensional systems [29]. In three dimensions, the region of the FFLO stability is mostly covered by an experimentally confirmed phase separation [30, 31], related to a first-order normal-to-superfluid transition. However, we expect that this effective narrow region at very low temperatures can be enlarged by the presence of a mass imbalance since, from mean-field calculations, it is already known that a majority of heavy atoms should favor FFLO pairing [32].

Thanks to the experimental observations in ultra-cold Fermi gases, the study of the BCS-BEC crossover has strongly developed also on the theory side [33,34]. Many theoretical methods, like many-body diagrammatic techniques, quantum Monte Carlo (QMC), diagrammatic Monte Carlo (DMC), functional renormalization group, epsilon and virial expansions, have been extensively used to describe the crossover.

In this work, we will focus on diagrammatic techniques based on the t-matrix approximation since, particularly in the context of attractive ultra-cold Fermi gases, this theoretical approach appears as a natural candidate to describe the system while it evolves throughout the BCS-BEC crossover. The first pioneering approach in this respect goes back to the work by Nozières and Schmitt-Rink (NSR) [9] in 1985. In that work, a simplified version of the non-self-consistent t-matrix approximation, obtained by extending the diagrammatic description of a dilute repulsive Fermi gas due to Galitskii [35], proved to highlight the main features of the crossover physics in the normal phase above the superfluid critical temperature. Later on, the NSR approach was extended to improve the treatment of the non-self-consistent t-matrix approximation, further improved in turn by its fully self-consistent version, known as Luttinger-Ward approach. This approach compares well with experimental data and Quantum Monte Carlo (QMC) calculations for several thermodynamic quantities for a balanced system, where the two species in the Fermi gas have the same population and mass [36–41].

In this thesis, we will use the fully self-consistent t-matrix to study the normal

phase of mass imbalanced and polarized ultra-cold Fermi gas. In particular, we will focus on the mixtures ^{40}K-^{161}Dy (potassium-dysprosium) and ^{6}Li-^{53}Cr (lithium-chromium), which are relevant for the ongoing experiments in Innsbruck [42, 43] and Florence [44], respectively. The results for the two mass imbalanced mixtures, which represent a new contribution of this thesis, will be often compared with the known results for a mass balanced mixture, which we have anyway reproduced for completeness. For the calculations presented in this work, we will use the numerical codes at both finite and zero temperature developed by Michele Pini [45–47]. The thesis is organized as follows:

- In Chapter 1, we review the main features of the BCS-BEC crossover, with particular interest to imbalanced ultra-cold Fermi gases, showing that the inclusion of pairing fluctuations above a mean-field approach is required to describe consistently this theory.

- In Chapter 2, we introduce the finite temperature diagrammatic Green's function formalism, which is a fundamental theoretical basis for a quantum many-body approach to the BCS-BEC crossover.

- In Chapter 3, we discuss and justify the t-matrix approximation, which select a certain class of diagrams, known as ladder diagrams, that are relevant to study an ultra-cold Fermi gas in the normal phase throughout the BCS-BEC crossover. Furthermore, we discuss the Luttinger-Ward approach, which improves the t-matrix approximation with the inclusion of full self-consistency.

- In Chapter 4, we describe the Landau Fermi liquid theory and its application to imbalanced ultra-cold Fermi gases, showing that a transition towards non-Fermi liquid behaviour is used to investigate the presence of a quantum critical point (QCP) in the phase diagram of the system.

- In Chapter 5, we introduce some considerations on experiments with imbalanced ultra-cold Fermi-Fermi mixtures. In particular, we focus on the ^{40}K-^{161}Dy and ^{6}Li-^{53}Cr mixtures, which will be the ones analyzed in our numerical calculations.

- In Chapter 6, we present the numerical results obtained within the Luttinger-Ward approach for different thermodynamic quantities at finite temperature, focusing on three different mass ratios. We also consider the high-temperature limit of the t-matrix approximation, which reduces to the quantum virial expansion in this regime.

- In Chapter 7, we present some numerical results obtained within the Luttinger-Ward approach at zero temperature. More precisely, we consider the zero temperature phase diagram for three different mass ratios and the behaviour of the quasi-particle residues and effective masses near the QCP. Finally, some results for the self-energies are reported.

Chapter 1

BCS-BEC Crossover and Ultra-cold Fermi Gases

In this chapter, we give a general introduction to the BCS-BEC crossover. We start by discussing the BCS theory with a mean-field approach and the Bose-Einstein condensation for a non-interacting gas. We see how these two phenomena can be smoothly connected through the variation of the size of the fermion pairs and why the mean-field approximation is not enough to get a consistent description of this crossover. Then we describe qualitatively the effects of an imbalance of the spin populations and the main aspects and achievements of the BCS–BEC crossover that have emerged with ultra-cold Fermi gases. Throughout this thesis, we use units where the reduced Planck constant $\hbar$ and the Boltzmann constant k_B are set equal to unity.

1.1 BCS Theory of Superconductivity

The first microscopic theory of superconductivity was formulated in 1957 and is widely known as *Bardeen–Cooper–Schrieffer theory* (BCS). In a general form, it considers an effective attractive interaction $V(\mathbf{r}-\mathbf{r}')$ between two different species of fermions at a distance $|\mathbf{r}-\mathbf{r}'|$ (conventionally denoted with spin $\uparrow$ and $\downarrow$), embedded in a continuous medium [48]. This interaction is responsible for the creation of fermion pairs in the medium, also known as *Cooper pairs*. For example, in conventional superconductors, this attraction is due to the electron-phonon interaction.

In some systems, like metallic superconductors or ultra-cold Fermi gases, a detailed knowledge of the form of the attractive interaction is not important and one can just consider the simplest form of the potential, i.e. a *contact potential* $V(\mathbf{r}) = v_0\delta(\mathbf{r})$, where v_0 is a negative constant. However, the price to pay for the use of this interaction is that, when dealing with a homogeneous system, the Fourier transform $V(\mathbf{k}) = v_0$ is a constant and therefore the 3-dimensional integrals over the wave vector $\mathbf{k}$ may diverge in the ultraviolet. This problem can be avoided by introducing a cut-off k_0, like the Debye frequency for metallic superconductors. For ultra-cold gases, on the other hand, we will deal with a more useful regularization procedure (see Section 3.1.3), related to the fact that also the two-body problem in vacuum is affected by a similar divergence.

To describe quantitatively this theory, it is more convenient to work in the *grand-canonical ensemble*, which allows for a variable number of particles. We therefore consider the grand-canonical Hamiltonian $K = H - \mu N$ with a zero-range interaction of strength v_0

$$K = \sum_{\mathbf{k}\sigma} \xi_{\mathbf{k}} c^\dagger_{\mathbf{k}\sigma} c_{\mathbf{k}\sigma} + v_0 \sum_{\mathbf{k}\mathbf{k}'} c^\dagger_{\mathbf{k}\uparrow} c^\dagger_{-\mathbf{k}\downarrow} c_{-\mathbf{k}'\downarrow} c_{\mathbf{k}'\uparrow}. \tag{1.1}$$

In this expression, $\xi_{\mathbf{k}} = \mathbf{k}^2/(2m) - \mu$, while $c^\dagger_{\mathbf{k}\sigma}$ ($c_{\mathbf{k}\sigma}$) is a fermionic creation (annihilation) operator for wave vector $\mathbf{k}$ and spin projection $\sigma = \uparrow, \downarrow$ (here we are considering equal densities $n_\uparrow = n_\downarrow$, and thus $\mu_\uparrow = \mu_\downarrow$, for simplicity).

We now use the *BCS mean-field* (or *Hartree-Fock-Bogoliubov*) *approximation*, which consists in decoupling the second term of (1.1) by including also particle non-conserving averages, i.e. $c^\dagger_\alpha c^\dagger_\beta c_\gamma c_\delta \to +\langle c^\dagger_\alpha c_\delta\rangle c^\dagger_\beta c_\gamma - \langle c^\dagger_\alpha c_\gamma\rangle c^\dagger_\beta c_\delta + \langle c^\dagger_\beta c_\gamma\rangle c^\dagger_\alpha c_\delta + \langle c^\dagger_\beta c_\delta\rangle c^\dagger_\alpha c_\gamma + \langle c^\dagger_\alpha c^\dagger_\beta\rangle c_\gamma c_\delta + \langle c_\gamma c_\delta\rangle c^\dagger_\alpha c^\dagger_\beta$, where $\langle \dots \rangle$ is the thermal average determined by K. As can be seen, the first four terms represent the usual HF approximation and have the effect of renormalizing the spectrum of free fermions. Since we will be mainly interested in the limit $v_0 \to 0^-$, in the following these terms will be neglected. Therefore, we can rewrite the mean-field grand-canonical Hamiltonian as

$$K_{mf} = \sum_{\mathbf{k}\sigma} \xi_{\mathbf{k}} c^\dagger_{\mathbf{k}\sigma} c_{\mathbf{k}\sigma} - \sum_{\mathbf{k}} \left(\Delta^* c_{-\mathbf{k}\downarrow} c_{\mathbf{k}\uparrow} + \Delta c^\dagger_{\mathbf{k}\uparrow} c^\dagger_{-\mathbf{k}\downarrow} \right) - \frac{|\Delta|^2}{v_0}, \tag{1.2}$$

where the parameter Δ is determined by the self-consistent relation

$$\Delta = -v_0 \sum_{\mathbf{k}} \langle c_{-\mathbf{k}\downarrow} c_{\mathbf{k}\uparrow} \rangle. \tag{1.3}$$

In mean-field theory, we approximate the effect of all the other bodies on any given individual by a single averaged effect, thus passing from a many-body problem to a one-body problem. The description of a system of fermions with a mutual attractive interaction within this approximation is appropriate when the inter-particle correlations extend much beyond the average inter-particle distance, such that different pairs strongly overlap with each other. This is definitely the case for conventional superconductors, to which the BCS theory of superconductivity was originally meant to apply.

The quadratic form (1.2) can be easily diagonalized introducing the *Bogoliubov* (or *quasi-particle*) *operators*

$$\gamma_{\mathbf{k}\uparrow} = u^*_{\mathbf{k}} c_{\mathbf{k}\uparrow} - v^*_{\mathbf{k}} c^\dagger_{-\mathbf{k}\downarrow}, \qquad \gamma^\dagger_{-\mathbf{k}\downarrow} = v_{\mathbf{k}} c_{\mathbf{k}\uparrow} + u_{\mathbf{k}} c^\dagger_{-\mathbf{k}\downarrow}, \tag{1.4}$$

with $|u_{\mathbf{k}}|^2 + |v_{\mathbf{k}}|^2 = 1$, which guarantees the fermionic nature of the γ-operators (i.e. the usual anti-commutation relations). In particular, one can further evaluate

$$|v_{\mathbf{k}}|^2 = 1 - |u_{\mathbf{k}}|^2 = \frac{1}{2}\left(1 - \frac{\xi_{\mathbf{k}}}{E_{\mathbf{k}}}\right), \tag{1.5}$$

where $E_{\mathbf{k}} = \sqrt{\xi^2_{\mathbf{k}} + |\Delta|^2}$ are the eigenvalues of the diagonalized Hamiltonian [49].

The BCS ground state $|\Phi_{BCS}\rangle$ (at $T = 0$) is by definition the vacuum for the quasi-particle operators, i.e. $\gamma_{\mathbf{k}\uparrow}|\Phi_{BCS}\rangle = \gamma_{-\mathbf{k}\downarrow}|\Phi_{BCS}\rangle = 0$, and can be obtained explicitly as

$$|\Phi_{BCS}\rangle = \prod_{\mathbf{k}} \left(u_{\mathbf{k}} + v_{\mathbf{k}} c^{\dagger}_{\mathbf{k}\uparrow} c^{\dagger}_{-\mathbf{k}\downarrow}\right)|0\rangle\,. \tag{1.6}$$

The evaluation of expectation values is considerably facilitated by this relation. One can easily show that $\langle\Phi_{BCS}| c^{\dagger}_{\mathbf{k}\sigma} c_{\mathbf{k}\sigma}|\Phi_{BCS}\rangle = |v_{\mathbf{k}}|^2$ is the *occupation number* $n_{\mathbf{k}}$ and that $\langle\Phi_{BCS}| c^{\dagger}_{-\mathbf{k}\downarrow} c_{\mathbf{k}\uparrow}|\Phi_{BCS}\rangle = u^*_{\mathbf{k}} v_{\mathbf{k}}$ is the so-called *anomalous density* $\phi_{\mathbf{k}}$ which characterizes the BCS wave function.

At $T \neq 0$ we can use the thermal averages $\langle\gamma^{\dagger}_{\mathbf{k}\uparrow}\gamma_{\mathbf{k}\uparrow}\rangle = 1 - \langle\gamma_{-\mathbf{k}\downarrow}\gamma^{\dagger}_{-\mathbf{k}\downarrow}\rangle = f(E_{\mathbf{k}})$, where $f(\varepsilon) = [e^{\beta\varepsilon} + 1]^{-1}$ is the *Fermi function* with $\beta = 1/T$, together with the definitions in (1.4), to readily get the mean-field *density equation*

$$n = \int \frac{d\mathbf{k}}{(2\pi)^3}\left(1 - \frac{\xi_{\mathbf{k}}}{E_{\mathbf{k}}}(1 - 2f(E_{\mathbf{k}}))\right). \tag{1.7}$$

Correspondingly, the self-consistent condition (1.3) reduces to

$$\Delta = -v_0 \sum_{\mathbf{k}} u_{\mathbf{k}} v^*_{\mathbf{k}} (1 - 2f(E_{\mathbf{k}})), \tag{1.8}$$

and, using the analytic expressions for $u_{\mathbf{k}}$, $v_{\mathbf{k}}$ in (1.5) and performing the *thermodynamic limit*, one finally gets the *gap equation*

$$-\frac{1}{v_0} = \int_{|\mathbf{k}|\leq k_0} \frac{d\mathbf{k}}{(2\pi)^3} \frac{1 - 2f(E_{\mathbf{k}})}{2E_{\mathbf{k}}} \equiv \int_{|\mathbf{k}|\leq k_0} \frac{d\mathbf{k}}{(2\pi)^3} \frac{\tanh(\beta E_{\mathbf{k}}/2)}{2E_{\mathbf{k}}}, \tag{1.9}$$

where k_0 is the ultraviolet cut-off introduced to avoid divergences, as discussed above. As we see from the definition of $E_{\mathbf{k}}$, the coefficient Δ originates a gap in the energetic spectrum which is maximum at $T = 0$, namely Δ_0, and non-zero only for $T < T_c^{BCS}$. For this reason, the gap Δ can be interpreted as the BCS *order parameter*.

At finite temperature, it is impossible to find an analytic solution for the density equation (1.7) and the gap equation (1.9) because of the presence of the Fermi function, so one has to search for numerical solutions. However, when approaching the critical temperature T_c^{BCS} from below, an exception occurs and one can obtain analytic results. At mean-field level indeed, the critical temperature T_c^{BCS} corresponds to a vanishing BCS gap parameter Δ: we will recover this value in Section 3.1.3, when we will introduce a proper regularization condition for ultra-cold Fermi gases.

1.2 Bose-Einstein Condensation (BEC)

A *Bose–Einstein condensate* (BEC) is a peculiar gaseous state at low temperatures, predicted by Einstein in 1925 and produced in the laboratory for the first time in 1995, in which a large fraction of bosons reside in the same lowest quantum state. The study of these condensates has become one of the most active areas of

research in contemporary physics, mainly because they exhibit quantum properties on a macroscopic scale [50].

The mean occupation number of the single-particle state ν for non-interacting bosons in thermodynamic equilibrium is given by the *Bose function* $[e^{\beta(\varepsilon_\nu-\mu)}-1]^{-1}$, where ε_ν is the energy of the single-particle state for a particular external potential under consideration. The condition that the total number of particles must be equal to the sum of the occupation numbers of the individual levels determines the chemical potential μ as a function of N and T. If we consider the energy of the lowest single-particle state to be zero, i.e. $\varepsilon_0 = 0$, we must have $\mu < 0$ above the transition temperature, in order to have a physical (i.e. positive) distribution, and $\mu = 0$ in the condensed state, up to terms of order $1/N$ which we shall generally neglect in the thermodynamic limit. At high temperatures the mean occupation number of any state is much less than unity and therefore the chemical potential is much less than zero. As the temperature is lowered, the mean occupation numbers increase and the chemical potential rises. This makes μ a non-increasing function with respect to temperature, i.e. $\partial\mu/\partial T \leq 0$.

Performing the thermodynamic limit, the computations of the thermodynamic properties of gases involve integrals, rather than sums over states, and the multiplicity of the levels is replaced by a *density of states* $g(\varepsilon)$, in which details of the level structure are smoothed out. However, this procedure fails for a Bose-Einstein condensed system, since the contribution from the ground state is not properly accounted for. Nonetheless, one can still get a good approximation to the contribution from excited states

$$N_{ex} = \int_0^\infty \frac{g(\varepsilon)d\varepsilon}{e^{\beta(\varepsilon-\mu)}-1}. \tag{1.10}$$

The transition temperature T_c^{BEC}, defined as the highest temperature at which a macroscopic occupation of the lowest state occurs, is determined by the condition that the total number of particles can be accommodated in excited states, imposing $\mu = 0$ in (1.10), that is

$$N = N_{ex}(T_c, \mu = 0) = \int_0^\infty \frac{g(\varepsilon)d\varepsilon}{e^{\varepsilon/T_c}-1}. \tag{1.11}$$

We can compute the density of state for a three-dimensional free particle with $2s+1$ spin states using a semi-classical approach. On average, there is one quantum state per phase-space volume $(2\pi)^3$ (in $\hbar$-units). The volume of the region of the momentum space for which the magnitude of the momentum is less than p is $4\pi p^3/3$ and, since the energy of a free particle of momentum $\mathbf{p}$ is by $\varepsilon_{\mathbf{p}} = \mathbf{p}^2/(2m)$, the total number of states $G(\varepsilon)$ with energy less than ε is given by

$$G(\varepsilon) = (2s+1)V\frac{4\pi}{3}\frac{(2m\varepsilon)^{3/2}}{(2\pi)^3}, \tag{1.12}$$

where V is the volume of the system. Therefore, the density of states $g(\varepsilon)$ is obtained by

$$g(\varepsilon) = \frac{dG(\varepsilon)}{d\varepsilon} = (2s+1)V\frac{m^{3/2}}{2^{1/2}\pi^2}\varepsilon^{1/2}. \tag{1.13}$$

Now we are ready to compute the transition temperature T_c^{BEC} for a free 3D Bose gas by inverting the relation (1.11) and using the density of states (1.13) as

$$T_c^{BEC} = \frac{2\pi}{m}\left[\frac{n}{(2s+1)\zeta(3/2)}\right]^{2/3}, \tag{1.14}$$

with the Riemann zeta function $\zeta(3/2) = \sum_{n=0}^{\infty} n^{-3/2} \simeq 2.612$.

We can also easily calculate the condensate fraction $\rho_0(T) = N_0/N$ which, in the thermodynamic limit, is different from zero only for $T < T_c$. In fact $\rho_0(T) = 1 - \rho_{ex}(T)$, where $\rho_{ex} = N_{ex}/N$ can be calculated from (1.10) below the transition temperature by setting $\mu = 0$. For particles in a box in three dimensions ρ_0 is therefore given by the well-known result

$$\rho_0(T) = 1 - \left(\frac{T}{T_c}\right)^{2/3}. \tag{1.15}$$

Bose-Einstein condensation occurs when the macroscopic majority of particles fall into the single-particle ground state, that is when the number of particles in the single-particle ground state N_0 is $N_0 \approx N$, and therefore $N_\nu/N \ll 1$ for $\nu \neq 0$. For this reason, it is convenient to write the field operator $\hat{\psi}(\mathbf{r})$, which annihilates a particle at position $\mathbf{r}$, as

$$\hat{\psi}(\mathbf{r}) = \varphi_0(\mathbf{r})a_0 + \sum_{\nu\neq 0} \varphi_\nu(\mathbf{r})a_\nu, \tag{1.16}$$

where a_ν is the bosonic annihilation operator in the single-particle state $\varphi_\nu(\mathbf{r})$. Considering that $|a_\nu\,|\ldots, N_\nu, \ldots\rangle\,| \sim N_\nu$, the second term in this expression may be considered to be a small fluctuation $\delta\hat{\psi}(\mathbf{r})$.

Now let us analyze the effect of the ground state annihilation operator a_0 on the Bose-Einstein condensed state. Since we deal with a macroscopic number of bosons in the ground state, the difference between N_0 and $N_0 - 1$ is negligible, and hence we can assume

$$a_0\,|N_0, \ldots\rangle = \sqrt{N_0}\,|N_0 - 1, \ldots\rangle \simeq \sqrt{N_0}\,|N_0, \ldots\rangle\,. \tag{1.17}$$

So, the unique effect of the ground state annihilation operator is to multiply the state with the real number $\sqrt{N_0}$. We can therefore replace this operator a_0 (and also its conjugate $a_0^\dagger$) with the real number $\sqrt{N_0}$. This is known as *Bogoliubov approximation* [51], which allows one to describe the field operator as a macroscopic wave function for the ground state plus a small fluctuation, negligible for sufficiently low temperatures

$$\hat{\psi}(\mathbf{r}) = \psi_0(\mathbf{r}) + \delta\hat{\psi}(\mathbf{r}), \tag{1.18}$$

where $\psi_0(\mathbf{r}) = \sqrt{N_0}\varphi_0(\mathbf{r})$. The classical field $\psi_0(\mathbf{r})$ is called *condensate wave function* and plays the role of the BEC *order parameter*.

The Bogoliubov ansatz (1.18) for the field operator implies that the expectation value $\langle\hat{\psi}(\mathbf{r})\rangle$, for low temperatures, is different from zero. This would not be possible if the condensate state is in a particle number eigenstate $|N_0\rangle$. From a quantum

field theoretical point of view, this spontaneous symmetry breaking means that the condensate state is in or close to a *coherent state* $|\alpha\rangle$ defined by

$$a_0 |\alpha\rangle = \alpha |\alpha\rangle , \qquad |\alpha\rangle = \sum_{N_0} \frac{e^{-|\alpha|^2/2}}{\sqrt{N_0!}} \alpha^{N_0} |N_0\rangle \equiv e^{-|\alpha^2|/2} e^{\alpha a_0^\dagger} |0\rangle , \tag{1.19}$$

where we notice that, if $|\alpha|^2 = N_0$, we recover $\psi_0(\mathbf{r}) = \langle\alpha| \varphi_0(\mathbf{r}) a_0 |\alpha\rangle = \sqrt{N_0}\varphi_0(\mathbf{r})$.

1.3 BCS-BEC Crossover

We now show that the BCS wave function (1.6) contains the BEC of composite bosons as a limit. If we set $g_\mathbf{k} = v_\mathbf{k}/u_\mathbf{k}$, the BCS ground state can be rewritten in the form

$$|\Phi_{BCS}\rangle = \left(\prod_{\mathbf{k}'} u_{\mathbf{k}'} \right) \exp \left[\sum_\mathbf{k} g_\mathbf{k} c_{\mathbf{k}\uparrow}^\dagger c_{-\mathbf{k}\downarrow}^\dagger \right] |0\rangle , \tag{1.20}$$

since $(c_{\mathbf{k}\sigma}^\dagger)^2 = 0$ for the Pauli principle. By direct comparison with (1.19), the BCS wave function is by definition a coherent state of Cooper pairs. We see that the operator $a_0^\dagger \equiv \sum_\mathbf{k} g_\mathbf{k} c_{\mathbf{k}\uparrow}^\dagger c_{-\mathbf{k}\downarrow}^\dagger$ contains fermion pairs but it is not a truly bosonic operator since the commutator $[a_0, a_0^\dagger] = \sum_\mathbf{k} |g_\mathbf{k}|^2 (1 - \hat{n}_{\mathbf{k}\uparrow} - \hat{n}_{-\mathbf{k}\downarrow})$ does not satisfy the proper bosonic commutation relations but explicitly contains the fermionic operators $\hat{n}_{\mathbf{k}\sigma} = c_{\mathbf{k}\sigma}^\dagger c_{\mathbf{k}\sigma}$. However, as long as $\langle\Phi_{BCS}| \hat{n}_{\mathbf{k}\sigma} |\Phi_{BCS}\rangle = |v_\mathbf{k}|^2 \ll 1$ for all $\mathbf{k}$ of physical relevance, one may consider that $[a_0, a_0^\dagger] \simeq 1$ for all practical purposes. As a consequence, $|\Phi_{BCS}\rangle = \exp\left(a_0^\dagger\right) |0\rangle$ represents a Bose-Einstein condensate, since it corresponds to a bosonic coherent state with a non-vanishing broken symmetry $\langle\Phi_{BCS}| a_0 |\Phi_{BCS}\rangle = \sum_\mathbf{k} |g_\mathbf{k}|^2 \neq 0$, exactly as discussed in the previous section.

Looking at the definition (1.5) it is clear that, if the fermionic chemical potential μ becomes large and negative, the condition $|v_\mathbf{k}|^2 \ll 1$ can be satisfied for all $\mathbf{k}$. This happens when the two-body problem in vacuum presents a bound state with a large binding energy ε_0. In this BEC limit μ approaches the value $-\varepsilon_0/2$, which is equivalent to saying that all fermions are paired up in tight (composite) bosons with a vanishing residual interaction among them. This result for μ can directly be obtained from the mean-field gap equation (at zero temperature) in the case of a wave-vector dependent interaction $V(\mathbf{k}, \mathbf{k}')$

$$\Delta_\mathbf{k} = -\int \frac{d\mathbf{k}'}{(2\pi)^3} V(\mathbf{k}, \mathbf{k}') \frac{\Delta_{\mathbf{k}'}}{2E_{\mathbf{k}'}}, \tag{1.21}$$

which is a generalization of the equation in (1.9). Using $\phi_\mathbf{k} = u_\mathbf{k}^* v_\mathbf{k} \equiv \Delta_\mathbf{k}/2E_\mathbf{k}$ and $|v_\mathbf{k}|^2 = n_\mathbf{k}$, we can rewrite the (1.21) in the form

$$2\xi_\mathbf{k}\phi_\mathbf{k} + (1 - 2n_\mathbf{k}) \int \frac{d\mathbf{k}'}{(2\pi)^3} V(\mathbf{k}, \mathbf{k}')\phi_{\mathbf{k}'} = 0. \tag{1.22}$$

Given $n_\mathbf{k} \ll 1$, this equation is nothing else than the *Schrödinger equation* for the relative motion of two particles of equal mass m, mutually interacting via the

potential V. The negative eigenvalue 2μ of this equation thus is equal to (minus) the two-body binding energy ε_0 as stated above.

The aspects underlined above suggest a crossover phenomenon, which connects smoothly the BCS superfluidity and the Bose-Einstein condensation through the reduction of the size of the fermion pairs, the fundamental entities in both phenomena. By varying the size, we pass from large values when Cooper pairs are strongly overlapping in the BCS limit, to small values when composite bosons are non-overlapping in the BEC limit. The fermionic chemical potential μ, which can be found by inverting a proper relation for the number density n, is therefore one of the driving fields which enables the system to pass from the BCS to the BEC limits of the BCS–BEC crossover. As an example, Figure 1.1 shows the occupation number $n_{\mathbf{k}} = |v_{\mathbf{k}}|^2$ at zero temperature for different values of the chemical potential μ. In particular, the curves $n_{\mathbf{k}}$ have an inflection point at $\varepsilon_{\mathbf{k}} = \mu$, which shows the presence of an underlying Fermi surface, only when $\mu > 0$, while the occupation number becomes quite small for all $\mathbf{k}$ and the Fermi sea gets completely dissolved when μ becomes negative.

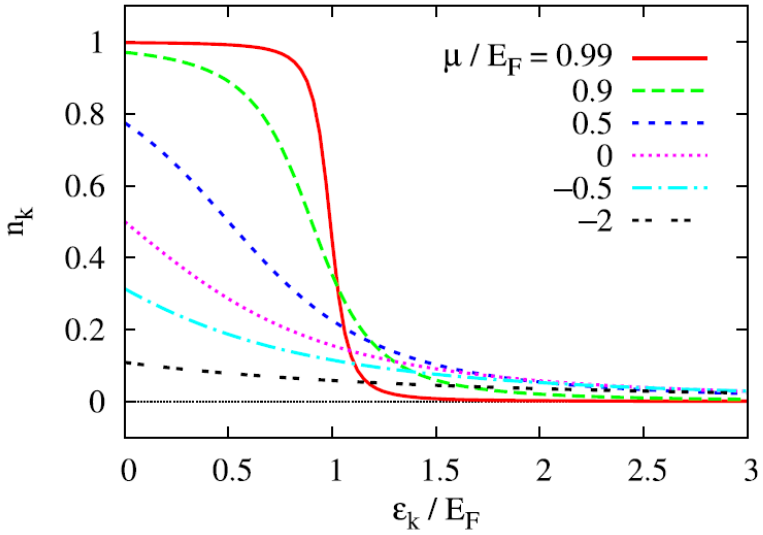

Figure 1.1: BCS occupation number $n_{\mathbf{k}} = |v_{\mathbf{k}}|^2$ at zero temperature in function of the the energy $\varepsilon_{\mathbf{k}} = \mathbf{k}^2/(2m)$ in units of the Fermi energy $E_F = (3\pi^2 n)^{2/3}/(2m)$, where n is the density, for different values of the chemical potential μ. *Source*: reproduced from Ref. [33].

Another quantity that is obviously crucial to drive the BCS-BEC crossover is the form and the strength of the interaction potential $V(\mathbf{r})$ between the fermions [52]. In particular we will see in Chapter 3 that, for short-range potentials and at low energies (i.e. temperatures), the crossover is described in terms of a single parameter: the *dimensionless coupling* $(k_F a)^{-1}$, where a is the *scattering length* associated to the interaction potential and $k_F = (3\pi^2 n)^{1/3}$ is the *Fermi wave vector*. If the strength of the potential increases from just below the critical value for binding to just above it, the coupling increases smoothly from negative to positive values. In Figure 1.2, a graphical representation of a Fermi gas in the broken-symmetry phase along

the BCS-BEC crossover is given as a function of the coupling $(k_F a)^{-1}$. Large and negative couplings $(k_F a)^{-1} \ll -1$ correspond to the *weak-coupling* (or BCS) regime, while large and positive couplings $(k_F a)^{-1} \gg 1$ correspond to the *strong-coupling* (or BEC) regime. The intermediate region $(k_F a)^{-1} = 0$, where pairs have a dimension that is comparable to the average inter-particle spacing, is usually called *unitary regime* or *unitarity*.

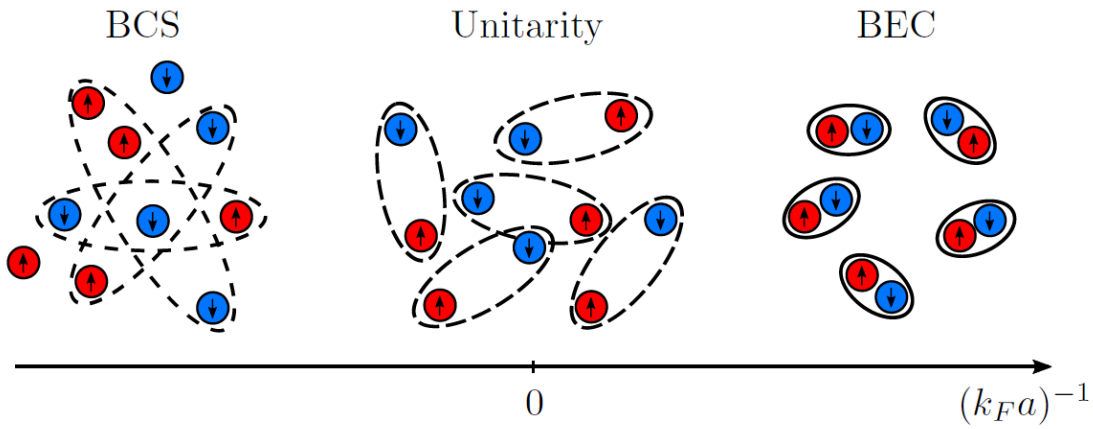

Figure 1.2: Two-component balanced Fermi gas in the ordered (broken-symmetry) phase across the BCS-BEC crossover by varying the dimensionless coupling $(k_F a)^{-1}$. *Source*: reproduced from Ref. [46].

1.3.1 Need of Pairing Fluctuations above Mean-field

As we discussed above, in this theory the range of the inter-particle correlations can become much smaller than the inter-particle distance. Therefore, it is clear that we need a proper inclusion of pairing fluctuations above mean-field to get a consistent description of the BCS–BEC crossover, especially at finite temperature when they are accompanied by thermal fluctuations.

As an example, let's try to recover the critical temperature in the strong-coupling (BEC) limit. We assume $|\mu| \gg T_c$ such that $\mu \simeq -\varepsilon_0/2$, i.e. the chemical potential reaches the large asymptotic value for the bound state discussed previously. In this way the density equation (1.7) at the critical temperature can be simplified as

$$n = 2\int \frac{d\mathbf{k}}{(2\pi)^3} \frac{1}{e^{\xi_{\mathbf{k}}/T_c}+1} \simeq 2\int \frac{d\mathbf{k}}{(2\pi)^3} e^{-\xi_{\mathbf{k}}/T_c}, \tag{1.23}$$

and we get an equation for T_c that can be solved iteratively yielding [53]

$$T_c \simeq \frac{\varepsilon_0}{2\ln\left(\frac{\varepsilon_0}{E_F}\right)^{3/2}}, \tag{1.24}$$

at leading order in $E_F/\varepsilon_0 \ll 1$, where $E_F = k_F^2/(2m)$ is the *Fermi energy*. Although $T_c \ll |\mu|$ consistently with our assumptions, the expression of T_c (1.24) diverges in the BEC limit at fixed density, instead of approaching as expected the finite value

T_c^{BEC} in (1.14) for the BEC of an ideal gas of bosons with mass $2m$ and density $n/2$. The reason for this failure to recover the BEC temperature from the mean-field density equation is that we have taken into account only internal degrees of freedom of the composite bosons, leaving aside the translational ones. To include these, pairing fluctuations beyond mean field need to be considered, as we will discuss in Section 3.2.2. Physically, the mean-field temperature (1.24) corresponds to the *pair dissociation temperature* T^* of the composite bosons, which is completely different from the BEC temperature at which quantum coherence is established by the system. Indeed, while in weak-coupling fermion pairs form and condense at the same temperature (that is $T^* \simeq T_c$), in strong-coupling pair formation occurs at a temperature higher than the condensation temperature (that is $T^* \gg T_c$).

With the introduction of the pair dissociation temperature T^* above, we understand that inclusion of pairing fluctuations is especially relevant in the normal phase above T_c, where the order parameter vanishes. This is also because, even though we lose the characteristic long-range order of the superfluid phase, a "local" order is expected to survive above T_c if the system is fluctuating. In a similar way to what occurs in the superfluid phase below T_c when the order parameter is instead non-zero, these considerations have led people to associate pairing fluctuations with the occurrence of a *pseudo-gap* above T_c [54].

To collect all these notions, Figure 1.3 presents a qualitative phase diagram of the BCS-BEC crossover in a dilute Fermi gas in the standard three dimensional case, obtained well before the era of cold atom experiments. Remarkably, many of its features have now been tested experimentally [55].

1.4 Spin Imbalanced (Polarized) Systems

What happens if not every spin up fermion can find a spin down partner? This question has intrigued physicists ever since the early days of BCS theory. In practice, unequal populations of up and down-spin electrons are very difficult to create in conventional superconductors, essentially because the orbital effects in the presence of a magnetic field destroy superconductivity long before the Zeeman splitting is able to induce an appreciable imbalance. Fortunately, in two-component ultra-cold Fermi gases, one can control the populations of different "spin" states (that correspond to different hyperfine states) independently from orbital effects. The first physicists who addressed this problem within the BCS approach were Clogston, Chandrasekhar and Sarma [22, 56, 57]. In their works, the orbital effects were completely neglected and therefore the spin-population imbalance was assumed to be produced by an external magnetic field acting only on the spins of the electrons.

The BCS mean-field approximation, which was discussed in the previous sections for a balanced system, can be easily generalized to the presence of different spin populations (and thus of different chemical potentials). The number equation (1.7) splits into an equation for the total density

$$n = n_\uparrow + n_\downarrow = \int \frac{d\mathbf{k}}{(2\pi)^3}\left(1 - \frac{\xi_\mathbf{k}}{E_\mathbf{k}}(1 - f(E_\mathbf{k}^+) - f(E_\mathbf{k}^-))\right), \tag{1.25}$$

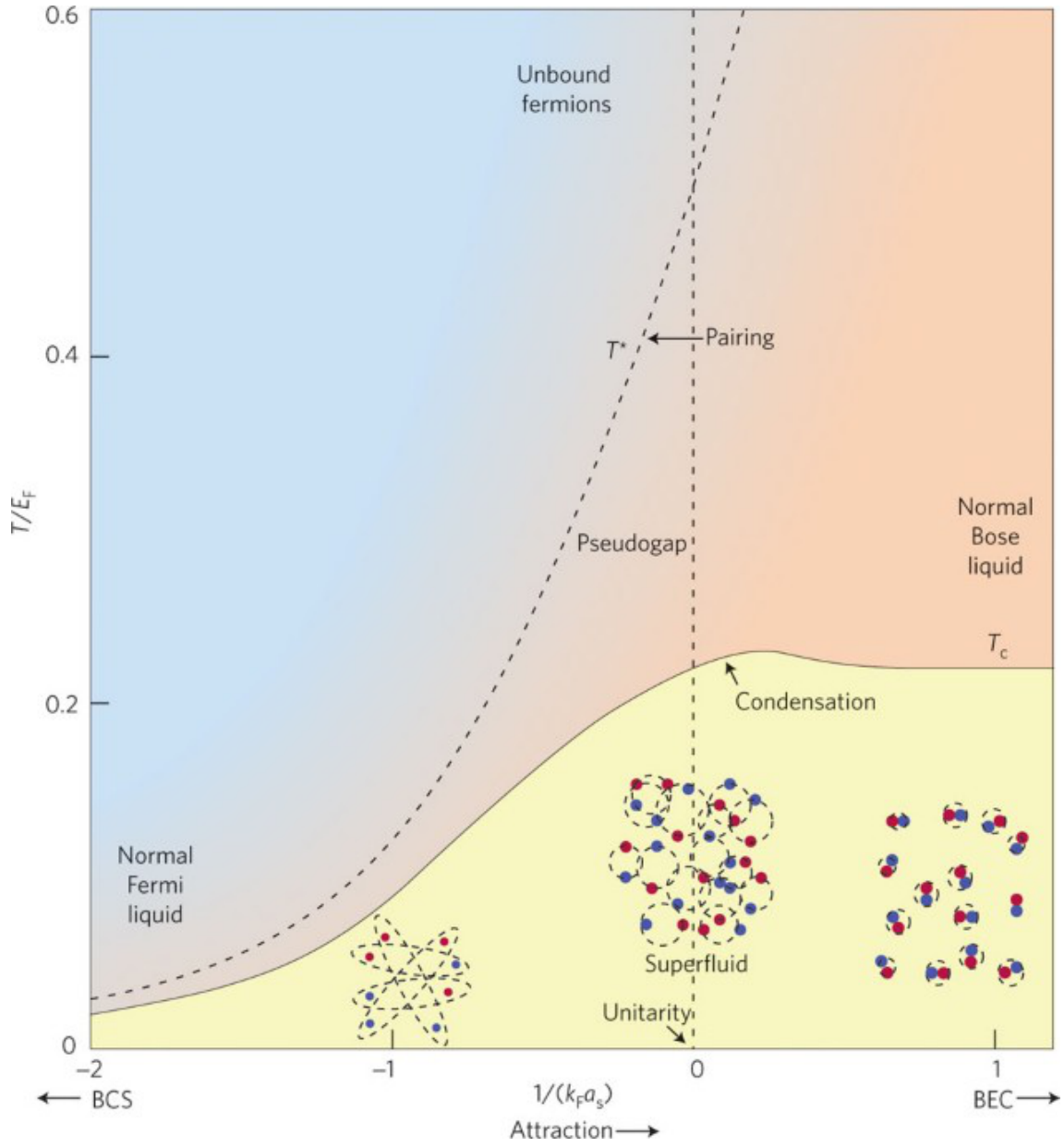

Figure 1.3: Qualitative phase diagram of the BCS-BEC crossover (temperature T/E_F vs coupling $(k_F a)^{-1}$). Increasing the relative attraction, the pair-dissociation temperature T^* diverges away from the transition temperature T_c below which a condensate exists. *Source*: reproduced from Ref. [34].

and an equation for the difference between the two densities

$$n_\uparrow - n_\downarrow = \int \frac{d\mathbf{k}}{(2\pi)^3}\Big(f(E^+_\mathbf{k}) - f(E^-_\mathbf{k})\Big), \tag{1.26}$$

while the gap equation (1.9) for a contact potential is modified as follows

$$-\frac{1}{v_0} = \int_{|\mathbf{k}|\leq k_0} \frac{d\mathbf{k}}{(2\pi)^3}\frac{1 - f(E^+_\mathbf{k}) - f(E^-_\mathbf{k})}{2E_\mathbf{k}}. \tag{1.27}$$

Here $E_\mathbf{k} = \sqrt{\xi^2_\mathbf{k} + |\Delta|^2}$ with $\xi_\mathbf{k} = (\xi_{\mathbf{k}\uparrow} + \xi_{\mathbf{k}\downarrow})/2$, and $E^\pm_\mathbf{k} = E_\mathbf{k} \pm \delta\xi_\mathbf{k}$ with $\delta\xi_\mathbf{k} = (\xi_{\mathbf{k}\uparrow} - \xi_{\mathbf{k}\downarrow})/2$, where $\xi_{\mathbf{k}\sigma} = \mathbf{k}^2/(2m) - \mu_\sigma$ is the single particle energy relative to the chemical potential μ_σ for the spin $\sigma =\uparrow,\downarrow$. At $T = 0$, one sees from (1.26) that the difference $n_\uparrow - n_\downarrow$ between the two densities is finite if one of the two single-particle excitation energies $E^\pm_\mathbf{k}$ become negative in a certain region of $\mathbf{k}$-space. Equivalently, in terms of the *imbalancing field* $h = (\mu_\uparrow - \mu_\downarrow)/2$ such that $E^\pm_\mathbf{k} = E_\mathbf{k} \mp h$, if $h > \min E_\mathbf{k}$ one obtains $n_\uparrow > n_\downarrow$ (for definiteness, in the following we shall assume $h > 0$ such that spin-$\uparrow$ fermions correspond to the majority species). Moreover, the above equations at $T = 0$ correspond to the following ground-state wave function [58]

$$|\Phi_S\rangle = \prod_{\mathbf{k}\in\mathcal{R}} c^\dagger_{\mathbf{k}\uparrow} \prod_{\mathbf{k}\notin\mathcal{R}} \left(u_\mathbf{k} + v_\mathbf{k} c^\dagger_{\mathbf{k}\uparrow} c^\dagger_{-\mathbf{k}\downarrow}\right)|0\rangle\,, \tag{1.28}$$

where $u_\mathbf{k}$ and $v_\mathbf{k}$ are defined as in (1.5). The region of $\mathbf{k}$-space with $E^+_\mathbf{k} < 0$ is denoted with $\mathcal{R}$ and is fully occupied by the $\uparrow$-fermions of the majority species, while outside this region Cooper pairing occurs. The state $|\Phi_S\rangle$, known as *Sarma state*, is determined by a sort of phase separation in $\mathbf{k}$-space between one region which is unpolarized and superfluid and a second region which is fully polarized and normal, accommodating at the same time superfluidity and a finite population imbalance. Depending on the value of $\mu = (\mu_\uparrow + \mu_\downarrow)/2$, two or one Fermi surfaces with gapless single-particle excitations enclose the normal region $\mathcal{R}$, respectively if $\mu > \delta\varepsilon$ or $\mu < \delta\varepsilon$, with $\delta\varepsilon = \sqrt{h^2 - \Delta^2}$. The phase described by (1.28) thus corresponds to a *gapless polarized BCS superfluid*.

A problem with the Sarma state (1.28) in weak-coupling is that it results energetically unstable. Specifically one finds that, by solving the gap equation (1.27) in the weak-coupling limit, the gap $\Delta(h)$ shows a re-entrant behavior below a certain temperature T_0. This re-entrant branch at $T = 0$ is then associated to the Sarma state. Furthermore, also the dependence of the critical temperature on h, which is obtained by setting $\Delta = 0$ in the gap equation (1.27), shows an analogous re-entrant behavior (full line in Figure 1.5(a)). However, due to comparisons between the (grand-canonical) free energies of the normal and superfluid phases, it was found that below the temperature T_0 the transition becomes of *first-order*, also known as *Clogston-Chandrasekhar transition*, with the gap dropping discontinuously to zero at the transition. Correspondingly, the re-entrant behavior below T_0 is completely eliminated by the transition curve (dashed line in Figure 1.5(a)). The analysis made by Sarma at $T = 0$ recovered this first-order transition at $h = \Delta_0/\sqrt{2}$, from an unpolarized BCS state to a polarized normal state, suppressing superfluidity when $h > \Delta_0/\sqrt{2}$.

1.4.1 Fulde-Ferrell-Larkin-Ovchinnikov Phase (FFLO)

Fulde and Ferrell (FF) [23] and, independently, Larkin and Ovchinnikov (LO) [24] proposed an alternative solution to the problem of superconductivity (superfluidity) in the presence of spin imbalance. The basic idea, presented schematically in Figure 1.4, is that a mismatch of the spin-up and spin-down Fermi surfaces due to spin imbalance should favour Cooper pairing for a finite value of the center-of-mass wave vector $\mathbf{Q}$. This is because the pairing states $|\mathbf{k}+\mathbf{Q}/2,\uparrow\rangle$ and $|-\mathbf{k}+\mathbf{Q}/2,\downarrow\rangle$ remain in the vicinity of both Fermi surfaces if we take $|\mathbf{Q}|$ of the order of $k_{F\uparrow}-k_{F\downarrow}$, with $k_{F\sigma}=(6\pi^2 n_\sigma)^{1/3}$. Specifically, this matching occurs only on one side of the respective Fermi surfaces as determined by $\mathbf{Q}$ itself, while on the other side pairing is completely suppressed. By making these regions completely empty/filled with $\downarrow$ / $\uparrow$ fermions respectively, one obtains a non-vanishing value of the polarization. As a consequence, pair condensation at finite $\mathbf{Q}$ leads to a space-dependent order parameter, which is given by a single plane wave in the Fulde–Ferrell analysis and by a superposition of two plane waves with the same $|\mathbf{Q}|$ and opposite direction in the Larkin–Ovchinnikov analysis. Therefore, the exotic FLLO phase corresponds to an *inhomogeneous superfluid*.

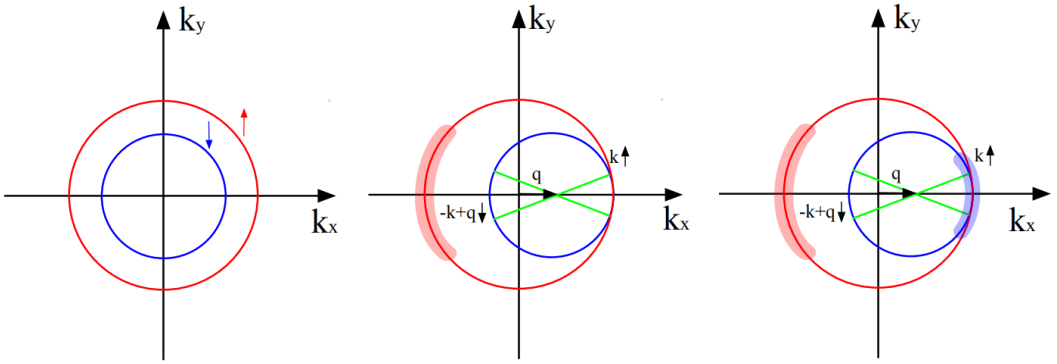

Figure 1.4: *Left*: Two different sizes of Fermi surfaces for the two components of a non-interacting density-imbalanced Fermi gas. *Middle*: FFLO phase, in which the pairs now carry the momentum $\mathbf{q}$. Pairing occurs such that the minority Fermi surface can be thought of as shifted by the wave vector $\mathbf{q}$. Examples of up and down spin particles that pair are represented by the green lines. In the red region pairing is suppressed and therefore are only present the unpaired majority particles. *Right*: For some parameters, unpaired minority particles may also appear in the blue region. Notice that the total net momentum of the system remains zero. *Source*: reproduced from Ref. [59].

We can readily extend the mean-field equations (1.25)-(1.27) to take into account the FF pairing. By setting

$$\Delta_{\mathbf{Q}} e^{i\mathbf{Q}\cdot\mathbf{r}} = -v_0 \int \frac{d\mathbf{k}}{(2\pi)^3} \langle c_{-\mathbf{k}+\mathbf{Q}/2\downarrow} c_{\mathbf{k}+\mathbf{Q}/2\uparrow} \rangle, \tag{1.29}$$

we can modify them via the replacements $(\xi_{\mathbf{k}}, E_{\mathbf{k}}, E^{\pm}_{\mathbf{k}}) \to (\xi_{\mathbf{k},\mathbf{Q}}, E_{\mathbf{k},\mathbf{Q}}, E^{\pm}_{\mathbf{k},\mathbf{Q}})$, where $E_{\mathbf{k},\mathbf{Q}} = \sqrt{\xi^2_{\mathbf{k},\mathbf{Q}} + |\Delta_{\mathbf{Q}}|^2}$ with $\xi_{\mathbf{k},\mathbf{Q}} = (\xi_{\mathbf{k}+\mathbf{Q}/2\uparrow} + \xi_{-\mathbf{k}+\mathbf{Q}/2\downarrow})/2$, and $E^{\pm}_{\mathbf{k},\mathbf{Q}} = E_{\mathbf{k},\mathbf{Q}} \pm \delta\xi_{\mathbf{k},\mathbf{Q}}$

with $\delta\xi_{\mathbf{k},\mathbf{Q}} = (\xi_{\mathbf{k}+\mathbf{Q}/2\uparrow} - \xi_{-\mathbf{k}+\mathbf{Q}/2\downarrow})/2$. Analogously to the Sarma phase, the FF solution at $T = 0$ then corresponds to the wave function [60]

$$|\Psi_{FF}\rangle = \prod_{\mathbf{k}\in\mathcal{R}_\uparrow} c^\dagger_{\mathbf{k}+\mathbf{Q}/2\uparrow} \prod_{\mathbf{k}\in\mathcal{R}_\downarrow} c^\dagger_{-\mathbf{k}+\mathbf{Q}/2\downarrow} \prod_{\mathbf{k}\notin\mathcal{R}_{\uparrow,\downarrow}} \left(u_{\mathbf{k}} + v_{\mathbf{k}} c^\dagger_{\mathbf{k}+\mathbf{Q}/2\uparrow} c^\dagger_{-\mathbf{k}+\mathbf{Q}/2\downarrow}\right)|0\rangle\,, \quad (1.30)$$

where in the region $\mathcal{R}_\uparrow$ ($\mathcal{R}_\downarrow$) the state $|\mathbf{k}+\mathbf{Q}/2,\uparrow\rangle$ is fully occupied (empty) and the state $|-\mathbf{k}+\mathbf{Q}/2,\downarrow\rangle$ is fully empty (occupied), while the remaining states are available for pairing. A finite population imbalance is present only when the difference between the volumes of the two regions $\mathcal{R}_\uparrow$ and $\mathcal{R}_\downarrow$ is different from zero. However, it is important to notice that no finite value of the current is associated with a finite value of $|\mathbf{Q}|$, because the current carried by the condensate is compensated by an opposite current of the unpaired fermions.

By minimizing the mean-field free-energy one can get the thermodynamic stability of the FF phase, together with the value of $|\mathbf{Q}|$. In weak-coupling, one obtains that at $T = 0$ the Clogston–Chandrasekhar transition is replaced by a first-order transition BCS-FF at essentially the same value of $h = \Delta_0/\sqrt{2}$, followed by a second-order transition FF-normal when $h = 0.754\Delta_0$. Correspondingly, $\mathbf{Q}$ changes from $1.28(k_{F\uparrow} - k_{F\downarrow})$ at the transition BCS-FF, to $1.2(k_{F\uparrow} - k_{F\downarrow})$ at the transition FF-normal. Also at finite temperature the transition FF-normal remains of second order, while the transition BCS-FF is of first order. The resulting phase diagram is reported in Figure 1.5(a): we notice in particular the presence of a *tricritical point*, where the three transition lines intersect, and a quite narrow region of existence of the FF phase.

In the LO approach a more general superposition of plane waves with the same $|\mathbf{Q}|$ was considered, corresponding in real space to a crystalline order for the order parameter. This surpassed the FF assumption of a single wave vector $\mathbf{Q}$, since it was found that near the transition point the solution $\Delta_{\mathbf{Q}} \cos(\mathbf{Q}\cdot\mathbf{r})$ has lower energy than the single plane-wave FF solution, and has also the lowest energy among the crystalline solutions. A refined phase diagram for the superfluid/normal transition in weak coupling, with more general solutions in the FFLO phase is reported, in Figure 1.5(b) [61]. One sees that the FFLO-normal phase transition is now of first-order and the FLLO phase still remains confined to a small corner of the phase diagram, although it is enlarged with respect to the FF solution.

Until this point, the Sarma and FLLO phases and their stability have been discussed only in the weak-coupling limit. Across the BCS-BEC crossover, theoretical and experimental works on ultra-cold polarized Fermi gases show the presence of a (real space) *phase separation* between the normal and superfluid phases, due to the fact that the transition has found to evolve from second-order to first-order [30]. Furthermore, also in this context, the Sarma phase turns out to be unstable against the FFLO phase or the phase separation unpolarized BCS-polarized normal phase, which is a manifestation of the Clogston-Chandraskhar first-order transition discussed above [62–64]. More precisely, by taking into account the FF phase (i.e. a single plane wave order parameter) and the phase separation, a complete $T = 0$ mean-field analysis for a polarized Fermi gas throughout the BCS-BEC crossover was carried out, searching for the global minima of the grand-canonical potential [65]. The resulting phase diagram (polarization vs coupling) in Figure 1.6 shows that

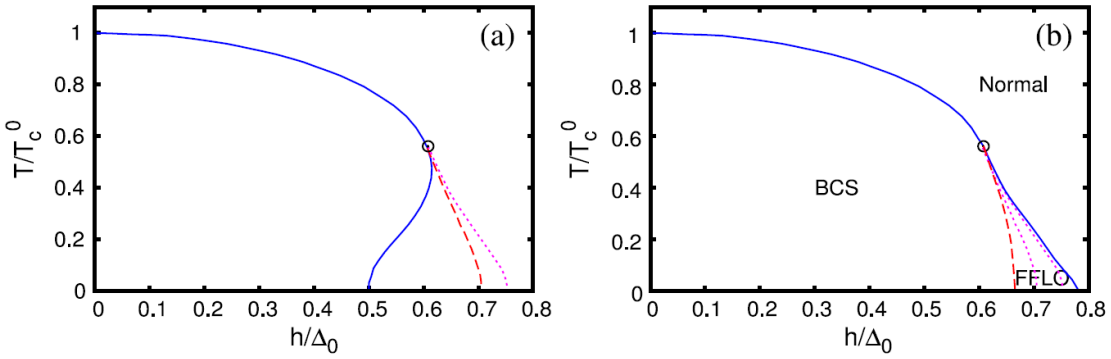

Figure 1.5: (**a**) Phase diagram for the superfluid/normal transition in the BCS limit (temperature in units of the critical temperature T_c^0 for $h = 0$ and $h = (\mu_\uparrow - \mu_\downarrow)/2$ in units of the zero-temperature gap Δ_0 at $h = 0$). *Full line*: critical temperature from the BCS gap equation, which corresponds to a true transition line only above the tricritical point (circle). *Dashed line*: first-order transition line separating the BCS superfluid from the normal phase. *Dotted line*: second-order transition line between the FF and normal phase. (**b**) Refined phase diagram for the superfluid/normal transition in weak-coupling, with more general solutions in the FFLO phase. *Full line*: transition line superfluid-normal phase, which becomes of first order below the tricritical point (circle). *Dashed line*: second-order transition line BCS-FFLO phases. For comparison are also reported the transition lines BCS-FF and FF-normal obtained by the simple FF solution (*dotted lines*). *Source*: reproduced from Ref. [33].

the phase separation normal-superfluid dominates, especially in the unitary limit, covering the normal-FLLO and the normal-Sarma transition lines. In the BEC side of the crossover, instead, the polarized superfluid (Sarma) phase is stable, where it corresponds to a mixture of composite bosons and excess fermions [66]. The FFLO phase is instead confined to a small region on the BCS side and so far, no evidence of the elusive FFLO phase has been found in ultra-cold gases.

Within mean-field theory, it has been possible to investigate the FF state in *mass imbalanced* ultra-cold Fermi gases through the BCS-BEC crossover [32]. It has been found that, when the heavy species is the majority, a stable FFLO phase persists throughout the crossover and the phase region is enlarged with respect to the mass balanced case. In contrast, when the light species is the majority, such an FFLO phase exists only in the BCS regime. As an example, in Figure 1.7 are reported the coupling-polarization phase diagrams for the mixture ^{6}Li -^{40}K at $T = 0$ for both positive and negative density imbalance. Despite the fact that a mean-field theory is not accurate enough to describe the problem, we expect that the findings about the enhancement effect of a large mass ratio on FFLO type of pairing remain valid also with the inclusion of pairing fluctuations.

With ultra-cold Fermi gases, also the interesting regime of the strongly imbalanced limit becomes accessible. In this case, the minority fermions act as dressed impurities, called *polarons*, immersed in a bath of majority fermions and the system is in the normal phase, even at zero temperature for not too strong attraction. As

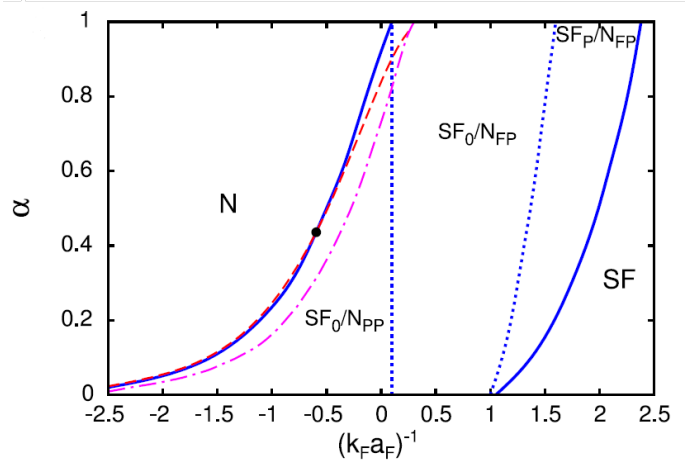

Figure 1.6: Mean-field $T = 0$ phase diagram for the population imbalance $\alpha = (n_\uparrow - n_\downarrow)/n$ vs the coupling parameter $(k_F a_F)^{-1}$. *Full lines*: phase separation (PS) boundaries normal-superfluid homogeneous phases $(N - SF)$. *Dotted lines*: boundaries inside the PS between balanced superfluid and partially polarized normal state, balanced superfluid and fully polarized normal state, polarized superfluid and fully polarized normal state $(SF_0/N_{PP} - SF_0/N_{FP} - SF_P/N_{FP})$. *Dashed line*: transition normal-FFLO phase. *Dashed–dotted line*: transition normal-Sarma phase (regardless its instability). *Source*: reproduced from Ref. [33].

we will see in Chapter 4, in this regime the system can be correctly described as a *Fermi liquid* of weakly-interacting quasi-particles.

1.5 Crossover in Ultra-cold Fermi Gases

Ultra-cold Fermi gases provide a unique opportunity for realizing experimentally the BCS–BEC crossover. This is because a method was found to vary the scattering length a_F of the two-fermion problem, while keeping the density of the system (and thus the Fermi wave vector k_F) fixed, from negative to positive values across the resonance where $a_F = \pm\infty$. In this way, a direct and unambiguous comparison between experiments and theory is allowed, because experimental data have been associated with the value of the dimensionless coupling parameter $(k_F a_F)^{-1}$ which is also used theoretically to drive the BCS–BEC crossover.

Special attention has been devoted to the *unitary limit* of the inter-particle interaction, when the scattering length diverges. The interesting fact of this unitary limit is that there are no length scales associated with the interaction, because the only length scale that remains at zero temperature is the average inter-particle spacing k_F^{-1} which is fixed by the density. More generally, the thermodynamic properties of the unitary Fermi gas depend only on density and temperature, paradoxically somehow just like for the non-interacting Fermi gas, and therefore a few universal functions of the dimensionless quantity T/E_F are sufficient to characterize the properties of the unitary Fermi gas. For this reason the unitary gas is often said to be *universal*.

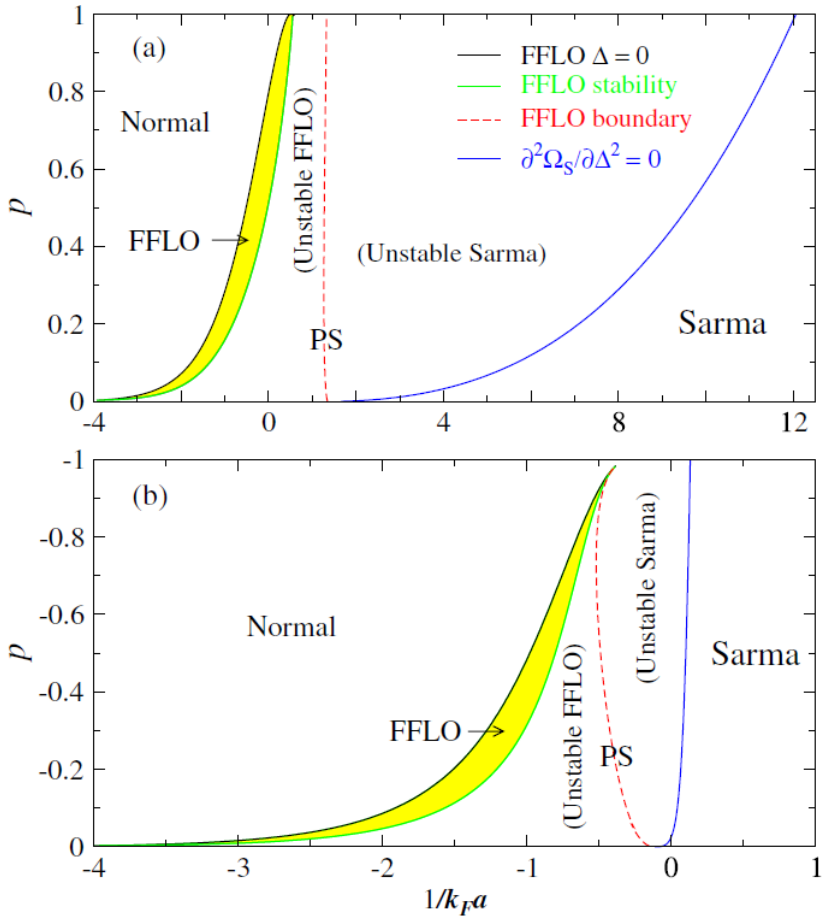

Figure 1.7: Mean-field $T = 0$ phase diagram of ^{6}Li -^{40}K mixture for the polarization $p = (n_\uparrow - n_\downarrow)/n$ vs the coupling parameter $(k_F a_F)^{-1}$. As a convention, we take the $m_\uparrow > m_\downarrow$, thus for $p > 0$ ($p < 0$) the heavy (light) species is the majority. Stable FFLO phase lives in the narrow yellow region. The phase separation (PS) (against unstable FFLO and Sarma) is divided by the red $\mathbf{Q} = 0$ line and delimited by the green and blue lines. *Source*: reproduced from Ref. [32].

1.5.1 Fano-Feshbach Resonance

As discussed above, ultra-cold Fermi gases offer an incredible benchmark for the experimental realization of the BCS-BEC crossover, because they are easily accessible and the strength of the interaction between the fermions is controllable by means of an external uniform magnetic field through a *Fano-Feshbach resonance* [67]. We stress again that, what is here meant by "spin" is the quantum number associated with the atomic *hyperfine levels* that are split apart by the magnetic field itself. The two hyperfine levels of lowest energy can be populated independently and are conventionally referred to as spin $\uparrow$ and spin $\downarrow$. For example, for B sufficiently large, in ^{6}Li the states $|\uparrow\rangle$ and $|\downarrow\rangle$ correspond to $\left|m_I = 0, m_J = -\frac{1}{2}\right\rangle$ and $\left|m_I = 1, m_J = -\frac{1}{2}\right\rangle$, respectively, where $I = 1$ and $J = \frac{1}{2}$ are the nuclear and electron spin quantum numbers with projections m_I and m_J.

A Fano-Feshbach resonance can occur upon collision of two slow atoms when

they temporarily stick together forming an unstable compound with short lifetime (so-called resonance). Specifically, it is a condition where the zero-energy scattering state of the two hyperfine species (which together define the *open channel*) is degenerate with the most weakly bound molecular state of a second pair of hyperfine species (the *closed channel*). The ability to tune the scattering length by a change of an external magnetic field B relies on the difference in the magnetic moments of the closed and open channels. Because of the Zeeman effect, a variation of B changes the position of closed channel bound states relative to the open channel threshold.

The atom–atom interaction can be varied from a condition when the resonant bound state is in the continuum above threshold, to a condition when a true bound state exists below threshold (see Figure 1.8(a)). Correspondingly, as we will show in Section 3.1.2, the scattering length a_F changes from negative to positive values and diverges when the bound state sets in (see Figure 1.8(b)). On a phenomenological level, Feshbach resonances are described by an effective pseudo-potential between atoms in the open channel with scattering length

$$a(B) = a_{bg}\left(1 - \frac{\Delta B}{B - B_0}\right). \tag{1.31}$$

Here a_{bg} is the background scattering length in the absence of the coupling to the closed channel while ΔB and B_0 describe the width and position of the resonance expressed in magnetic field units.

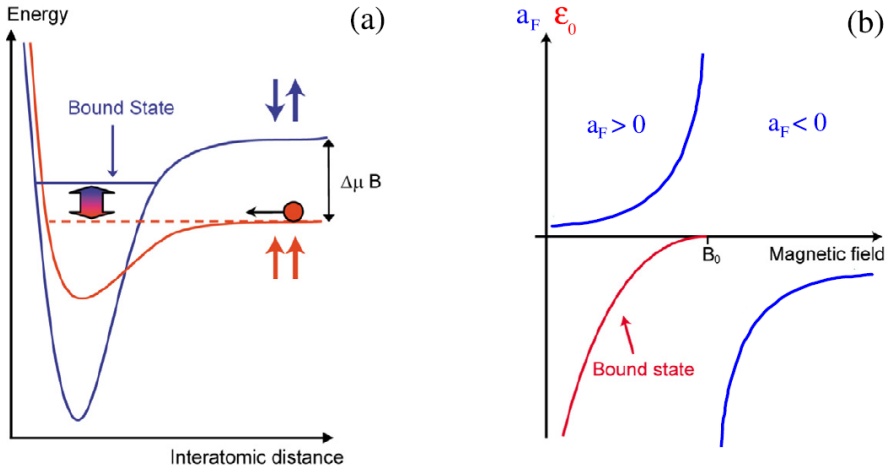

Figure 1.8: (**a**) Coupling between closed (blue) and open (red) scattering channels, which can be displaced relative to each other by varying the magnetic field B. (**b**) The corresponding scattering length as a function of B. When $a_F > 0$, a bound state with binding energy ε_0 sets in. *Source*: reproduced from Ref. [33].

In general one needs a two-channel model to describe such kind of resonance. However, essentially all crossover experiments are performed in the so-called "broad" Feshbach resonance limit where the width of the resonance is much larger than the Fermi energy. In this limit, an effective single-channel model is sufficient [68]. The broad Fano-Feshbach resonances are fundamental for using ultra-cold atoms to simulate the BCS–BEC crossover universally, i.e. independently on the details of the inter-atomic interaction.

While in principle the BCS limit corresponds to $(k_F a_F)^{-1} \ll -1$ and the BEC limit to $(k_F a_F)^{-1} \gg 1$, the evolution from the BCS to BEC limits is best studied in the limited range $-1 \lesssim (k_F a_F)^{-1} \lesssim 1$. This is because this limited range is sufficient in practice for realizing theoretically the BCS–BEC crossover in most physical quantities.

1.5.2 Tan's Contact

The *contact* C is a quantity that characterizes many-body systems with short-range interaction (like ultra-cold Fermi gases) and connects the strength of short-range two-body correlations to the thermodynamics. [69–71].

Physically, the contact C describes how the two-body problem locally merges into the surrounding many-body problem and can be defined by considering the short-distance behavior of the *pair correlation function* for opposite spin fermions

$$g_{\uparrow\downarrow}(\boldsymbol{\rho}) = \langle \psi_\uparrow^\dagger(\frac{\boldsymbol{\rho}}{2})\psi_\downarrow^\dagger(-\frac{\boldsymbol{\rho}}{2})\psi_\downarrow(-\frac{\boldsymbol{\rho}}{2})\psi_\uparrow(\frac{\boldsymbol{\rho}}{2})\rangle - n_\uparrow n_\downarrow, \tag{1.32}$$

that is given by

$$g_{\uparrow\downarrow}(\boldsymbol{\rho}) \xrightarrow{\rho\to 0} \frac{C}{(4\pi)^2}\left(\frac{1}{\rho^2} - \frac{2}{a_F\rho} + \dots\right), \tag{1.33}$$

where $\rho = |\boldsymbol{\rho}|$. In this sense, the contact C is related to the probability of finding two opposite spin fermions at short distances. Indeed, if we consider a small sphere of radius $\delta\rho$ centered on a particle, the probability for unit of volume to find a particle with opposite spin inside the sphere is given by

$$P(|\boldsymbol{\rho}| < \delta\rho)/V_{\delta\rho} = \int_{|\boldsymbol{\rho}|<\delta\rho} d\boldsymbol{\rho}\; g_{\uparrow\downarrow}(\boldsymbol{\rho}) \simeq \frac{C}{4\pi}\delta\rho, \tag{1.34}$$

where $V_{\delta\rho} = 4\pi(\delta\rho)^3/3$ is the volume of the sphere and we have assumed that $\delta\rho$ is much smaller than the scattering length a_F and all the other relevant lengths in the system. Note that, as the probability must be dimensionless, this relation defines the units of the contact as the inverse of a length to the fourth power.

Alternatively, the contact can be defined via the large wave-vector tail of the fermionic distributions $n_\sigma(k)$ with $k = |\mathbf{k}|$, which behaves asymptotically as

$$n_\sigma(k) \xrightarrow{k\to\infty} \frac{C}{k^4}. \tag{1.35}$$

The contact enters in several thermodynamics relations. For instance, with a zero-range inter-particle interaction, the internal energy density E/V and the pressure P can be expressed in terms of the contact as

$$\begin{aligned} \frac{E}{V} &= \frac{C}{4\pi a_F m} + \int \frac{d\mathbf{k}}{(2\pi)^3}\frac{k^2}{2m}\left(n_\sigma(k) - \frac{C}{k^4}\right), \\ P &= \frac{2}{3}\frac{E}{V} + \frac{C}{12\pi a_F m}, \end{aligned} \tag{1.36}$$

where V is the volume occupied by the system. One can also prove the following *adiabatic relations*, which relate the derivative of the energy (at constant entropy)

and of the free energy (at constant temperature) with respect to the scattering length to the contact, as

$$\begin{aligned}\left(\frac{\partial E}{\partial a_F^{-1}}\right)_S &= -\frac{CV}{4\pi m},\\ \left(\frac{\partial F}{\partial a_F^{-1}}\right)_T &= -\frac{CV}{4\pi m}.\end{aligned} \tag{1.37}$$

At the mean-field level and zero temperature, $n(k)$ is given by the factor $|v_{\mathbf{k}}|^2 = (1 - \xi_{\mathbf{k}}/E_{\mathbf{k}})/2$ that enters the BCS wave function (1.6). Expanding this factor for large k, one obtains

$$n(k) = |v_{\mathbf{k}}|^2 \simeq \frac{\Delta^2}{4\xi_{\mathbf{k}}^2} \simeq \frac{(m\Delta)^2}{k^4}, \tag{1.38}$$

which allows one to approximate the contact C with the quantity $(m\Delta)^2$. However, this value cannot properly represent the contact, in particular in the BCS limit at $T = 0$ where the gap Δ_0 is exponentially small in the coupling. Indeed, the leading coupling dependence of the free energy at $T = 0$ in weak-coupling is given by $\pi a_F n^2/m$, therefore C must reduce to the expression $(2\pi a_F n)^2$, as it can be readily obtained from the adiabatic relation above. This is another reason why we need the inclusion of pairing fluctuations to modify the mean-field results and recover the correct value of C, that will be obtained within the t-matrix approximation in Section 3.2.4.

Chapter 2

Finite Temperature Green's Functions Formalism

As discussed in the previous chapter, to describe consistently the whole BCS-BEC crossover at finite temperature, it is necessary to consider an approach that goes beyond the BCS mean-field approach and includes pair fluctuations. For this reason, in this chapter we introduce the finite temperature Green's function diagrammatic formalism, which is the fundamental theoretical basis for a quantum many-body approach. In this formalism, two different kinds of Green's functions are defined: the temperature Green's function $\mathcal{G}$, which has a simple perturbation expansion and enable us to evaluate the equilibrium thermodynamic properties; and the real-time Green's function G, which instead describes the excitation properties and the linear response of the system to an external perturbation. In the following sections, we will introduce the formalism for both of them and show that they are connected by an analytic continuation[1].

2.1 Temperature Green's Function

Let us consider a Hamiltonian $\hat{H}$ that describes a system of N particles at thermal equilibrium at the temperature T. As in the previous sections, it is useful to describe the system in the grand-canonical ensemble and use the grand-canonical Hamiltonian $\hat{K} = \hat{H} - \mu\hat{N}$. We can then introduce the following modified K-Heisenberg picture for the field operators $\hat{\psi}_\sigma$

$$\begin{aligned} \hat{\psi}_\sigma(\mathbf{x},\tau) &= e^{\hat{K}\tau}\hat{\psi}_\sigma(\mathbf{x})e^{-\hat{K}\tau}, \\ \hat{\psi}^\dagger_\sigma(\mathbf{x},\tau) &= e^{\hat{K}\tau}\hat{\psi}^\dagger_\sigma(\mathbf{x})e^{-\hat{K}\tau}, \end{aligned} \tag{2.1}$$

where τ is the imaginary time (or *euclidean time*) and σ is the spin index. The *single-particle temperature Green's function* (or *single-particle propagator*) is defined

[1] We just notice that this separation into two different Green's functions is not required in the ground-state (zero-temperature) formalism. However, within the finite temperature formalism, the perturbative analysis arises more naturally without requiring any assumption, like the *adiabatic "switching on"* [72].

in terms of these field operators as

$$\mathcal{G}_{\sigma\sigma'}(\mathbf{x},\tau,\mathbf{x}',\tau') = -\langle T_\tau[\hat{\psi}_\sigma(\mathbf{x},\tau)\hat{\psi}^\dagger_{\sigma'}(\mathbf{x}',\tau')]\rangle, \tag{2.2}$$

where T_τ is the *time-ordering operator*, which brings the field operators evaluated at later time on the left (including a factor $(-1)^P$, where P is the number of permutations of fermion operators), and the symbol $\langle\cdots\rangle$ represents the thermal average of an operator

$$\langle\hat{\mathcal{O}}\rangle = \mathrm{Tr}[\hat{\rho}_G\hat{\mathcal{O}}] = \sum_n \langle\varphi_n|\,\hat{\rho}_G\hat{\mathcal{O}}\,|\varphi_n\rangle\,. \tag{2.3}$$

This trace is the sum of the expectation values over the states $|\varphi_n\rangle$, which form a complete basis for the Hilbert space of the system. The operator $\hat{\rho}_G$ is the *grand-canonical density matrix*, defined as

$$\hat{\rho}_G = \frac{1}{\mathcal{Z}}e^{-\beta\hat{K}} = e^{\beta(\Omega-\hat{K})}, \tag{2.4}$$

where Ω is the *grand-potential* (or grand-canonical free energy) and $\mathcal{Z}$ is the *grand-canonical partition function*

$$\mathcal{Z} = e^{-\beta\Omega} = \mathrm{Tr}[e^{-\beta\hat{K}}]. \tag{2.5}$$

If the Hamiltonian is time-independent and the system is homogeneous, i.e. we assume space-time translational invariance, the temperature Green's function (2.2) depends only on $\mathbf{x}-\mathbf{x}'$ and $\tau-\tau'$. We can therefore introduce its *Fourier transform* to momentum space

$$\mathcal{G}_{\sigma\sigma'}(\mathbf{k},\tau) = \int d\mathbf{x}\; e^{-i\mathbf{k}\cdot\mathbf{x}}\;\mathcal{G}_{\sigma\sigma'}(\mathbf{x},\tau), \tag{2.6}$$

and the corresponding anti-Fourier transform

$$\mathcal{G}_{\sigma\sigma'}(\mathbf{x},\tau) = \int \frac{d\mathbf{k}}{(2\pi)^3}\; e^{i\mathbf{k}\cdot\mathbf{x}}\;\mathcal{G}_{\sigma\sigma'}(\mathbf{k},\tau). \tag{2.7}$$

Furthermore, the temperature Green's function for bosons (fermions) is *periodic* (*anti-periodic*) in the τ variable with period $\beta = 1/T$

$$\mathcal{G}_{\sigma\sigma'}(\mathbf{k},\tau+\beta) = \pm\mathcal{G}_{\sigma\sigma'}(\mathbf{k},\tau), \tag{2.8}$$

where the upper (lower) sign refers to bosons (fermions). Without loss of generality, the imaginary time τ can then be taken only in the interval $(0,\beta)$. Using these periodicity properties, the bosonic and fermionic Green's functions can be expanded in *Fourier series* as

$$\mathcal{G}_{\sigma\sigma'}(\mathbf{k},\tau) = \frac{1}{\beta}\sum_n e^{-i\omega_n\tau}\;\mathcal{G}_{\sigma\sigma'}(\mathbf{k},\omega_n), \tag{2.9}$$

where ω_n are the *Matsubara frequencies* defined as

$$\begin{aligned}\omega_n &= \frac{\pi}{\beta}(2n+1) \quad \text{for fermions,}\\ \omega_n &= \frac{\pi}{\beta}2n \quad \text{for bosons,}\end{aligned} \tag{2.10}$$

with n integer. The Fourier coefficients in the series (2.9) are given by

$$\mathcal{G}_{\sigma\sigma'}(\mathbf{k},\omega_n) = \int_0^\beta d\tau\; e^{i\omega_n\tau}\;\mathcal{G}_{\sigma\sigma'}(\mathbf{k},\tau). \tag{2.11}$$

2.1.1 Relation to Observables

The single-particle temperature Green's function (2.2) includes information on the thermal average of all the single-particle observables of the system. Let us consider a single-particle operator, which can in general be written in the form

$$\hat{J} = \int d\mathbf{x}\, \hat{\mathcal{J}}(\mathbf{x}) = \int d\mathbf{x} \sum_{\sigma\sigma'} \hat{\psi}^\dagger_{\sigma'}(\mathbf{x}) J_{\sigma'\sigma}(\mathbf{x}) \hat{\psi}_\sigma(\mathbf{x}), \tag{2.12}$$

where $\hat{\mathcal{J}}(\mathbf{x})$ is the second-quantized density of the first-quantized operator $J_{\sigma'\sigma}(\mathbf{x})$. Therefore, its thermal average can be written as

$$\langle \hat{J} \rangle = \mp \int d\mathbf{x} \lim_{\mathbf{x}'\to\mathbf{x}} \lim_{\tau'\to\tau^+} \sum_{\sigma\sigma'} J_{\sigma'\sigma}(\mathbf{x}) \mathcal{G}_{\sigma\sigma'}(\mathbf{x},\tau,\mathbf{x}',\tau'), \tag{2.13}$$

where $\tau^+ = \tau + 0^+$. The expression (2.13) is readily obtained using the cyclic property of the trace, together with the definitions of field operators in the K-Heisenberg picture (2.1), of the temperature Green's function (2.2) and of thermal average (2.3). This means that the thermal average of any single-particle operator $\hat{J}$ can be obtained by operating with its first-quantized version $J_{\sigma'\sigma}(\mathbf{x})$ on the Green's function and then summing over the spin indices and integrating on $\mathbf{x}$. For example, we can consider the *number operator*

$$\hat{N} = \int d\mathbf{x}\, \hat{n}(\mathbf{x}) = \int d\mathbf{x} \sum_{\sigma} \hat{\psi}^\dagger_{\sigma}(\mathbf{x}) \hat{\psi}_\sigma(\mathbf{x}), \tag{2.14}$$

where the first-quantized operator is simply the identity matrix $J_{\sigma'\sigma} = \delta_{\sigma'\sigma}$. The thermal average of the number of particles is then given by

$$N \equiv \langle \hat{N} \rangle = \mp \int d\mathbf{x} \lim_{\tau'\to\tau^+} \sum_{\sigma} \mathcal{G}_{\sigma\sigma}(\mathbf{x},\tau,\mathbf{x},\tau'). \tag{2.15}$$

For a homogeneous system in a volume V, it is useful to use the Fourier transformations (2.7) and (2.9) and write the previous number equation in transformed space

$$n = \mp \int \frac{d\mathbf{k}}{(2\pi)^3} \frac{1}{\beta} \sum_n e^{i\omega_n 0^+} \sum_\sigma \mathcal{G}_{\sigma\sigma}(\mathbf{k},\omega_n), \tag{2.16}$$

where $n = N/V$ is the total density of the system and $e^{i\omega_n 0^+}$ is a convergence factor that comes from the imaginary-time ordering.

Similarly to the particle number N, the *mean kinetic energy* can be obtained as

$$\langle \hat{T} \rangle = \mp \int d\mathbf{x} \lim_{\mathbf{x}'\to\mathbf{x}} \lim_{\tau'\to\tau^+} \sum_\sigma \left[-\frac{\nabla^2_{\mathbf{x}}}{2m} \right] \mathcal{G}_{\sigma\sigma}(\mathbf{x},\tau,\mathbf{x}',\tau'). \tag{2.17}$$

An interesting question now arises: is it possible to construct the mean potential energy from the two-body operator

$$\hat{V} = \frac{1}{2} \sum_{\sigma,\sigma'} \int d\mathbf{x} \int d\mathbf{x}'\, V(\mathbf{x}-\mathbf{x}') \hat{\psi}^\dagger_\sigma(\mathbf{x}) \hat{\psi}^\dagger_{\sigma'}(\mathbf{x}') \hat{\psi}_{\sigma'}(\mathbf{x}') \hat{\psi}_\sigma(\mathbf{x}), \tag{2.18}$$

and thereby determine the total *internal energy* $E \equiv \langle \hat{T}+\hat{V}\rangle$? Since $\hat{V}$ involves four field operators, we might expect to need the two-particle Green's function. However, thanks to the *Heisenberg equation of motion*

$$\frac{\partial}{\partial\tau}\hat{\psi}_\sigma(\mathbf{x},\tau) = [\hat{K}, \hat{\psi}_\sigma(\mathbf{x},\tau)], \tag{2.19}$$

we can express $\langle\hat{V}\rangle$ solely in terms of the single-particle Green's function as

$$\langle\hat{V}\rangle = \mp\frac{1}{2}\int d\mathbf{x} \lim_{\mathbf{x}'\to\mathbf{x}}\lim_{\tau'\to\tau^+}\sum_\sigma\left[-\frac{\partial}{\partial\tau}+\frac{\nabla^2_{\mathbf{x}}}{2m}+\mu\right]\mathcal{G}_{\sigma\sigma}(\mathbf{x},\tau,\mathbf{x}',\tau'), \tag{2.20}$$

and this allows to get the internal energy

$$E = \mp\frac{1}{2}\int d\mathbf{x} \lim_{\mathbf{x}'\to\mathbf{x}}\lim_{\tau'\to\tau^+}\sum_\sigma\left[-\frac{\partial}{\partial\tau}-\frac{\nabla^2_{\mathbf{x}}}{2m}+\mu\right]\mathcal{G}_{\sigma\sigma}(\mathbf{x},\tau,\mathbf{x}',\tau'). \tag{2.21}$$

The mean interaction potential (2.20) can also be used to obtain the grand-potential Ω (or equivalently the grand-canonical partition function $\mathcal{Z}$), by means of an integration over a variable coupling constant, known as *link clustered expansion* [72]. This calculation consists in replacing the two-body interaction $\hat{V}$ with $\lambda\hat{V}$, where $\lambda\in[0,1]$ is a numerical coupling constant, and evaluate

$$\Omega[\mathcal{G}]-\Omega_0 \equiv -\frac{1}{\beta}[\ln(\mathcal{Z}[\mathcal{G}])-\ln(\mathcal{Z}_0)] = \int_0^1\frac{d\lambda}{\lambda}\langle\lambda\hat{V}\rangle, \tag{2.22}$$

where Ω_0 is the grand-potential for the non-interacting system and $\langle\lambda\hat{V}\rangle$ can be calculated using (2.20), in terms of the single-particle Green's function $\mathcal{G}^\lambda_{\sigma\sigma'}$ for a system with grand-canonical Hamiltonian $\hat{K}(\lambda)=\hat{K}_0+\lambda\hat{V}$.

2.1.2 Non-interacting System

As a simple example, it is very useful to compute the temperature Green's function $\mathcal{G}^0_{\sigma\sigma'}(\mathbf{x},\tau,\mathbf{x}',\tau')$ for a non-interacting system. Since we are interested in the properties of the bulk medium, we assume *periodic boundary conditions* (PBC) in a box of volume V, with the *thermodynamic limit* to be performed at the end of the calculations. In this way the single-particle states are plane waves, i.e. $\varphi_{\mathbf{k}}(\mathbf{x}) = V^{-1/2}e^{i\mathbf{k}\cdot\mathbf{x}}$, and we can therefore expand the field operators in terms of the time-dependent creation and annihilation operators as

$$\begin{aligned}\hat{\psi}_\sigma(\mathbf{x},\tau) &= \frac{1}{\sqrt{V}}\sum_{\mathbf{k}} e^{i\mathbf{k}\cdot\mathbf{x}}\, a_{\mathbf{k}\sigma}e^{-\xi_{\mathbf{k}}\tau},\\ \hat{\psi}^\dagger_\sigma(\mathbf{x},\tau) &= \frac{1}{\sqrt{V}}\sum_{\mathbf{k}} e^{-i\mathbf{k}\cdot\mathbf{x}}\, a^\dagger_{\mathbf{k}\sigma}e^{\xi_{\mathbf{k}}\tau},\end{aligned} \tag{2.23}$$

with $\xi_{\mathbf{k}} = \mathbf{k}^2/(2m)-\mu$. Using the definition (2.2), we can easily get

$$\mathcal{G}^0_{\sigma\sigma'}(\mathbf{x},\tau) = -\frac{\delta_{\sigma\sigma'}}{V}\sum_{\mathbf{k}} e^{i\mathbf{k}\cdot\mathbf{x}}e^{-\xi_{\mathbf{k}}\tau}\left[\theta(\tau)\langle a_{\mathbf{k}\sigma}a^\dagger_{\mathbf{k}\sigma}\rangle_0 \pm \theta(-\tau)\langle a^\dagger_{\mathbf{k}\sigma}a_{\mathbf{k}\sigma}\rangle_0\right], \tag{2.24}$$

where the thermal average $\langle a_{\mathbf{k}\sigma} a^\dagger_{\mathbf{k}\sigma}\rangle_0 = 1 \pm \langle a^\dagger_{\mathbf{k}\sigma} a_{\mathbf{k}\sigma}\rangle_0$ for a non-interacting system is well known from statistical mechanics, since it corresponds to a Bose (Fermi) function for bosons (fermions)

$$\langle a^\dagger_{\mathbf{k}\sigma} a_{\mathbf{k}\sigma}\rangle_0 = \frac{1}{e^{\beta\xi_{\mathbf{k}}} \mp 1}. \tag{2.25}$$

As expected, $\mathcal{G}^0$ is diagonal in the matrix indices. It is also interesting to evaluate the mean number of particles N^0 and the mean internal energy E^0 with (2.15) and (2.21), respectively. A straightforward calculation recovers the well known results

$$\begin{aligned} N^0 &= (2s+1)\sum_{\mathbf{k}} \frac{1}{e^{\beta\xi_{\mathbf{k}}} \mp 1}, \\ E^0 &= (2s+1)\sum_{\mathbf{k}} \frac{\mathbf{k}^2/(2m)}{e^{\beta\xi_{\mathbf{k}}} \mp 1}, \end{aligned} \tag{2.26}$$

where s is the spin of the particles.

In the thermodynamic limit, we perform the substitution $V^{-1}\sum_{\mathbf{k}} \to (2\pi)^{-3}\int d\mathbf{k}$ to get an expression for $\mathcal{G}^0_{\sigma\sigma'}(\mathbf{k},\tau)$ from (2.6). We can therefore perform the integral over τ, as suggested by (2.11), to get the non-interacting Green's function in the transformed space, which assume the simpler form

$$\mathcal{G}^0_{\sigma\sigma'}(\mathbf{k},\omega_n) = \frac{\delta_{\sigma\sigma'}}{i\omega_n - \xi_{\mathbf{k}}}. \tag{2.27}$$

To get the density equation (2.16) for the non-interacting system, we need to evaluate the sum over the Matsubara frequencies, which can be carried out analytically with a contour integration [72] leading to

$$\sum_n \frac{e^{i\omega_n 0^+}}{i\omega_n - x} = \mp\frac{\beta}{e^{\beta x} \mp 1}. \tag{2.28}$$

Compatibly with the first expression in (2.26), the result simply reduce to the $\mathbf{k}$-integral of the Bose (Fermi) distribution

$$n^0 = (2s+1)\int \frac{d\mathbf{k}}{(2\pi)^3}\ \frac{1}{e^{\beta\xi_{\mathbf{k}}} \mp 1}. \tag{2.29}$$

2.2 Perturbation Theory and Feynman Rules

In addition to the relation with the thermodynamic quantities, another important reason to introduce the temperature Green's function is that $\mathcal{G}$, commonly referred to as *dressed* Green's function, has a simple perturbative expansion in terms of the *bare* (i.e. non-interacting) one $\mathcal{G}^0$. For simplicity we consider a homogeneous system of fermions, in order to work in the momentum-frequency space, and we assume the common situation in which the Hamiltonian can be written as the sum of a one-body term and a two-body term, i.e. $\hat{K} = \hat{K}_0 + \hat{V}$. Therefore, we are going to work with the Fourier transform of the potential $V(\mathbf{x}-\mathbf{x}')$ given by

$$V(\mathbf{k}) = \int d\mathbf{x}\ e^{-i\mathbf{k}\cdot\mathbf{x}}\, V(\mathbf{x}). \tag{2.30}$$

Without going into details of the derivation, which would require the introduction of the *interaction picture* and a generalized version of the *Wick theorem* at finite temperature [72], we now enunciate the *Feynman rules* for the n-th order contribution to the dressed temperature Green's function $\mathcal{G}_{\sigma\sigma'}(\mathbf{k}, \omega_n)$

1. Draw all topologically distinct *connected* graphs with n interaction lines and $2n + 1$ directed particle lines
2. Assign a direction to each interaction line. Associate a wave vector and a Matsubara frequency with each line and impose *frequency-momentum conservation* at every vertex.
3. Associate a factor $\mathcal{G}^0_{\sigma\sigma'}(\mathbf{k}, \omega_n)$ (as defined in (2.27)) with each particle line.
4. Associate a factor $V(\mathbf{k})$ (as defined in (2.30)) with each interaction line.
5. Integrate over all n independent internal wave vectors and sum over all n independent internal Matsubara frequencies.
6. The spin indices form a matrix product along any continuous particle line. Evaluate all matrix sums.
7. Multiply everything by a factor $[-\beta(2\pi)^3]^{-n}(-1)^F$, where F is the number of closed fermionic loops.
8. Whenever a particle line either closes on itself or is joined by the same interaction line, insert a convergence factor $e^{i\omega_n 0^+}$.

For instance, once we summed over the spin indices, the zero and first-order diagrams, represented in Figure 2.1, are given by

$$\begin{aligned}\mathcal{G}(\mathbf{k}, \omega_n) &= \mathcal{G}^0(\mathbf{k}, \omega_n) \\ &- \mathcal{G}^0(\mathbf{k}, \omega_n)^2 \frac{1}{\beta} \sum_m e^{i\omega_m 0^+} \int \frac{d\mathbf{p}}{(2\pi)^3} [-(2s+1)V(0) + V(\mathbf{p}-\mathbf{k})] \mathcal{G}^0(\mathbf{p}, \omega_m),\end{aligned} \tag{2.31}$$

where we have assumed that we can write $\mathcal{G}_{\sigma\sigma'}(\mathbf{k}, \omega_n) = \delta_{\sigma\sigma'}\mathcal{G}(\mathbf{k}, \omega_n)$ because of the spin-independent interaction, while the factor $(2s+1)$ comes from the sum over the spin indices. The first-order contribution to the dressed Green's function consists of two diagrams, which are known as *Hartree-Fock diagrams*.

2.2.1 Self-Energy and Dyson Equation

It is possible to classify the various contribution in a generic Feynman diagram. This procedure yields the *Dyson equation*, which summarizes the perturbation theory in a particularly compact form. We start with the *self-energy insertion* $\Sigma'_{\sigma\sigma'}(\mathbf{k}, \omega_n)$, defined as any part of a diagram that is connected to the rest of it by two particle lines (one in and one out), and so

$$\mathcal{G}_{\sigma\sigma'}(\mathbf{k}, \omega_n) = \mathcal{G}^0_{\sigma\sigma'}(\mathbf{k}, \omega_n) + \sum_{\lambda\lambda'} \mathcal{G}^0_{\sigma\lambda}(\mathbf{k}, \omega_n) \Sigma'_{\lambda\lambda'}(\mathbf{k}, \omega_n) \mathcal{G}^0_{\lambda'\sigma'}(\mathbf{k}, \omega_n). \tag{2.32}$$

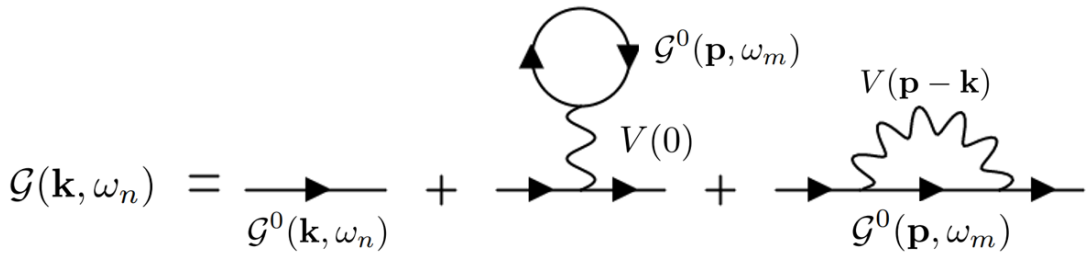

Figure 2.1: Zero and first-order diagrammatic contributions to the dressed temperature Green's function: the zero order is just the bare green function (left), while the first order is made by the Hartree (middle) and Fock (right) diagrams.

We next introduce the *proper self-energy insertion* $\Sigma_{\sigma\sigma'}(\mathbf{k},\omega_n)$, which is a self-energy insertion that cannot be separated into two pieces by cutting a single particle line, i.e. contains information on the so-called *one-particle irreducible* (1PI) diagrams. It follows from these definitions that the self-energy can be written as a sum of all possible repetitions of the proper self-energy

$$\Sigma'_{\sigma\sigma'}(\mathbf{k},\omega_n) = \Sigma_{\sigma\sigma'}(\mathbf{k},\omega_n) + \sum_{\lambda\lambda'} \Sigma_{\sigma\lambda}(\mathbf{k},\omega_n)\mathcal{G}^0_{\lambda\lambda'}(\mathbf{k},\omega_n)\Sigma_{\lambda'\sigma'}(\mathbf{k},\omega_n) + \dots \tag{2.33}$$

Correspondingly, the Green's function in (2.32) can be summed formally, after replacing the expression (2.33) for the self-energy, to yield an algebraic self-consistent equation known as *Dyson equation*

$$\mathcal{G}_{\sigma\sigma'}(\mathbf{k},\omega_n) = \mathcal{G}^0_{\sigma\sigma'}(\mathbf{k},\omega_n) + \sum_{\lambda\lambda'} \mathcal{G}^0_{\sigma\lambda}(\mathbf{k},\omega_n)\Sigma_{\lambda\lambda'}(\mathbf{k},\omega_n)\mathcal{G}_{\lambda'\sigma'}(\mathbf{k},\omega_n), \tag{2.34}$$

which connects the (proper) self-energy, the dressed and the bare temperature Green's function. We just notice that the algebraic form of the equation in the frequency-momentum space is replaced by an integral form in coordinates space, which is obviously much more complicated.

In the usual case, these quantities are all diagonal in the spin indices, and the Dyson equation (2.34) can be solved explicitly as

$$\mathcal{G}(\mathbf{k},\omega_n) = \frac{1}{\mathcal{G}^0(\mathbf{k},\omega_n)^{-1} - \Sigma(\mathbf{k},\omega_n)} = \frac{1}{i\omega_n - \xi_{\mathbf{k}} - \Sigma(\omega_n,\mathbf{k})}. \tag{2.35}$$

2.3 Real-time Green's Function

We have seen that the temperature Green's function can be used to calculate the thermodynamic properties of our system and has a simple perturbative expansion. However, it is not convenient to work with imaginary time to get dynamical quantities, since these are in general obtained from real-time responses to external perturbations. For this reason, we complete the description by introducing the

single-particle real-time Green's function

$$G_{\sigma\sigma'}(\mathbf{x},t,\mathbf{x}',t') = -i\langle T_t[\hat{\psi}_\sigma(\mathbf{x},t)\hat{\psi}^\dagger_{\sigma'}(\mathbf{x}',t')]\rangle, \tag{2.36}$$

where now t is a real time, T_t is the time ordering operator for real times and $\hat{\psi}_\sigma$ is a true K-Heisenberg field operator

$$\hat{\psi}_\sigma(\mathbf{x},t) = e^{i\hat{K}t}\hat{\psi}_\sigma(\mathbf{x})e^{-i\hat{K}t}. \tag{2.37}$$

If we consider a homogeneous system with a time-independent Hamiltonian, the Green's function (2.36) can be Fourier transformed to the frequency-momentum space to get

$$G_{\sigma\sigma'}(\mathbf{k},\omega) = \int d\mathbf{x}\; e^{-i\mathbf{k}\cdot\mathbf{x}} \int dt\; e^{i\omega t}\; G_{\sigma\sigma'}(\mathbf{x},t). \tag{2.38}$$

The real-time Green's function contains information on the excitations of the system related to the addition or the removal of a particle. To show this, consider a system of fermions and assume for simplicity that the Green's function is diagonal in the spin indices, i.e. $G_{\sigma\sigma'} = \delta_{\sigma\sigma'}G$ (this is always true for a balanced Fermi gas in the normal phase). One can therefore express $G(\mathbf{k},\omega)$ in the *Lehmann representation*

$$\begin{aligned} G(\mathbf{k},\omega) =& e^{\beta\Omega}\sum_{mn}(2\pi)^3\delta(\mathbf{k}-(\mathbf{P}_n-\mathbf{P}_m))e^{-i\mathbf{k}\cdot\mathbf{x}}|\,\langle m|\,\hat{\psi}_\sigma(0)\,|n\rangle\,|^2 \\ &\times\Big[\frac{e^{-\beta K_m}}{\omega-(K_n-K_m)+i0^+}+\frac{e^{-\beta K_n}}{\omega-(K_n-K_m)-i0^+}\Big], \end{aligned} \tag{2.39}$$

where $|n\rangle$, $|m\rangle$ are exact eigenstates of $\hat{H}$, $\hat{\mathbf{P}}$ and $\hat{N}$ and can refer to excited states. This shows that $G(\mathbf{k},\omega)$ is a meromorphic function of ω with simple poles at $K_n - K_m = E_n - E_m - \mu(N_n - N_m)$ and the corresponding residue vanishes unless $N_n = N_m + 1$, being proportional to $|\,\langle m|\,\hat{\psi}\,|n\rangle\,|^2$.

The Lehmann representation (2.39) is also used to show that, in general, the real-time Green's function has the following *spectral representation*

$$G(\mathbf{k},\omega) = \int_{-\infty}^{\infty} d\omega'\; A(\mathbf{k},\omega')\left[\frac{1-f(\omega)}{\omega-\omega'+i0^+}+\frac{f(\omega)}{\omega-\omega'-i0^+}\right], \tag{2.40}$$

where $f(\omega) = [e^{\beta\omega}+1]^{-1}$ is the Fermi function and $A(\mathbf{k},\omega)$ is the *single-particle spectral weight function*, which contains the important physical properties of the system. Specifically, it can be thought as the probability density to excite eigenstates with energy ω and momentum $\mathbf{k}$ (with respect to the ground state) by adding or subtracting a particle with momentum $\mathbf{k}$ to the equilibrium system at given temperature T. Indeed, it is semi-positive defined

$$A(\mathbf{k},\omega) \geq 0 \qquad \forall\,\mathbf{k},\omega, \tag{2.41}$$

and it satisfies the *sum rule*

$$\int_{-\infty}^{\infty} d\omega\; A(\mathbf{k},\omega) = 1. \tag{2.42}$$

For many purposes, it is more convenient to deal with the *retarded* or *advanced* real-time Green's Function

$$G^R_{\sigma\sigma'}(\mathbf{x},t,\mathbf{x}',t') = -i\theta(t-t')\langle\{\hat{\psi}_\sigma(\mathbf{x},t),\hat{\psi}^\dagger_{\sigma'}(\mathbf{x}',t')\}\rangle, \tag{2.43}$$

$$G^A_{\sigma\sigma'}(\mathbf{x},t,\mathbf{x}',t') = i\theta(t'-t)\langle\{\hat{\psi}_\sigma(\mathbf{x},t),\hat{\psi}^\dagger_{\sigma'}(\mathbf{x}',t')\}\rangle, \tag{2.44}$$

where $\{\cdot,\cdot\}$ is the anti-commutator. Also the retarded (advanced) Green's function admits a spectral representation

$$G^R_A(\mathbf{k},\omega) = \int_{-\infty}^{\infty} d\omega' \, \frac{A(\mathbf{k},\omega')}{\omega - \omega' \pm i0^+}, \tag{2.45}$$

which shows that G^R (G^A) is *analytic* in the upper (lower) half of the complex plane ω and, using (2.40), we get

$$G(\mathbf{k},\omega) = (1-f(\omega))G^R(\mathbf{k},\omega) + f(\omega)G^A(\mathbf{k},\omega). \tag{2.46}$$

In particular, the sum rule (2.42) allows one to evaluate the large-frequency behaviour of the Green's function as

$$G(\mathbf{k},\omega) = G^R(\mathbf{k},\omega) = G^A(\mathbf{k},\omega) \sim \frac{1}{\omega} \qquad |\omega| \to \infty, \tag{2.47}$$

which remains correct for an arbitrary interacting system, since in this limit the kinetic energy of the single-particle excitation dominates any interaction effects. Moreover, the spectral weight function A can be obtained by inverting the relation (2.45), obtaining

$$A(\mathbf{k},\omega) = \mp\frac{1}{\pi}\,\mathrm{Im}\, G^R_A(\mathbf{k},\omega). \tag{2.48}$$

In general, knowledge of $A(\mathbf{k},\omega)$ allows one to physically characterize the dynamic properties of the system. From it, one can also obtain the *density of states* by integrating over all momenta $\mathbf{k}$

$$N(\omega) = \frac{dn(\omega)}{d\omega} = \int \frac{d\mathbf{k}}{(2\pi)^3} A(\mathbf{k},\omega), \tag{2.49}$$

such that $N(\omega)d\omega$ corresponds to the number of available states with energies between ω and $\omega + d\omega$.

2.3.1 Analytic Continuation

As discussed above, the real-time Green's function G in (2.36) contains some relevant information, however most of the finite temperature calculations are performed just in terms of the temperature Green's function $\mathcal{G}$ in (2.2). Fortunately, there is a connection between them: using the Lehmann representation (2.39), one can prove that the same spectral weight function $A(\mathbf{k},\omega)$ introduced previously determines also the temperature Green's function [72]

$$\mathcal{G}(\mathbf{k},\omega_n) = \int_{-\infty}^{\infty} d\omega' \, \frac{A(\mathbf{k},\omega')}{i\omega_n - \omega'}. \tag{2.50}$$

If we now define the following function of complex variable z

$$\tilde{G}(\mathbf{k}, z) = \int_{-\infty}^{\infty} d\omega' \, \frac{A(\mathbf{k}, \omega')}{z - \omega'}, \tag{2.51}$$

we see that the temperature Green's function corresponds to the value of $\tilde{G}$ at discrete points on the imaginary axis, $\mathcal{G}(\mathbf{k}, \omega_n) = \tilde{G}(\mathbf{k}, i\omega_n)$. We therefore perform an *analytic continuation* to retrieve $\tilde{G}(\mathbf{k}, z)$ on the whole complex plane and we evaluate it just above the real axis at $z = \omega + i0^+$ to obtain the retarded Green's function, $G^R(\mathbf{k}, \omega) = \tilde{G}(\mathbf{k}, \omega + i0^+)$ (or just below the real axis at $z = \omega - i0^+$ to get the advanced Green's function). At the end, the spectral weight function is just obtained using the relation in (2.48).

Without further information, the analytic continuation is not unique: both $\tilde{G}(\mathbf{k}, z)$ and $e^{2\pi l z/\omega_n}\tilde{G}(\mathbf{k}, z)$ (for any integer l) are possible continuations, because they both reduce to $\mathcal{G}(\mathbf{k}, \omega_n)$ at the points $i\omega_n$. Fortunately, since the sum rule (2.42) requires that $\tilde{G}(\mathbf{k}, z) \sim z^{-1}$ as $|z| \to \infty$, we are thus able to choose the proper analytic continuation, which is now guaranteed to be unique.

It is usually simplest to compute the spectral function directly from the temperature Green's function by formally considering $i\omega_n$ as a continuous variable, and therefore performing the substitution $i\omega_n \to \omega + i0^+$. However, one has to be careful because this procedure is correct only if the substitution is made after the analytical evaluation of the sums over Matsubara frequencies.

As an example, consider the *bubble diagram* Π^0 for the *polarization insertion*, diagrammatically represented in Figure 2.2 and defined using the Feynman rules as

$$\Pi^0(\mathbf{q}, \nu_n) = \frac{2}{\beta} \int \frac{d^3p}{(2\pi)^3} \sum_{\omega_1} \left[\frac{1}{i\omega_1 - \xi_{\mathbf{p}}} \frac{1}{i(\omega_1 + \nu_n) - \xi_{\mathbf{p}+\mathbf{q}}} \right]. \tag{2.52}$$

The sum over the Matsubara frequencies ω_1 can be evaluated using a partial fraction decomposition and the result in (2.28), leading to

$$\Pi^0(\mathbf{q}, \nu_n) = -2 \int \frac{d^3p}{(2\pi)^3} \frac{f(\xi_{\mathbf{q}+\mathbf{p}}) - f(\xi_{\mathbf{p}})}{i\nu_n - (\xi_{\mathbf{p}+\mathbf{q}} - \xi_{\mathbf{p}})}, \tag{2.53}$$

where we used $e^{-i\beta\nu_n} = 1$ for bosonic frequencies. Now we can substitute $i\nu_n \to \omega + i0^+$, obtaining a correct result for $\Pi^0(\mathbf{q}, \omega)$. On the contrary, if we make the previous substitution before the evaluation of the frequency sum, we get a different and incorrect result

$$\Pi^0(\mathbf{q}, \omega) = -2 \int \frac{d^3p}{(2\pi)^3} \frac{f(\xi_{\mathbf{p}+\mathbf{q}} - \omega) - f(\xi_{\mathbf{p}})}{\omega - (\xi_{\mathbf{p}+\mathbf{q}} - \xi_{\mathbf{p}}) + i0^+}. \tag{2.54}$$

In practical cases, one knows the temperature Green's function only at a finite number N of Matsubara frequencies. The problem of obtaining a unique spectral weight function A from this set of N data is well known to be *ill-posed*. For this reason, we need to constraint the Green's function using numerical methods, and therefore performing an approximate analytic continuation.

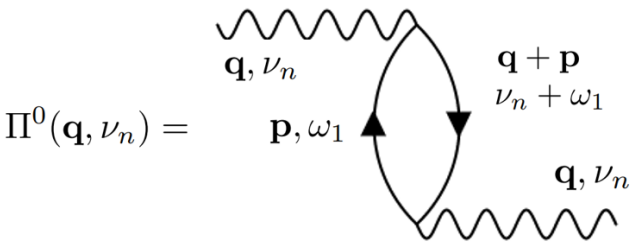

Figure 2.2: Diagrammatic representation of the one-bubble diagram contained in the polarization insertion. The internal momentum-frequency couple is $(\mathbf{p}, \omega_1)$.

Chapter 3

Ladder Diagrams and t-Matrix Approximation

Practically, it is impossible to evaluate the temperature Green's function to all orders in perturbation theory, so we have to perform an approximation and select certain classes of diagrams that are relevant to our physical system. In this chapter, we show that the set of diagrams selected to study the normal phase of an ultra-cold Fermi gas throughout the BCS-BEC crossovers are the so-called ladder diagrams and the corresponding method is known as t-matrix approximation. The justification to this many-body approach is found in the two-body scattering theory which, in the context of ultra-cold Fermi gases, can be simplified with the s-wave approximation. Furthermore, this non-self-consistent t-matrix approach can be improved with the inclusion of different degrees of self-consistency: we will focus on the fully self-consistent method, also known as Luttinger-Ward approach[1].

3.1 Two-body Scattering Theory

To understand which class of diagrams are important for our many-body system, it is first crucial to know the two-body physics [74]. Let us start from the scattering problem of two particles with masses $m_\uparrow$ and $m_\downarrow$, interacting via a potential $V(\mathbf{r})$ that depends only on the relative position $\mathbf{r} = \mathbf{r}_1 - \mathbf{r}_2$. It is not difficult to show that the corresponding Schrödinger equation separates into a part describing the center-of-mass motion and a part describing the relative motion. The center-of-mass part behaves as a free particle with mass $m_B = m_\uparrow + m_\downarrow$, whereas the relative part behaves as a single particle with *reduced mass* $m_{red} = m_\uparrow m_\downarrow/(m_\uparrow + m_\downarrow)$. The relative wave function is then the solution of the time-independent Schrödinger equation

$$\left(-\frac{\nabla^2}{2m_{red}} + V(\mathbf{r}) \right)\psi(\mathbf{r}) \equiv \big(\hat{H}_0 + V(\mathbf{r})\big)\psi(\mathbf{r}) = E\psi(\mathbf{r}), \tag{3.1}$$

[1]It is important to notice that the many-body formalism presented in this chapter refers to the normal phase of the Fermi gas up to the critical temperature of the superfluid transition. To study the superfluid phase, the formalism must be extended to take into account the so-called *anomalous* Green's functions, i.e. the off-diagonal terms in the *Nambu representation* [73], but this extension will not be treated in this thesis.

where E is the energy eigenvalue. If the potential $V(\mathbf{r})$ is *short-ranged* and the relative distance is large, then (3.1) is the Schrödinger equation for a free particle with an energy $E = \mathbf{k}^2/(2m_{red}) \equiv \varepsilon_{\mathbf{k}}$, which is conserved since we are interested in elastic scattering processes. In this way, we can rewrite the Schrödinger equation in a basis-independent (bra-ket) notation as

$$(\varepsilon_{\mathbf{k}} - \hat{H}_0)\,|\psi_{\mathbf{k}}\rangle = \hat{V}\,|\psi_{\mathbf{k}}\rangle\,, \tag{3.2}$$

whose solution is given by the *Lippmann-Schwinger equation*

$$|\psi_{\mathbf{k}}\rangle = |\mathbf{k}\rangle + \frac{1}{\varepsilon_{\mathbf{k}} - \hat{H}_0 + i0^+}\hat{V}\,|\psi_{\mathbf{k}}\rangle\,, \tag{3.3}$$

where we introduced $i0^+$ to deal with the singular nature of the operator $1/(E-\hat{H}_0)$. The choice $+i0^+$, rather than $-i0^+$, is physical and will become apparent when we obtain the solution for the scattering state. To find the scattering wave function $\psi_{\mathbf{k}}(\mathbf{r})$, we multiply (3.3) by $\langle\mathbf{r}|$

$$\psi_{\mathbf{k}}(\mathbf{r}) = e^{i\mathbf{k}\cdot\mathbf{r}} + \int d\mathbf{r}'\,\langle\mathbf{r}|\,\frac{1}{\varepsilon_{\mathbf{k}} - \hat{H}_0 + i0^+}\,|\mathbf{r}'\rangle\,\langle\mathbf{r}'|\,\hat{V}\,|\psi_{\mathbf{k}}\rangle\,, \tag{3.4}$$

where we used $\langle\mathbf{r}|\mathbf{k}\rangle = e^{i\mathbf{k}\cdot\mathbf{r}}$, that is an incoming plane wave. The second term requires more work and gives

$$\begin{aligned}
&\int d\mathbf{r}'\,\langle\mathbf{r}|\,\frac{1}{\varepsilon_{\mathbf{k}} - \hat{H}_0 + i0^+}\,|\mathbf{r}'\rangle\,\langle\mathbf{r}'|\,\hat{V}\,|\psi_{\mathbf{k}}\rangle \\
&= \int d\mathbf{r}' \int \frac{d\mathbf{k}'}{(2\pi)^3}\frac{e^{i\mathbf{k}'\cdot(\mathbf{r}-\mathbf{r}')}}{\varepsilon_{\mathbf{k}} - \varepsilon_{\mathbf{k}'} + i0^+}\,\langle\mathbf{r}'|\,\hat{V}\,|\psi_{\mathbf{k}}\rangle \\
&= -2m_{red}\int d\mathbf{r}'\frac{e^{ik|\mathbf{r}-\mathbf{r}'|}}{4\pi|\mathbf{r}-\mathbf{r}'|}\,\langle\mathbf{r}'|\,\hat{V}\,|\psi_{\mathbf{k}}\rangle\,,
\end{aligned} \tag{3.5}$$

where we inserted the completeness relation of the momentum eigenstates in the first step and integrated in the second step. Since we are dealing with a short-ranged potential, we are primarily interested in the behaviour of the wave function at distances which are larger than its range. For this reason, we can expand the interatomic distance for $r \gg r'$ as $|\mathbf{r}-\mathbf{r}'| \simeq r - \mathbf{r}'\cdot\hat{\mathbf{r}}$ and define $\mathbf{k}' = k\hat{\mathbf{r}}$, which has the same magnitude as $\mathbf{k}$ but points in the direction $\hat{\mathbf{r}} = \mathbf{r}/r$. Putting all the pieces together, we get the crucial result

$$\psi_{\mathbf{k}}(\mathbf{r}) = e^{i\mathbf{k}\cdot\mathbf{r}} + f(\mathbf{k}',\mathbf{k})\frac{e^{ikr}}{r}, \tag{3.6}$$

which shows that, at distances much larger than the interaction range, the total wave function can be written as the sum of an incoming plane wave and an outgoing modulated spherical wave. The modulation factor $f(\mathbf{k}',\mathbf{k})$ is the *scattering amplitude*, defined as

$$f(\mathbf{k}',\mathbf{k}) = -\frac{1}{4\pi}2m_{red}\,\langle\mathbf{k}'|\,\hat{V}\,|\psi_{\mathbf{k}}\rangle\,. \tag{3.7}$$

Now, we are also able to understand the reason for adding the $+i0^+$ term in (3.3): a small negative imaginary part $-i0^+$ would have led to a description of the time-reversed scattering process, i.e. an incoming spherical wave.

3.1.1 Two-body t-Matrix

To solve the scattering problem in a more convenient way without dealing with the scattering state, we introduce the operator $\hat{T}$ known as *two-body transition operator*, and defined by the relation

$$\hat{V}\,|\psi_{\mathbf{k}}\rangle = \hat{T}\,|\mathbf{k}\rangle\,. \tag{3.8}$$

The matrix elements of $\hat{T}$ are directly related to the scattering amplitude $f(\mathbf{k}', \mathbf{k})$, as we can readily see by substituting the previous relation into (3.7), obtaining

$$f(\mathbf{k}', \mathbf{k}) = -\frac{1}{4\pi} 2m_{red}\, t(\mathbf{k}', \mathbf{k}), \tag{3.9}$$

where $t(\mathbf{k}', \mathbf{k}) \equiv \langle \mathbf{k}'|\,\hat{T}\,|\mathbf{k}\rangle$ is the *two-body t-matrix*. The Lippmann-Schwinger equation (3.3) becomes a self-consistent equation for the T-operator

$$\hat{T} = \hat{V} + \hat{V}\frac{1}{E - \hat{H}_0 + i0^+}\hat{T}, \tag{3.10}$$

where $\hat{G}_0 \equiv (E - \hat{H}_0 + i0^+)^{-1}$ is an operator that gives rise to a *non-interacting propagator* $G_0(\mathbf{r}, \mathbf{r}') \equiv \langle \mathbf{r}|\,\hat{G}_0\,|\mathbf{r}'\rangle$ for the outgoing wave[2], since it is a solution of the differential equation

$$\left(E + \frac{\nabla^2}{2m_{red}}\right) G_0(\mathbf{r} - \mathbf{r}') = \delta(\mathbf{r} - \mathbf{r}'). \tag{3.11}$$

The equation (3.10) can be solved iteratively, resulting in the *Born series* given by

$$\hat{T}(z) = \hat{V} + \hat{V}\hat{G}_0(z)\hat{V} + \hat{V}\hat{G}_0(z)\hat{V}\hat{G}_0(z)\hat{V} + \ldots, \tag{3.12}$$

where the operator $\hat{G}_0(z) = (z - \hat{H}_0)^{-1}$ corresponds to the non-interacting propagator of the particles at a (complex) energy z. The *on-shell* t-matrix $t(\mathbf{k}', \mathbf{k})$, that appears in (3.9), is obtained by calculating the matrix element $\langle \mathbf{k}'|\,\hat{T}(z)\,|\mathbf{k}\rangle$ on the energy shell $|\mathbf{k}| = |\mathbf{k}'|$ for $z = \varepsilon_{\mathbf{k}} + i0^+$ [75].

A common approximation is to take only the first term of the Born series (3.12) into account, which is called *Born approximation*. However, this is not our case: in the ultra-cold Fermi gases across the BCS-BEC crossover the potential can be really strong, and we are obliged to solve the equation exactly at all orders to correctly take into account the effects of the interaction potential on the scattering wave function. As we will shown in the next section, this is still possible if we limit ourselves to the low-energy scattering, that is usually the only relevant process in ultra-cold gases.

The Born series for the on-shell t-matrix (or, equivalently using (3.9), for the scattering amplitude) of the two-body problem is given by

$$\begin{aligned} t(\mathbf{k}', \mathbf{k}) &= V(\mathbf{k}' - \mathbf{k}) + \int \frac{d\mathbf{p}}{(2\pi)^3} V(\mathbf{k}' - \mathbf{p}) G_0(\mathbf{p}) t(\mathbf{p}, \mathbf{k}) \\ &\equiv V(\mathbf{k}' - \mathbf{k}) + \int \frac{d\mathbf{p}}{(2\pi)^3} V(\mathbf{k}' - \mathbf{p}) G_0(\mathbf{p}) V(\mathbf{p} - \mathbf{k}) \\ &+ \int \frac{d\mathbf{p}}{(2\pi)^3} \int \frac{d\mathbf{p}'}{(2\pi)^3} V(\mathbf{k}' - \mathbf{p}) G_0(\mathbf{p}) V(\mathbf{p} - \mathbf{p}') G_0(\mathbf{p}') V(\mathbf{p}' - \mathbf{k}) + \ldots, \end{aligned} \tag{3.13}$$

[2]Notice that this quantity is mathematically a Green's function since is a solution to (3.11), but has nothing to do with the many-body Green's functions defined in (2.2) and (2.36).

where $G_0(\mathbf{p}) = (\varepsilon_{\mathbf{k}} - \varepsilon_{\mathbf{p}} + i0^+)^{-1}$, and is schematically represented in Figure 3.1. We see that any term of the series for the scattering amplitude is a repetition of interactions V and propagations G_0 of the pair of interacting particles: this is exactly the structure of the *ladder diagrams* that we will choose in the many-body approach, and explains the reason why this choice of diagrams is called *t-matrix approximation*.

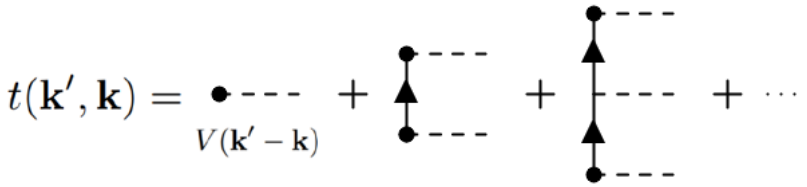

Figure 3.1: Diagrammatic representation of the born series for the on-shell t-matrix. Notice that these are not Feynman diagrams but are just a way of keeping track of the terms that contribute to the expansion.

It is relevant to notice that the formal solution of the operator equation for the transition operator (3.10) is given by

$$\hat{T}(z) = \hat{V} + \hat{V}\frac{1}{z - \hat{H}}\hat{V}, \tag{3.14}$$

where $\hat{H} = \hat{H}_0 + \hat{V}$. Inserting a complete set of eigenstates $|\alpha\rangle$ for $\hat{H}$, we get

$$\hat{T}(z) = \hat{V} + \sum_{\alpha} \hat{V}\frac{|\alpha\rangle\langle\alpha|}{z - \varepsilon_\alpha}\hat{V}, \tag{3.15}$$

where the summation over α is discrete for possible *bound states* of the interaction potential with $\varepsilon_\alpha < 0$, or becomes an integration for continuum of scattering states with $\varepsilon_\alpha > 0$. This means that the poles of the T-operator in the complex-energy plane correspond to bound states, while its branch cut on the positive real axis is related to the continuum of scattering states.

3.1.2 s-Wave Scattering

For most physical systems with short-range interactions, the potential is not known with precision. Fortunately, the exact knowledge is not necessary in the low-energy scattering limit, a very well verified condition for ultra-cold atoms, since the two-body interactions are characterized by a single parameter that can be measured experimentally, namely, the *scattering length*.

Consider the relative Schrödinger equation in the center-of-mass frame (3.1), where now the potential V is a typical spherically symmetric molecular potential, i.e. $V(\mathbf{r}) \equiv V(r)$. We can therefore expand the scattering wave function into

$$\psi_{\mathbf{k}}(\mathbf{r}) = \sum_{l=0}^{\infty}\sum_{m_l=-l}^{l} \frac{u_{\mathbf{k}l}(r)}{r} Y_{lm_l}(\theta, \phi), \tag{3.16}$$

where Y_{lm_l} are the spherical harmonics of angular momentum quantum number l. We notice that, since the scattering problem does not depends on ϕ, we omit the functions with $m \neq 0$, i.e only $Y_{l0}(\theta)$ are non-zero. By substituting this expansion in the Schrödinger equation, we find a one-dimensional equation along the direction of $\mathbf{k}$ for each radial wave $u_{\mathbf{k}l}$

$$\left(\frac{1}{2m_{red}}\frac{d^2}{dr^2} + \varepsilon_{\mathbf{k}}\right) u_{\mathbf{k}l}(r) = V_{eff}^{(l)}(r) u_{\mathbf{k}l}(r), \tag{3.17}$$

where we introduced the *effective potential*, which is given by the sum of the potential $V(r)$ and a centrifugal contribution due to the angular momentum

$$V_{eff}^{(l)}(r) = V(r) + \frac{l(l+1)}{r^2}. \tag{3.18}$$

If the energy $\varepsilon_{\mathbf{k}}$ is much lower than the height of the centrifugal barrier $l(l+1)/r_0^2$, where r_0 is the range of the potential, the system will not experience the short-range potential $V(r)$ and will be simply reflected by the centrifugal barrier. We therefore expect that in the limit of low energy the only relevant contribution to the scattering will be given by the $l = 0$ quantum number. As the latter is also denoted with s, this process is usually called *s-wave scattering*.

For spherically symmetric interaction potentials, the scattering amplitude (3.7) depends only on the magnitude of the incoming momentum k and the scattering angle θ, i.e. $f(\mathbf{k}', \mathbf{k}) \equiv f(k, \theta)$. We can therefore decompose the scattering amplitude, using the *partial waves expansion*, into

$$f(k, \theta) = \sum_{l=0}^{\infty} (2l+1) f_l(k) P_l(\cos\theta), \tag{3.19}$$

where $P_l(x)$ are the Legendre polynomials. To see the meaning of $f_l(k)$, we first use the identity

$$e^{i\mathbf{k}\cdot\mathbf{r}} = \sum_{l=0}^{\infty} (2l+1) i^l j_l(kr) P_l(\cos\theta), \tag{3.20}$$

where, for large r, we use the asymptotic behaviour of the spherical Bessel functions $j_l(kr)$, obtaining

$$e^{i\mathbf{k}\cdot\mathbf{r}} \simeq \sum_{l=0}^{\infty} (2l+1) P_l(\cos\theta) \left(\frac{e^{ikr} - e^{-i(kr - l\pi)}}{2ikr}\right). \tag{3.21}$$

This shows that the plane-wave part of the scattering wave function can be written as a sum of incoming and outgoing spherical waves. By combining (3.6), (3.19) and (3.21), we see that the presence of an interaction potential changes the coefficient of the outgoing spherical wave according to

$$\frac{e^{ikr}}{r} \to \frac{(1 + 2ikf_l(k))e^{ikr}}{r}, \tag{3.22}$$

where the magnitude of the coefficient $1 + 2ikf_l(k)$ must be equal to one, owing to the conservation of probability flux. We can therefore express the coefficient as an exponential

$$1 + 2ikf_l(k) \equiv e^{2i\delta_l(k)}, \tag{3.23}$$

where $\delta_l(k)$ is the *phase shift*. As a result, at large distances, the change in the wave function due to the collision process is solely given by a shift in the phase of every outgoing partial wave.

For the s-wave scattering we can define the *scattering length*

$$a \equiv -\lim_{k\to 0^+} \frac{\delta_0(k)}{k}, \tag{3.24}$$

and using (3.23), we then find that

$$f(\mathbf{k}', \mathbf{k}) \simeq f_0(k) = \frac{1}{k\cot\delta_0(k) - ik} \simeq -\frac{1}{a^{-1} + ik}, \tag{3.25}$$

where in the last expression we approximated $\cot x \simeq 1/x$ for low-energies ($k \to 0$). The relation in (3.25) shows indeed that all the scattering properties are described in terms of the s-wave scattering length a. The on-shell t-matrix, related to the scattering amplitude with (3.9), can be analytically continued to

$$t(\mathbf{k}', \mathbf{k}; z) \simeq \frac{4\pi a}{2m_{red}} \frac{1}{1 - a\sqrt{-2m_{red}z}}, \tag{3.26}$$

which shows a pole, i.e. a bound state, for $a > 0$ with the negative binding energy, just below the continuum threshold, given by

$$E_b = -\varepsilon_0 = -\frac{1}{2m_{red}a^2}. \tag{3.27}$$

3.1.3 Contact Potential and BCS-MF Critical Temperature

Since the form of the potential for the s-wave scattering is not important, the idea is to use the simplest one, which is a contact (zero-range) potential $V(\mathbf{r}) = v_0\delta(\mathbf{r})$, where v_0 is a negative constant chosen in a way to reproduce correctly the s-wave scattering. However, with this choice we must pay a price: for homogeneous systems the Fourier transform $V(\mathbf{k}) = v_0$ is constant and this can make the integrals in $\mathbf{k}$-space diverge for large k. To overcome this problem, we introduce an ultraviolet cut-off k_0 such that we can define an effective separable potential in momentum space as

$$V(\mathbf{k}' - \mathbf{k}) = v_0\theta(k_0 - |\mathbf{k}'|)\theta(k_0 - |\mathbf{k}|), \tag{3.28}$$

where $\theta(x)$ is the Heaviside step function. Notice that the choice of a potential that is separable in $\mathbf{k}$ and $\mathbf{k}'$ is just an useful theoretical trick that becomes irrelevant in the $k_0 \to \infty$ limit to recover the contact potential. We can now insert this separable potential in the equation for the on-shell t-matrix (3.13) and use the s-wave form of the scattering amplitude (3.25), together with the relation (3.9), to get an important relation that connects the scattering length a_F between two fermions to the parameters v_0 and k_0

$$\frac{2m_{red}}{4\pi a_F} = \frac{1}{v_0} + \int_{|\mathbf{k}|\le k_0} \frac{d\mathbf{k}}{(2\pi)^3} \frac{2m_{red}}{\mathbf{k}^2}. \tag{3.29}$$

This expression gives us a correct *regularization procedure* for the contact potential, since we can take simultaneously the limits $k_0 \to \infty$ and $v_0 \to 0^-$ such that the scattering length a_F is kept at the desired value without incurring in any divergence.

As an example, with the regularization condition (3.29) we can modify the mean-field gap equation (1.9) as

$$-\frac{m}{4\pi a_F} = \int \frac{d\mathbf{k}}{(2\pi)^3}\left(\frac{1-2f(E_\mathbf{k})}{2E_\mathbf{k}} - \frac{m}{\mathbf{k}^2}\right), \tag{3.30}$$

where now $m_{red} = m/2$ since we consider the case of a mass-balanced system. This expression now allows one to get the mean-field critical temperature in the BCS limit $(k_F a_F)^{-1} \ll -1$. As the coupling gets weaker, we expect that the system tends to a non-interacting Fermi gas: indeed from the mean-field density equation (1.7) we get a chemical potential $\mu \simeq E_F$, provided $T_c \ll E_F$. Therefore, by imposing $\Delta = 0$ in (3.30), we get [74]

$$T_c^{BCS} \equiv \frac{e^\gamma}{\pi}\Delta_0 = \frac{8e^\gamma E_F}{\pi e^2}\exp\left(\frac{\pi}{2k_F a_F}\right), \tag{3.31}$$

where γ is the Euler constant and Δ_0 is the zero temperature BCS gap parameter. Notice that, consistently with our assumptions, $T_c^{BCS} \ll E_F$. It is also possible to obtain a compact expression for T_c^{BCS} in the imbalanced case, by solving the gap equation (1.27). This is given by [76]

$$T_c^{BCS} = \frac{m_{red}}{\sqrt{m_\uparrow m_\downarrow}}\frac{\Delta_0}{2\pi}\exp\left[-\frac{1}{2}\mathcal{F}\left(\frac{1}{2T_c^{BCS}}\frac{m_\uparrow\mu_\uparrow - m_\downarrow\mu_\downarrow}{m_\uparrow + m_\downarrow}\right)\right], \tag{3.32}$$

where $\mathcal{F}(x) \equiv \Psi(\frac{1}{2} + \frac{ix}{\pi}) + \Psi(\frac{1}{2} - \frac{ix}{\pi})$, Ψ being the *digamma function*, defined as $\Psi(z) = \Gamma'(z)/\Gamma(z)$, where z is a complex number with a positive real component and Γ is the gamma function. Due to the highly non-linear term $\mathcal{F}$ in this equation, it is possible to find analytical solutions for T_c^{BCS} only when the system is spin-balanced, i.e. $\sqrt{2m_\uparrow\mu_\uparrow} = \sqrt{2m_\downarrow\mu_\downarrow}$. This reads

$$T_c^{BCS} \equiv \frac{2m_{red}}{\sqrt{m_\uparrow m_\downarrow}}\frac{e^\gamma}{\pi}\Delta_0 = \frac{2m_{red}}{\sqrt{m_\uparrow m_\downarrow}}\frac{8e^\gamma E_F}{\pi e^2}\exp\left(\frac{\pi}{2k_F a_F}\right), \tag{3.33}$$

where the Fermi energy is now expressed as $E_F = k_F^2/(4m_{red})$. In the BCS limit, we will try to recover this result within our many-body approach (see Section 3.2.3)[3].

We conclude this section with a crucial consideration: at low energy, an interaction between two identical fermions is possible only if they are in different spin states, i.e. they are distinguishable. This happen because of the anti-symmetrization principle of the wave-function for indistinguishable fermions, which states that

[3]Actually, it is important to notice that the mean-field result (3.31) is the correct weak-coupling asymptotic result for T_c only with logarithmic accuracy (i.e. it is the correct asymptotic behaviour of $\log T_c$ rather than T_c). The correct asymptotic result for T_c is obtained by including the *Gor'kov-Melik-Barkhudarov corrections* (GMB) [77], that are responsible for the suppression of T_c by a factor $(4e)^{1/3} \simeq 2.2$ in a balanced three dimensional ultra-cold Fermi gas. This screening of the interaction is related to many-body effects, or simply the effects of the medium, on the two-body interaction.

$\psi_{\mathbf{k}}(\mathbf{r}) = -\psi_{\mathbf{k}}(-\mathbf{r})$. Knowing that the parity of spherical harmonic functions $Y_{l0}(\theta)$ is $(-1)^l$, we see that in the expansion (3.16) only the odd l terms survive for fermions and contribute to the scattering. Therefore, the s-wave scattering ($l = 0$ even) is suppressed for fermions with the same spin state, i.e. indistinguishable fermions. In the case of the contact potential, this consideration is seen immediately because $\delta(\mathbf{r})\psi_{\mathbf{k}}(\mathbf{r}) = 0$ for identical fermions, due to the anti-symmetrization imposed on the wave function by the fermionic statistics.

3.2 Non-self-consistent t-Matrix Approach

We have to generalize what we have discussed until now to the many-body problem. First of all, we introduce the fundamental class of diagrams that we will use in our theory, the *ladder diagrams*, justified in Section 3.1.1 and presented in the upper part of Figure 3.2. The sum of all these ladder diagrams Γ_0 is called *particle-particle propagator* or *vertex of ladder diagrams*. The definition of Γ_0 is conveniently expressed in a self-consistent manner, as shown in the lower part of Figure 3.2, by applying the Feynman rules of Section 2.2. In this way, using the four-momentum compact notation $Q = (\mathbf{Q}, \Omega_\nu)$ and $p = (\mathbf{p}, \omega_n)$, we get the *Bethe-Salpeter equation*

$$\begin{aligned}\Gamma_0(\mathbf{k}', \mathbf{k}, Q) = &-V(\mathbf{k}' - \mathbf{k}) \\ &- \int \frac{d\mathbf{p}}{(2\pi)^3} \frac{1}{\beta} \sum_n V(\mathbf{k}' - \mathbf{p}) \mathcal{G}^0_\uparrow(p + Q) \mathcal{G}^0_\downarrow(-p) \Gamma_0(\mathbf{p}, \mathbf{k}, Q),\end{aligned} \tag{3.34}$$

where ω_n and Ω_ν are respectively the fermionic and bosonic Matsubara frequencies as defined in (2.10), while $\mathcal{G}^0_\sigma \equiv \mathcal{G}^0_{\sigma\sigma}$ is the spin-σ bare propagator, defined similarly as in (2.27)

$$\mathcal{G}^0_\sigma(\mathbf{k}, \omega_n) = \frac{1}{i\omega_n - \xi_{\mathbf{k}\sigma}}, \qquad \xi_{\mathbf{k}\sigma} = \frac{\mathbf{k}^2}{2m_\sigma} - \mu_\sigma, \tag{3.35}$$

to take now into account the possibility of spin and mass imbalance in the system. Notice that, to write the expression (3.34), we used the consideration made in Section (3.1.3) in which the interaction potential is non-zero only for fermions with different spin; therefore the only possible choice for two propagator connected by the same interaction line is $\mathcal{G}^0_\uparrow \mathcal{G}^0_\downarrow$.

If we directly compare the Bethe-Salpeter (3.34) equation with the self-consistent equation for the two-body t-matrix (3.13), we immediately see that the structure is very similar: Γ_0 takes the role of $-t$ (the minus sign is related to our convention), noticing however that Γ_0 depends also on the four-momentum of the pair $Q = (\mathbf{Q}, \Omega_\nu)$, while $\beta^{-1} \sum_n \mathcal{G}^0_\uparrow \mathcal{G}^0_\downarrow$ takes the role of G_0. This comparison explains why Γ_0 is also reasonably denoted as *many-body t-matrix*. A more precise relation between the two-body and many-body t-matrix will be obtained in the strong-coupling limit, discussed in Section 3.2.2.

As previously discussed, to study the normal phase of an ultra-cold Fermi gas throughout the BCS-BEC crossover, we can just focus specifically on the contact potential (3.28). We therefore get

$$\Gamma_0(Q) = -v_0 - v_0 \int_{|\mathbf{p}| \leq k_0} \frac{d\mathbf{p}}{(2\pi)^3} \frac{1}{\beta} \sum_n \mathcal{G}^0_\uparrow(p + Q) \mathcal{G}^0_\downarrow(-p) \Gamma_0(Q), \tag{3.36}$$

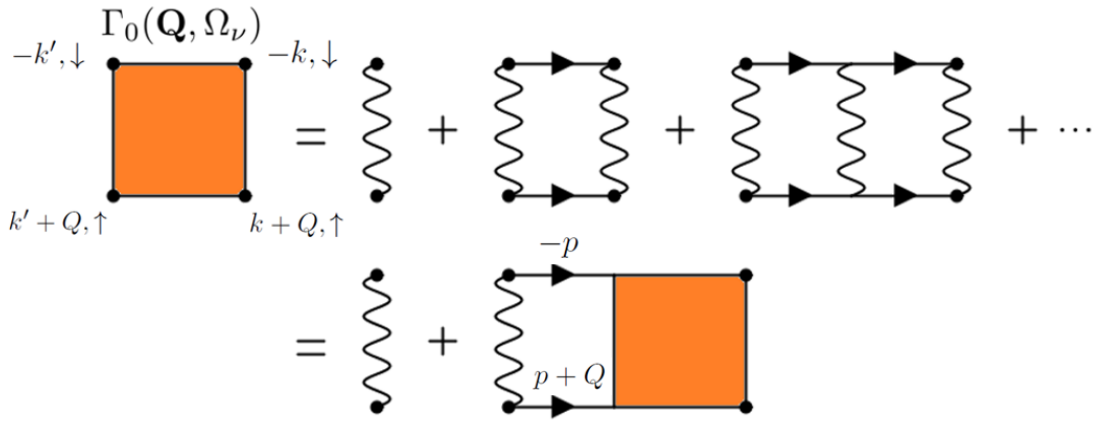

Figure 3.2: Diagrammatic representation of the particle-particle propagator Γ_0, defined as the sum of all the ladder diagrams (above). It can also be expressed self-consistently (below) through the Bethe-Salpeter equation.

where now we see that Γ_0 is only a function of the pair four-momentum Q, and therefore we can take it out from the integral to write it in the simpler form

$$\Gamma_0(Q) = -\frac{v_0}{1 + v_0 \chi^0_{pp}(Q)}, \tag{3.37}$$

with χ^0_{pp}, denoted as *particle-particle bubble*, given by

$$\chi^0_{pp}(Q) = \int_{|\mathbf{p}|\leq k_0} \frac{d\mathbf{p}}{(2\pi)^3} \frac{1}{\beta} \sum_n \mathcal{G}^0_\uparrow(p+Q)\mathcal{G}^0_\downarrow(-p). \tag{3.38}$$

This expression is still ultraviolet divergent in the limit $k_0 \to \infty$. This divergence can be eliminated with the regularization condition (3.29), expressing $1/v_0$ in terms of the fermionic scattering length a_F, obtaining

$$\Gamma_0(Q) = -\frac{1}{2m_{red}/(4\pi a_F) + R^0_{pp}(Q)}, \tag{3.39}$$

where R^0_{pp} is now the *renormalized particle-particle bubble*

$$R^0_{pp}(Q) = \int \frac{d\mathbf{p}}{(2\pi)^3} \left(\frac{1}{\beta} \sum_n \mathcal{G}^0_\uparrow(p+Q)\mathcal{G}^0_\downarrow(-p) - \frac{2m_{red}}{\mathbf{p}^2} \right). \tag{3.40}$$

The sum over the Matsubara frequencies ω_n can be carried out analytically after a partial fraction decomposition, with the relation (2.28), and gives the result

$$R^0_{pp}(Q) = \int \frac{d\mathbf{p}}{(2\pi)^3} \left(\frac{1 - f(\xi_{\mathbf{p}+\mathbf{Q}\uparrow}) - f(\xi_{\mathbf{p}\downarrow})}{\xi_{\mathbf{p}+\mathbf{Q}\uparrow} + \xi_{\mathbf{p}\downarrow} - i\Omega_\nu} - \frac{2m_{red}}{\mathbf{p}^2} \right), \tag{3.41}$$

where $f(\xi) = (e^{\beta\xi} + 1)^{-1}$ is the Fermi function. The ultraviolet divergence that appears in (3.38) is now eliminated by the counter-term $-2m_{red}/\mathbf{p}^2$, so the $k_0 \to \infty$ limit can be taken without problems.

We can now proceed to define the *t-matrix self-energy* in the following way: if we treat the particle-particle propagator Γ_0 as an effective interaction in the medium, the self-energy corresponds to an Hartree-like term (compare with Figure 2.1) of this interaction, as shown in Figure 3.3. Notice that we are not considering any Fock-like term (i.e. connect the bottom right and the top left vertices with a bare propagator), because in our problem this is exactly zero due to the absence of same-spin interaction[4]. Using the Feynman rules with a four-momentum notation, the expression for the self-energy is therefore given by

$$\Sigma^0_\sigma(k) = -\int \frac{d\mathbf{Q}}{(2\pi)^3}\frac{1}{\beta}\sum_\nu \Gamma_0(Q)\mathcal{G}^0_{\bar{\sigma}}(Q-k), \tag{3.42}$$

where σ and $\bar{\sigma}$ are opposite spin indices.

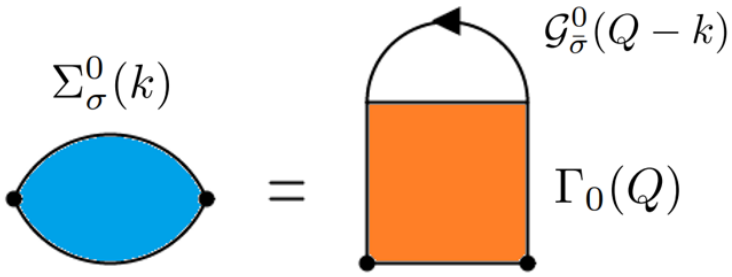

Figure 3.3: Diagrammatic representation of the t-matrix self-energy Σ^0_σ, interpreted as an Hartree-like diagram with effective interaction Γ_0.

We have now all what is necessary to calculate the dressed Green's function of our system. We first compute the renormalized particle-particle bubble R^0_{pp} with (3.41) from which we obtain the many-body t-matrix Γ_0 with (3.39), then we get the self-energy Σ^0_σ with (3.42) and we finally obtain the single-particle Green's function $\mathcal{G}_\sigma$ via the Dyson equation (2.35)

$$\mathcal{G}_\sigma(k) = \frac{1}{\mathcal{G}^0_\sigma(k)^{-1} - \Sigma^0_\sigma(k)}, \tag{3.43}$$

as shown in Figure 3.4.

This procedure is known in the literature as *non-self-consistent t-matrix* approach (check the upper flowchart in Figure 3.5). In this approximation we have four free parameters: the temperature T, the scattering length a_F and the chemical potentials for the two species in the Fermi gas $\mu_\uparrow$ and $\mu_\downarrow$, which can be found in terms of the densities n_σ by inverting the densities equations (2.16)

$$n_\sigma = \int \frac{d\mathbf{k}}{(2\pi)^3}\frac{1}{\beta}\sum_n e^{i\omega_n 0^+}\mathcal{G}_\sigma(\mathbf{k},\omega_n). \tag{3.44}$$

[4]In his original paper on the diagrammatic description of a dilute repulsive Fermi gas [35], Galitskii considered this Fock-like term.

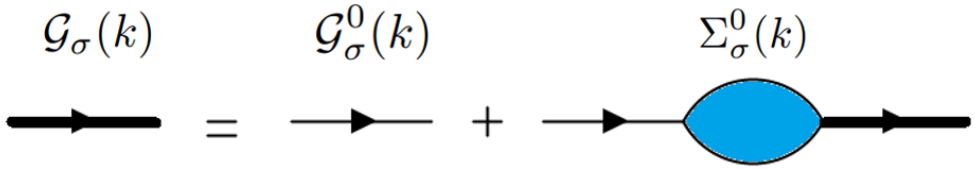

Figure 3.4: Diagrammatic representation of the t-matrix Dyson equation, which relates the dressed propagator $\mathcal{G}_\sigma$ to the bare propagator $\mathcal{G}^0_\sigma$ and t-matrix self-energy Σ^0_σ.

However, if we re-scale all the quantities in terms of the total density $n = n_\uparrow + n_\downarrow$, which is fixed, we reduce this number to three dimensionless parameters:

- The *coupling* $(k_F a_F)^{-1}$, where $k_F = (3\pi^2 n)^{1/3}$.
- The *temperature* T/E_F, where $E_F = k_F^2/(4m_{red})$.
- The *polarization* or *density imbalance* $p = (n_\uparrow - n_\downarrow)/n$.

It is crucial to notice that, since we are dealing with a mass imbalanced system (conventionally with $m_L \equiv m_\uparrow < m_H \equiv m_\downarrow$), the value of the polarization p must be analyzed also for negative values because the situation in which the majority of atoms is heavier (H), i.e. $p < 0$, could be physically much different from the case in which the majority is lighter (L), i.e. $p > 0$. In the mass balanced case $m_\uparrow = m_\downarrow = m$, one can simply study the system for positive polarization, since for negative values we have a completely symmetric situation.

3.2.1 Thouless Criterion and Pair Susceptibility

Within the non-self-consistent t-matrix approach it is possible to recover the correct superfluid critical temperature both in the BEC and BCS limits (albeit only with logarithmic accuracy in the latter case). In order to do this, it is convenient to introduce the *Thouless criterion*, [78] which states that the particle-particle propagator shows a pole at $\mathbf{Q} = 0$ and $\Omega_\nu = 0$ for a spin-balanced system at $T = T_c$, signaling an instability of the normal phase due to a macroscopic accumulation (condensation) of fermionic pairs in the state of momentum $\mathbf{Q} = 0$

$$[\Gamma_0(\mathbf{Q} = 0, \Omega_\nu = 0)|_{T=T_c}]^{-1} = 0. \tag{3.45}$$

The justification for this criterion resides in the notion of t-matrix: as we already discussed above, the particle-particle propagator can be thought as the many-body generalization of the two-body t-matrix introduced in Section 3.1.1. There, it was shown that the poles of the t-matrix correspond to two-body bound states in the interaction potential. This observation may be generalized to the many-body case,

such that the onset of a pole in the particle-particle propagator corresponds to long-lived pairs occurring in the system, that is our superfluid phase.

When dealing with an imbalanced system, one of the main aspects to study is the temperature-coupling-polarization phase diagram. In a standard normal-to-superfluid (Sarma) second-order transition, the Thouless criterion is easily generalized to find the *transition line*: the condition for the critical temperature (3.45) that now depends on the polarization p, i.e. $T = T_c(p)$, is still valid, and in addition we have a condition to find critical polarization p_c as a function of the temperature T

$$[\Gamma_0(\mathbf{Q} = 0, \Omega_\nu = 0)|_{p=p_c(T)}]^{-1} = 0. \tag{3.46}$$

The situation is quite different if one considers the normal-to-FFLO transition: in this transition the particle-particle propagator should have a divergence at finite momentum $\mathbf{Q}_0$, therefore the condition (3.45) becomes

$$[\Gamma_0(\mathbf{Q} = \mathbf{Q}_0, \Omega_\nu = 0)|_{T=T_c^{FLLO}}]^{-1} = 0. \tag{3.47}$$

However, in the limit $\mathbf{Q} \to \mathbf{Q}_0$ at finite temperature, $\Gamma_0(Q)$ would diverge as $(|\mathbf{Q}| - |\mathbf{Q}_0|)^{-2}$ and this divergence is non-integrable in the expression of the self-energy (3.42), in contrast to the standard $\mathbf{Q}_0 = 0$ case where the $|\mathbf{Q}|^{-2}$ divergence is compensated by the factor $|\mathbf{Q}|^2$ of the spherical integration over $\mathbf{Q}$ [79]. Notice that this problem would be solved if the normal-FFLO phase transition was indeed of first-order, like in the weak-coupling regime as we have seen in Section 1.4.1, since the transition would happen in a region where the divergence of Γ_0 is still not reached. However, in this context, we are treating the normal-FFLO transition as second-order because the study of a first-order transition would require an approach working also in the broken-symmetry phase, that will not be treated in this thesis. As a consequence, within any t-matrix diagrammatic approach, the FFLO phase can be found only at $T = 0$, while the system remains in the normal phase for any $T \neq 0$.

Nevertheless, the t-matrix approach allows one to analyze the presence of strong FFLO pairing fluctuations in the normal phase, which are precursors of a FFLO superfluid phase [80]. This is done by calculating the *pair susceptibility* $\chi_{pair}(\mathbf{Q})$, that describes the tendency of the normal Fermi gas towards superfluid ordering with pair center-of-mass momentum $\mathbf{Q}$. Within our approximation, the pair susceptibility is identified with

$$\chi_{pair}(\mathbf{Q}) = \Gamma_0(\mathbf{Q}, \Omega_\nu = 0), \tag{3.48}$$

such that a pole in the particle-particle propagator would correspond to a divergent χ_{pair} (see also Section 6.4). Therefore, the presence of strong FFLO fluctuations in the normal phase is signaled by a peak in the pair susceptibility at finite momentum $\mathbf{Q}_0$, which is strongly enhanced as the temperature is progressively lowered.

3.2.2 Strong-coupling (BEC) Limit

As we have seen in Section 1.3, in the strong-coupling limit $(k_F a_F)^{-1} \gg 1$ the dominant energy scale is the chemical potential $\mu = (\mu_\uparrow + \mu_\downarrow)/2$, which becomes large and negative since it approaches to half of the dimer binding energy, i.e. $\mu \simeq -\varepsilon_0/2$.

From (3.27), we know now that $\varepsilon_0 = (2m_{red}a_F^2)^{-1}$. In the following, we assume spin balance in the system, i.e. $n_\uparrow = n_\downarrow$. Therefore, by taking the $\beta|\mu| \gg 1$ limit, we can neglect the Fermi functions in the renormalized particle-particle bubble (3.41) and the integral can be carried out analytically, yielding

$$R_{pp}^{0,SC}(Q) = -\frac{(2m_{red})^{3/2}}{4\pi}\sqrt{\frac{\mathbf{Q}^2}{2m_B} - 2\mu - i\Omega_\nu}, \tag{3.49}$$

where $m_B = m_\uparrow + m_\downarrow$. By inserting this expression in (3.39), we obtain the particle-particle propagator Γ_0 in the BEC limit

$$\Gamma_0^{SC}(Q) = -\frac{4\pi a_F}{2m_{red}}\frac{1}{1 - a_F\sqrt{2m_{red}\left(\frac{\mathbf{Q}^2}{2m_B} - 2\mu - i\Omega_\nu\right)}}, \tag{3.50}$$

or, by rearranging the previous expression

$$\Gamma_0^{SC}(Q) = -\frac{4\pi}{(2m_{red})^2 a_F}\frac{1 + \sqrt{1 + \left(\frac{\mathbf{Q}^2}{2m_B} - \mu_B - i\Omega_\nu\right)\varepsilon_0^{-1}}}{i\Omega_\nu - \left(\frac{\mathbf{Q}^2}{2m_B} - \mu_B\right)}, \tag{3.51}$$

where we defined the bosonic chemical potential $\mu_B = 2\mu + \varepsilon_0$. These two expressions above hide two important results, that we will now discuss. First of all, by comparing the many-body t-matrix in the strong-coupling limit (3.50) and the two-body t-matrix in (3.26), we see immediately that

$$\Gamma_0^{SC}(Q) \equiv -t(z = i\Omega_\nu - \mathbf{Q}^2/(2m_B) + 2\mu), \tag{3.52}$$

so the two expressions coincide up to a minus sign due to our definition of Γ_0. Secondly we notice that, within the square root in (3.51), the term multiplied by ε_0^{-1} is sub-leading in the strong-coupling limit, so to the lowest order the particle-particle propagator assumes the familiar form

$$\Gamma_0^{SC}(Q) \simeq -\frac{8\pi}{(2m_{red})^2 a_F}\frac{1}{i\Omega_\nu - \xi_{\mathbf{Q}}^B}, \tag{3.53}$$

with $\xi_{\mathbf{Q}}^B = \mathbf{Q^2}/(2m_B) - \mu_B$. Therefore, in the strong-coupling limit, the particle-particle propagator reduces to a non-interacting single-particle propagator (2.27) for composite bosons, up to a multiplicative factor.

For the self-energy (3.42) in the strong-coupling limit, we can neglect the Q dependence of $\mathcal{G}_\sigma^0$ since $|\mu|$ is the dominant scale in the denominator, so we obtain

$$\Sigma_\sigma^{0,SC}(k) \simeq -\mathcal{G}_{\bar{\sigma}}^0(-k)\int\frac{d\mathbf{Q}}{(2\pi)^3}\frac{1}{\beta}\sum_\nu e^{i\Omega_\nu 0^+}\Gamma_0^{SC}(Q), \tag{3.54}$$

and for the same reason, we can truncate the Dyson equation (3.43) as

$$\mathcal{G}_\sigma(k) \simeq \mathcal{G}_\sigma^0(k) + \mathcal{G}_\sigma^0(k)\Sigma_\sigma^{0,SC}(k)\mathcal{G}_\sigma^0(k). \tag{3.55}$$

If we now integrate $\mathcal{G}_\sigma(k)$ to get the density as in (3.44), we have

$$n \simeq n^0 - 2\int \frac{d\mathbf{k}}{(2\pi)^3}\frac{1}{\beta}\sum_n e^{i\omega_n 0^+}\mathcal{G}^0_\sigma(k)^2\mathcal{G}^0_{\bar{\sigma}}(-k)\int \frac{d\mathbf{Q}}{(2\pi)^3}\frac{1}{\beta}\sum_\nu e^{i\Omega_\nu 0^+}\Gamma^{SC}_0(Q), \quad (3.56)$$

where n^0 is simply a free fermion density as in (2.29), that is suppressed in the limit $\beta|\mu| \gg 1$ and can be neglected. By computing the sum over the frequencies ω_n and the $\mathbf{k}$-integral, we evaluate

$$\int \frac{d\mathbf{k}}{(2\pi)^3}\frac{1}{\beta}\sum_n e^{i\omega_n 0^+}\mathcal{G}^0_\sigma(k)^2\mathcal{G}^0_{\bar{\sigma}}(-k) \simeq -\frac{(2m_{red})^2}{8\pi\sqrt{4m_{red}|\mu|}} \simeq -\frac{(2m_{red})^2 a_F}{8\pi}, \quad (3.57)$$

and we notice that this constant factor compensates the factor in the bare bosonic propagator (3.53). Now we can evaluate the sum over the bosonic frequencies Ω_ν with (2.28) to get the density

$$n \simeq 2\int \frac{d\mathbf{k}}{(2\pi)^2}\frac{1}{e^{\beta\xi^B_{\mathbf{Q}}}-1} \equiv 2n_B. \quad (3.58)$$

Therefore, in the BEC limit, the non-self-consistent t-matrix approach correctly recovers a system of non-interacting composite bosons with with mass m_B and density $n_B = n/2$. Indeed, as we know from Section 1.2, we can recover the correct value of the BEC critical temperature by letting $\mu_B \to 0^-$, obtaining

$$T_c^{BEC} = \frac{2\pi}{m_B}\left[\frac{n_B}{\zeta(3/2)}\right]^{2/3}. \quad (3.59)$$

It is interesting to notice that the condition $\mu_B = 0$, used to get the BEC temperature, is equivalent to require that the particle-particle propagator in (3.53) shows a pole at $Q = 0$, i.e. $\Gamma^{SC}_0(Q=0)^{-1} = 0$, that is the Thouless criterion (3.45).

3.2.3 Weak-coupling (BCS) Limit

Let us consider the weak-coupling limit $(k_F a_F)^{-1} \ll -1$ and let us try to recover the mean-field BCS critical temperature (3.33) within the non-self-consistent t-matrix approach. To do this, we impose the Thouless criterion (3.45), which can be rewritten as

$$\frac{2m_{red}}{4\pi a_F} + R^0_{pp}(Q=0)|_{T=T_c} = 0. \quad (3.60)$$

It is important to notice that, by comparing (3.30) with (3.41), the Thouless criterion (3.60) is equivalent to the condition of vanishing gap parameter $\Delta = 0$ in the BCS theory. In the weak-coupling limit, we expect the system to get closer to a non-interacting Fermi gas and, consequently, the critical temperature T_c to be very low. We can therefore take the limit $\mu/T_c \gg 1$ in the renormalized particle-particle bubble, with $\mu = (\mu_\uparrow + \mu_\downarrow)/2$, to obtain

$$R^{0,WC}_{pp}(Q=0)|_{T=T_c} \simeq \frac{(4m_{red})^{3/2}\sqrt{\mu}}{4\pi^2}\left[\ln\left(\frac{2m_{red}}{\sqrt{m_\uparrow m_\downarrow}}\frac{8\mu e^\gamma}{\pi T_c}\right) - 2\right], \quad (3.61)$$

where γ is the Euler constant[5]. By inserting this expression in (3.60) we get

$$T_c \simeq \frac{2m_{red}}{\sqrt{m_\uparrow m_\downarrow}} \frac{8\mu e^\gamma}{\pi e^2} \exp\left(\frac{\pi}{2k_F a_F}\sqrt{\frac{E_F}{\mu}}\right), \tag{3.62}$$

which is exponentially suppressed for $(k_F a_F)^{-1} \ll -1$, as expected. However, we need to understand if μ has some corrections of order $(k_F a_F)$ to E_F, i.e. $\mu \simeq E_F(1 + Ak_F a_F)$, because in that case we would not recover the BCS critical temperature (3.31) precisely due to a constant factor, i.e. $\exp(-\pi A/4)$). To this aim, one can replace the expression (3.62) for T_c in the particle-particle bubble to see that $R_{pp}^{0,WC}(Q)$ is linear in $(k_F a_F)$ for most values of Q (except for $Q \simeq 0$ because of the Thouless criterion) [82], and therefore is sub-leading with respect to $2m_{red}/(4\pi a_F)$. Thus the particle-particle propagator can be approximated as

$$\Gamma_0^{WC}(Q) \simeq -\frac{4\pi a_F}{2m_{red}}, \tag{3.63}$$

while the self-energy reads

$$\Sigma_\sigma^{0,WC}(k) \simeq \frac{4\pi a_F}{2m_{red}} \int \frac{d\mathbf{Q}}{(2\pi)^3} T_c \sum_\nu \frac{1}{i\Omega_\nu - i\omega_n + \xi_{\mathbf{Q}-\mathbf{k}\bar{\sigma}}} = \frac{2\pi a_F}{2m_{red}} n^0, \tag{3.64}$$

where n^0 is the density of non-interacting fermions as in 2.29. In the limit $\mu/T_c \gg 1$ this is given by

$$n^0 = 2\int \frac{d\mathbf{Q}}{(2\pi)^3} \frac{1}{e^{\xi_{\mathbf{Q}\sigma}/T_c} + 1} \simeq 2\int \frac{d\mathbf{Q}}{(2\pi)^3} \theta(\xi_{\mathbf{Q}\sigma}) \simeq \frac{k_\mu^3}{3\pi^2}, \tag{3.65}$$

where $k_\mu = \sqrt{2m_\sigma \mu_\sigma}$. From (3.64), we notice that the self-energy reduces to a constant Σ_σ^0, linear in a_F at leading order. As we will see below, this simply correspond to a *mean-field shift* of the chemical potential. Since $(k_F a_F) \to 0^-$, we can expand the Dyson equation to first order in Σ_σ^0

$$\mathcal{G}_\sigma(k) \simeq \mathcal{G}_\sigma^0(k) + \Sigma_\sigma^0 \mathcal{G}_\sigma^0(k)^2. \tag{3.66}$$

Integrating $\mathcal{G}_\sigma(k)$ as in (3.44) to obtain the total density n, we find a first term that is simply the free contribution n^0 and a second term that is obtained by

$$\begin{aligned} &\int \frac{d\mathbf{k}}{(2\pi)^3} T_c \sum_n e^{i\omega_n 0^+} \Sigma_\sigma^0 \mathcal{G}_\sigma^0(k)^2 \simeq \\ &\frac{2\pi a_F}{m} n^0 \int \frac{d\mathbf{k}}{(2\pi)^3} T_c \sum_n \frac{1}{(i\omega_n - \xi_{\mathbf{k}\sigma})^2} \simeq -\frac{k_\mu}{\pi} n^0 a_F. \end{aligned} \tag{3.67}$$

Therefore, the density in the weak-coupling limit is given by

$$n \simeq n^0 \left(1 - \frac{2k_\mu}{\pi} a_F\right). \tag{3.68}$$

[5]It is important to point out that the result 3.61 holds only in the spin-balanced case. In this way, the integral is computed by splitting it into two parts [81]: one in the range $|k - K_\mu| > k_0$ (with $K_\mu = \sqrt{4m_{red}\mu}$) where the hyperbolic tangent can be set to one, and the other in the range $|k - K_\mu| < k_0$, with k_0 chosen such that $K_\mu k_0/(2m_{red}) \ll T_c$ and $k_0 \ll K_\mu$.

From this relation, by using the expression $n = k_F^3/(3\pi^2)$ for the total density, we can get the chemical potential at first order in $(k_F a_F)$ as

$$\mu \simeq E_F\left(1 + \frac{4k_F a_F}{3\pi}\right), \tag{3.69}$$

and, if we insert this in (3.62), we get the weak-coupling critical temperature

$$T_c \simeq \frac{2m_{red}}{\sqrt{m_\uparrow m_\downarrow}} \frac{8E_F e^\gamma}{\pi e^2} \exp\left(\frac{\pi}{2k_F a_F} - \frac{1}{3}\right) = e^{-1/3}\, T_c^{BCS}. \tag{3.70}$$

This means that, within the non-self-consistent t-matrix approach, the BCS critical temperature is recoverd up to a "spurious" $e^{-1/3}$ factor. However, this factor can be corrected by self-consistently including the self-energy constant Σ_σ^0 (3.64) in the bare propagator $\mathcal{G}_\sigma^0$ within the definition (3.40) for the renormalized particle-particle bubble R_{pp}^0. This is equivalent to perform the shift $\mu_\sigma \to \mu_\sigma - \Sigma_\sigma^0$ in (3.61, which allows one to recover the mean-field result $T_c \simeq T_c^{BCS}$ in (3.33).

3.2.4 Contact in the t-Matrix Approach

As discussed at the end of Section 1.5.2, within the t-matrix approximation we can recover the correct value of the contact C in both weak-coupling and strong-coupling limits. The most straightforward way to obtain C is to relate it to the trace of the particle-particle propagator Γ_0, denoted with Δ_∞^2, as

$$C = (2m_{red}\Delta_\infty)^2 \equiv (2m_{red})^2 \int \frac{d\mathbf{Q}}{(2\pi)^3} \frac{1}{\beta} \sum_\nu e^{i\Omega_\nu 0^+} \Gamma_0(Q). \tag{3.71}$$

This is because, for large $\mathbf{k}$, the approximation performed in the integrand of (3.56) holds up for any coupling, and one obtains

$$n_\sigma(\mathbf{k}) \xrightarrow{k\to\infty} -\Delta_\infty^2 \frac{1}{\beta} \sum_n \mathcal{G}_\sigma^0(k)^2 \mathcal{G}_{\bar\sigma}^0(-k). \tag{3.72}$$

If one now performs the sum over the fermionic Matsubara frequencies on the right hand side, for large $\mathbf{k}$ one obtains

$$\Delta_\infty^2 \frac{1}{\beta} \sum_n \mathcal{G}_\sigma^0(k)^2 \mathcal{G}_{\bar\sigma}^0(-k) \simeq -\Delta_\infty^2 \frac{1}{(\xi_{\mathbf{k}\sigma} + \xi_{\mathbf{k}\bar\sigma})^2} \simeq -\Delta_\infty^2 \frac{(2m_{red})^2}{\mathbf{k}^4} \tag{3.73}$$

and therefore, using the definition in (1.35), the identification in (3.71) is immediate.

The quantity Δ_∞^2, therefore the contact C, can be evaluated analytically in the BCS and BEC limits in the spin-balanced case. In the strong-coupling limit, using the approximate form for Γ_0 in (3.53), we get

$$C^{SC} \simeq -\frac{8\pi}{a_F} \int \frac{d\mathbf{Q}}{(2\pi)^3} \frac{1}{\beta} \sum_\nu e^{i\Omega_\nu 0^+} \frac{1}{i\Omega_\nu - \xi_{\mathbf{Q}}^B} = \frac{8\pi}{a_F} n_B = \frac{4\pi}{a_F} n. \tag{3.74}$$

This result coincides with the one obtained from the adiabatic relation 1.37 with the leading-order expression for the energy $E = -\frac{N}{2}\varepsilon_0 = -N/(4m_{red}a_F^2)$ in this limit. In the weak-coupling limit, we expand Γ_0 to second order in $4\pi a_F/(2m_{red})$, so that

$$\Gamma_0^{WC}(Q) \simeq -\frac{4\pi a_F}{2m_{red}}\left(1 - \frac{4\pi a_F}{2m_{red}}R_{pp}^0(Q)\right), \tag{3.75}$$

and this yields

$$C^{WC} \simeq (4\pi a_F)^2 \int \frac{d\mathbf{Q}}{(2\pi)^3}\frac{1}{\beta}\sum_\nu \int \frac{d\mathbf{k}}{(2\pi)^3}\frac{1}{\beta}\sum_n \mathcal{G}_\uparrow^0(k+Q)\mathcal{G}_\downarrow^0(-k) = (2\pi a_F n)^2, \tag{3.76}$$

which agrees with what reported at the end of Section 1.5.2.

3.3 Luttinger-Ward Approach

When dealing with spin imbalanced systems, the non-self-consistent t-matrix approach presents a problem: the *spin susceptibility* $\chi_s = dM/dh$, where $M = n_\uparrow - n_\downarrow$ is the magnetization and $h = (\mu_\uparrow - \mu_\downarrow)/2$ is the imbalancing field, is negative for the balanced system near unitarity slightly above T_c [83]. This means that, for this approach, there is a region where a small imbalance of the chemical potentials $\mu_\uparrow > \mu_\downarrow$ produces the non-physical result of an opposite imbalance of the densities $n_\uparrow < n_\downarrow$.

More generally, we can make an improvement of the non-self-consistent t-matrix with the inclusion of self-consistency in the equations. One can consider the partial or full inclusion of self-consistency, but in this thesis we will consider just the latter case, known as *Luttinger-Ward approach* [84] or simply *fully self-consistent t-matrix* [45, 46]. This approach compares well with experimental data and Quantum Monte Carlo (QMC) calculations for several thermodynamic quantities in the balanced case [36–41]. In addition, as we will see below and in Section (4.3.1) respectively, the fully self-consistent approach respects the requirement of *conserving approximation* and therefore satisfies the *Luttinger theorem* for the Fermi surfaces of the two spin components, a property which is particularly important to describe in a consistent way the spin-imbalanced Fermi liquid phase.

The main idea of the Luttinger-Ward approach is very simple: we take all the equations introduced in the non-self-consistent t-matrix and we substitute all the bare propagators $\mathcal{G}^0$ with dressed propagators $\mathcal{G}$ in the ladder and self-energy diagrams. Therefore, we get the following t-matrix equations:

$$\mathcal{G}_\sigma(k) = \frac{1}{\mathcal{G}_\sigma^0(k)^{-1} - \Sigma_\sigma(k)}, \tag{3.77}$$

$$\Sigma_\sigma(k) = -\int \frac{d\mathbf{Q}}{(2\pi)^3}\frac{1}{\beta}\sum_\nu \Gamma(Q)\mathcal{G}_{\bar\sigma}(Q-k), \tag{3.78}$$

$$\Gamma(Q) = -\frac{1}{2m_{red}/(4\pi a_F) + R_{pp}(Q)}, \tag{3.79}$$

$$R_{pp}(Q) = \int \frac{d\mathbf{k}}{(2\pi)^3}\left(\frac{1}{\beta}\sum_n \mathcal{G}_\uparrow(k+Q)\mathcal{G}_\downarrow(-k) - \frac{2m_{red}}{\mathbf{k}^2}\right). \tag{3.80}$$

Within this approach, all the considerations done for the non-self-consistent t-matrix in Section 3.2 still apply: the chemical potentials μ_σ can be obtained by inverting the density equations (3.44), while the transition line normal-superfluid can be found by generalizing the Thouless criterion in Section 3.2.1 to the dressed particle-particle propagator, i.e. simply by substituting Γ_0 with Γ. In particular, this substitution also holds for the contact in (3.71). Notice that this approach automatically includes the mean-field shift Σ^0 discussed in Section 3.2.3, and therefore correctly recovers the BCS critical temperature in the weak-coupling limit without any spurious factor.

Obviously, the only possibility to solve the self-consistent equations (3.77-3.80) is via numerical methods. Therefore, in order to calculate the Green's function $\mathcal{G}$, the simplest method is to solve them iteratively and try to converge to a stable solution. In this procedure it is convenient to Fourier transform $\mathcal{G}$, Γ, Σ and R_{pp}, from the $(\mathbf{k},\omega_n)$ and $(\mathbf{Q},\Omega_n)$ spaces to the $(\mathbf{x},\tau)$ space, with the relations

$$\mathcal{G}_\sigma(\mathbf{x},\tau) = \int \frac{d\mathbf{k}}{(2\pi)^3}\frac{1}{\beta}\sum_n e^{i(\mathbf{k}\cdot\mathbf{x}-\omega_n\tau)}\mathcal{G}_\sigma(\mathbf{k},\omega_n), \tag{3.81}$$

$$\Gamma(\mathbf{x},\tau) = \int \frac{d\mathbf{Q}}{(2\pi)^3}\frac{1}{\beta}\sum_n e^{i(\mathbf{Q}\cdot\mathbf{x}-\Omega_\nu\tau)}\Gamma(\mathbf{Q},\Omega_\nu), \tag{3.82}$$

and analogous expressions for $\Sigma_\sigma(\mathbf{k},\omega_n)$ and $R_{pp}(\mathbf{Q},\Omega_\nu)$. These transformations are very useful because allows one to pass from convolution products in (3.78) and (3.80) to simple algebraic products in the transformed space

$$\Sigma_\sigma(\mathbf{x},\tau) = -\Gamma(\mathbf{x},\tau)\mathcal{G}_{\bar\sigma}(-\mathbf{x},-\tau), \tag{3.83}$$

$$R_{pp}(\mathbf{x},\tau) = \mathcal{G}_\uparrow(\mathbf{x},\tau)\mathcal{G}_\downarrow(\mathbf{x},\tau) - \Lambda\delta(\mathbf{x})\delta(\tau), \tag{3.84}$$

where $\Lambda = \int_{|\mathbf{k}|\leq k_0} d\mathbf{k}/(2\pi)^3[2m_{red}/\mathbf{k}^2]$ is a divergent constant in the $k_0\to\infty$ limit for the contact potential, introduced in Section 3.1.3. Therefore, we will always work with the difference

$$\Delta R_{pp}(\mathbf{x},\tau) \equiv R_{pp}(\mathbf{x},\tau) - R^0_{pp}(\mathbf{x},\tau) = \mathcal{G}_\uparrow(\mathbf{x},\tau)\mathcal{G}_\downarrow(\mathbf{x},\tau) - \mathcal{G}^0_\uparrow(\mathbf{x},\tau)\mathcal{G}^0_\downarrow(\mathbf{x},\tau), \tag{3.85}$$

such that we avoid dealing with the diverging constant Λ. In this way, we recover $R_{pp}(\mathbf{Q},\Omega_\nu)$ by transforming back (3.85) and then by adding the non-self-consistent bubble $R^0_{pp}(\mathbf{Q},\Omega_\nu)$. In Figure 3.5 we reported the two flowcharts for the non-self-consistent t-matrix and Luttinger-Ward approaches, in which the self-consistent iterative procedure is represented by a cycle. Notice that, in the first iteration of the self-consistent cycle, the value of $\mathcal{G}_\sigma(\mathbf{k},\omega_n)$ is obtained from non-self-consistent approach.

Most of the functions that we are going to Fourier transform in the self-consistent cycle show a slowly decaying tail in the variables $(\mathbf{k},\omega_n)$ and $(\mathbf{Q},\Omega_\nu)$, which corresponds to a singular behavior for $(\mathbf{x},\tau)\to 0^+$. Because of the periodicity properties of these functions, these singularities typically occur also for $\tau\to\beta^-$. Therefore, the functions to be transformed should be evaluated on scales that accumulate points

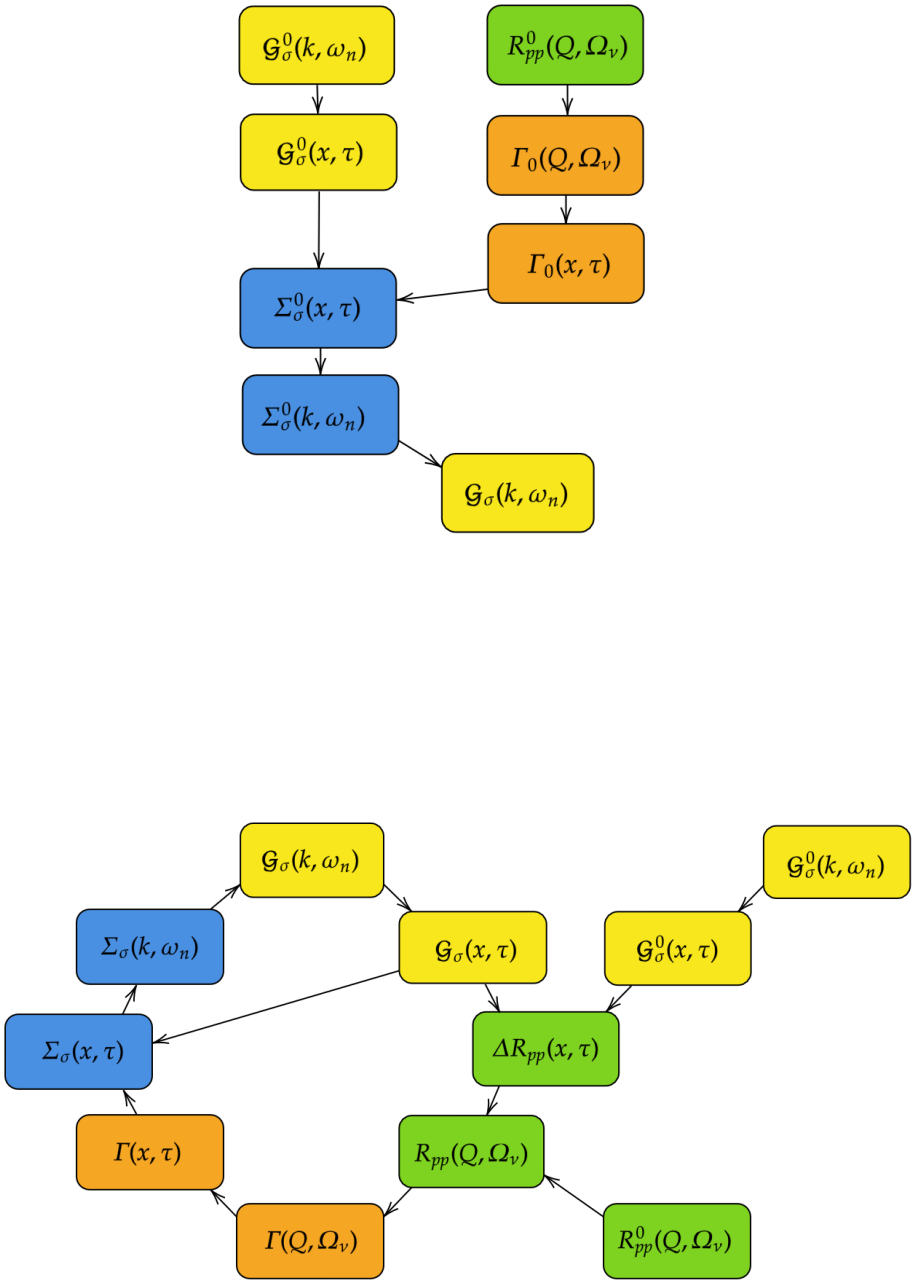

Figure 3.5: Flowcharts of the procedures in the t-matrix approximation: obtaining the dressed Green's function in the non-self-consistent approach (above) and achievement of full self-consistency in the Luttinger-Ward approach (below).

near these peaks, but clearly in this case, a standard fast Fourier transformation (FFT) cannot be applied because a constant step width would be needed. Nonetheless, consistent Fourier transforms for a generic grid of points can be obtained following the *Haussmann's prescriptions* [85, 86], discussed in Appendix A[6].

As discussed in detail in Appendix B, it is also necessary to subtract some appropriate semi-analytic expressions from the functions to be Fourier transformed in order to make their singular behavior weaker, or equivalently, their slow decay faster. Moreover, we need some optimization procedures to achieve the convergence toward self-consistency, which are particularly important close to T_c. This is because, as shown in Appendix C, in that region the iterative procedure in Figure 3.5 does not work properly.

3.3.1 Conserving Approximations

Even if we have included full self-consistency, the expression (3.78) for the self-energy is obviously not exact because we are still working in the t-matrix approximation. However, it is important to check if our approximation still respects conservation laws that are valid for the exact theory, like the particles number, the momentum and the energy. If these laws still hold in the approximated theory, this is said to be *conserving*. A general method for generating conserving approximations is given by the *Baym-Kadanoff theorem* [87,88]. This theorem states that a sufficient condition for an approximated theory to be conserving is that its self-energy Σ can be written as a functional derivative

$$\Sigma_{\sigma\sigma'}(x, x') = \frac{\delta\Phi}{\delta\mathcal{G}_{\sigma\sigma'}(x, x')}, \tag{3.86}$$

where Φ is a functional of only dressed single-particle Green's functions $\mathcal{G}$ and interaction lines V. Here, we used the compact notation $x \equiv (\mathbf{x}, \tau)$. In terms of Feynman diagrams, as shown in Figure 3.6, the functional derivative simply consists of removing a particle line in the term for Φ, leading to the self-energy contribution of the t-matrix approximation. Notice that only the Luttinger-Ward approach respects this requirement, as it is the only one that can be derived by a functional Φ that is not built also with bare Green's functions $\mathcal{G}^0$. Indeed, the non-self-consistent t-matrix approximation and all the other partially self-consistent versions are clearly non-conserving.

Conserving approximations are particularly useful in non-equilibrium phenomena like transport, but they have also some important implications on the equilibrium properties of the theory, which are the ones we will focus on in this thesis. Consider, for instance, the link clustered expansion in (2.22) for a Φ-derivable conserving theory. In this case, we can rewrite the expansion for the grand-potential Ω in

[6]It is important to point out at least two other cases in which a Fourier transform that accumulates points near specific regions becomes essential. The first one is in the presence of strong FFLO fluctuations, where the particle-particle propagator $\Gamma(\mathbf{Q}, \Omega_\nu)$ for a spin-imbalanced system is strongly peaked near a finite momentum $\mathbf{Q}_0$. The second one is in weak-coupling limit and at low temperatures, where the functions can exhibit the presence of sharp Fermi surfaces.

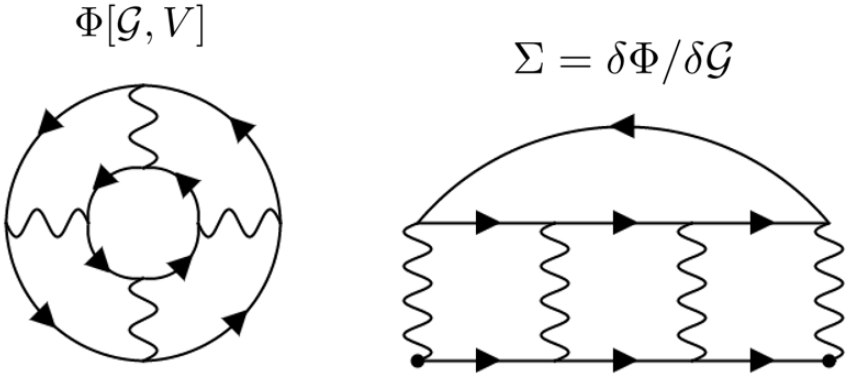

Figure 3.6: Diagrammatic representation of the functional $\Phi[\mathcal{G}, V]$ for a typical term in the t-matrix approximation (left) a the corresponding self-energy Σ (right). In particular, in the figure is reported the 4-th order diagram for Φ and Σ.

terms of the functional Φ as

$$\Omega[\mathcal{G}] = \mp\frac{1}{\beta}(\Phi[\mathcal{G}] - \mathrm{Tr}[\mathcal{G}\Sigma] + \mathrm{Tr}[\ln(-\mathcal{G})]), \tag{3.87}$$

where with the symbol trace we mean integration over all the $\mathbf{x}$ and τ variables and sum over all the spin indices σ, i.e.

$$\mathrm{Tr}[X] = \int d\mathbf{x}\, d\mathbf{x}' \int_0^\beta d\tau\, d\tau' \sum_{\sigma,\sigma'} X_{\sigma\sigma'}(\mathbf{x}\tau, \mathbf{x}'\tau'). \tag{3.88}$$

An important aspect of conserving approximations is that the thermodynamic quantities derived by the grand-canonical potential (3.87) or directly by the Green's function of the system are the same, so that we have a consistent picture of thermodynamic properties. As a concrete example, we consider the average total number of particles, derived from the grand-potential as

$$N \equiv \langle \hat{N} \rangle = \frac{\partial \Omega}{\partial \mu}. \tag{3.89}$$

This value is guaranteed to coincide with the same calculated directly from the single-particle Green's function in (2.15) only if the the approximation is conserving. On the contrary, in the non-self-consistent or partially self-consistent approaches, we do not expect that they satisfy these thermodynamic relations, and therefore we must specify in which way we are calculating the different quantities[7].

[7]The first original work on pairing fluctuations within the BCS-BEC crossover is known as *Nozières-Schmitt-Rink approach* (NSR) [9]. In this work, differently from the non-self-consistent t-matrix, the density was derived from a thermodynamic potential that is obtained by closing the ladder diagrams. Except when the self-energy corrections are small, the non-self-consistent t-matrix and NSR approaches are not equivalent since they are both non-conserving, and the former might yield a sensible result when the latter does not.

The same happens also with the Tan's contact, discussed in Section 1.5.2. The value of C obtained with the definition (1.35) and the one obtained using the adiabatic relations (1.37) are guaranteed to coincide only if we work with conserving approximations, like the Luttinger-Ward approach.

Chapter 4

Landau Theory of Fermi Liquids

For large polarization and not too strong interactions, our mixture of ultra-cold Fermi gases remains in the normal phase even at zero temperature. Therefore, in this region, the system is well described by the Landau theory of Fermi liquids. In this chapter we present the main aspects of the Landau phenomenological theory, based on physical arguments (for a review of Fermi liquid theory see Refs. [89–91]). Then, we connect it to a microscopic description in terms of the diagrammatic many-body approaches, relating the quasi-particle properties to the fermionic self-energy and the spectral weight function. Furthermore, we consider the $T = 0$ formulation of the Luttinger-Ward approach, which satisfies the important Luttinger theorem, and we briefly show how the Fermi liquid description breaks down in our system at the superfluid quantum critical point (QCP).

4.1 The Quasi-particle Concept

The phenomenological theory of *Fermi liquids*, originally developed by Landau for the description of liquid ^{3}He [92–94], deals with the properties of interacting many-fermion systems at low temperatures (much lower than the Fermi energy, i.e. $T \simeq 0$). It has applications in many fields of physics, from the low-energy behavior of electrons in metals to ultra-cold Fermi gases.

The main assumption of this theory is a continuous one-to-one correspondence between the eigenstates (ground state and excited states) of the non-interacting system (Fermi gas) and interacting system (Fermi liquid), as the interaction is *adiabatically switched-on*. It is crucial to notice that this adiabatic continuity assumption can be acceptable only if the interactions do not lead to any form of phase transition or symmetry-broken ground state[1]. In this way, the elementary excitations of a Fermi liquid, known as *quasi-particles* and *quasi-holes*, are in direct correspondence with the (particle or hole) excitations of the ideal Fermi gas[2]. Consequently, they carry the same quantum numbers and satisfy the Fermi-Dirac statistics.

[1] It is also interesting to point out that, in a 1D interacting fermion gas, Fermi liquid theory breaks down without the occurrence of a broken symmetry state. In this case, the correct theoretical counterpart of a Fermi liquid is known in literature as *Luttinger liquid*.

[2] Generally, the term "quasi-particles" refers to the elementary excitations whatever their relation to the bare particles. As we will see, in the Fermi liquid theory, it has a narrower sense.

As a starting point, it is useful to introduce the concept of quasi-particle by extending the concept of particle of the non-interacting system. Let us start with the ideal Fermi gas at $T = 0$ and for simplicity consider a three-dimensional balanced and isotropic system. The ground state consists in a sphere in momentum space, i.e. the *Fermi sphere*, filled with fermions up to the Fermi momentum k_F. The mean particle density n is then related to k_F by the well-known relation

$$n = 2 \int \frac{d\mathbf{k}}{(2\pi)^3} \theta(k_F - |\mathbf{k}|) = \frac{k_F^3}{3\pi^2}, \tag{4.1}$$

while the ground state energy is given by

$$E^0 = 2V \int \frac{d\mathbf{k}}{(2\pi)^3} \varepsilon_{\mathbf{k}}^0 \theta(k_F - |\mathbf{k}|) = \frac{3}{5} N E_F, \tag{4.2}$$

where $\varepsilon_{\mathbf{k}}^0 = \mathbf{k}^2/(2m)$ is the free fermion dispersion and $E_F = k_F^2/(2m) \equiv \mu(T = 0)$ the Fermi energy. If we consider a deviation $\delta n_{\mathbf{k}\sigma}$ from the distribution function $n_{\mathbf{k}}^0 = \theta(k_F - |\mathbf{k}|)$, the corresponding change in total energy is

$$\delta E[\delta n_{\mathbf{k}\sigma}] = V \sum_{\sigma} \int \frac{d\mathbf{k}}{(2\pi)^3} \varepsilon_{\mathbf{k}}^0 \delta n_{\mathbf{k}\sigma}. \tag{4.3}$$

For the non-interacting system, an *elementary excitation* corresponds to a particle added to or removed from the ground state (hole). Correspondingly, from (4.3), we get that the energy of any excited state is obtained by summing the energy of the added particle or hole.

Let us now add a particle with momentum $\mathbf{k}$ ($|\mathbf{k}| > k_F$) and spin σ to the ground state of the ideal gas. As soon as one adiabatically switches on the interactions, the particle is no longer in an eigenstate of the system and it may undergo several decay processes; in other words, it is damped and acquires a finite lifetime. Central to Fermi liquid theory is the fact that the lifetime becomes larger and larger at low energy ($|\mathbf{k}| \to k_F$)[3]. Thus, the state obtained by adding a low-lying ($|\mathbf{k}| \simeq k_F$) particle to the non-interacting Fermi sea evolves into a quasi-eigenstate of the interacting system, which is referred to as a quasi-particle. Similarly, one can define a quasi-hole by removing a particle with momentum $|\mathbf{k}| \simeq k_F$ from the non-interacting Fermi sea. Because of the one-to-one correspondence between particle (or hole) excitations in the ideal Fermi gas and quasi-particle excitations in the Fermi liquid, the quasi-particles are fermions and therefore follow the Fermi-Dirac statistics. Furthermore, conserved quantities like spin and charge are unchanged, whereas the interaction affects the value of other quantities like the quasi-particle dispersion, the particle momentum distribution and the (effective) mass.

[3]More precisely, one gets $\tau_{\mathbf{k}}^{-1} \propto (\pi T)^2 + \xi_{\mathbf{k}}^2$. This result is correctly obtained from the collision term of the *Boltzmann equation*, used to describe non-equilibrium situations in the system [89]. Actually, the long lifetime of quasi-particles close to the Fermi surface has also an explanation in terms of phase-space arguments. Consider the process where a particle in the state $\mathbf{k}$ above the Fermi sea is scattered into the state $\mathbf{k} + \mathbf{q}$ by creating a particle-hole pair $(\mathbf{k}', \mathbf{k}' - \mathbf{q})$. Because of energy conservation, the phase phase available for this scattering process is proportional to $(|\mathbf{k}| - k_F)^2$ [90].

In the interacting Fermi liquid at $T = 0$, the change in energy due a change $\delta n_{\mathbf{k}\sigma}$ in the quasi-particle distribution function $n^0_{\mathbf{k}} = \theta(k_F - |\mathbf{k}|)$ (not to be confused with the particle distribution in the interacting system) reads

$$\delta E[\delta n_{\mathbf{k}\sigma}] = V \sum_{\sigma} \int \frac{d\mathbf{k}}{(2\pi)^3} \varepsilon_{\mathbf{k}} \delta n_{\mathbf{k}\sigma}, \tag{4.4}$$

where $\varepsilon_{\mathbf{k}}$ is the quasi-particle dispersion which, for $|\mathbf{k}| > k_F$ ($|\mathbf{k}| < k_F$), represents the energy of a single quasi-particle (quasi-hole). The expression (4.4) is correct only if the number of quasi-particles is small enough to neglect interactions among them. If this is not the case, the energy variation can be written as

$$\delta E[\delta n_{\mathbf{k}\sigma}] = V \sum_{\sigma} \int \frac{d\mathbf{k}}{(2\pi)^3} \tilde{\varepsilon}_{\mathbf{k}} \delta n_{\mathbf{k}\sigma} + \frac{V}{2} \sum_{\sigma\sigma'} \int \frac{d\mathbf{k} d\mathbf{k}'}{(2\pi)^6} f_{\sigma\sigma'}(\mathbf{k}, \mathbf{k}') \delta n_{\mathbf{k}\sigma} \delta n_{\mathbf{k}'\sigma'}, \tag{4.5}$$

where we now denoted with $\tilde{\varepsilon}_{\mathbf{k}}$ the energy of a quasi-particle alone. The *Landau function* $f_{\sigma\sigma'}(\mathbf{k}, \mathbf{k}')$ characterizes the interaction between the quasi-particles and it is completely determined by a small number of multipole phenomenological parameters called *Landau parameters*[4] [91]. Indeed, the power of the Landau Fermi liquid theory lies in its ability to parameterize the interactions in terms of these few values.

The "dressed" dispersion $\varepsilon_{\mathbf{k}}$, corresponding to the energy of a quasi-particle surrounded by a gas of quasi-particles of density $n_{\mathbf{k}\sigma}$, is defined as the variation of the total energy of the system due to the introduction of this quasi-particle. Mathematically, this means that $\varepsilon_{\mathbf{k}}$ is given by the functional derivative

$$\varepsilon_{\mathbf{k}} = \frac{\delta E}{\delta n_{\mathbf{k}\sigma}} = \tilde{\varepsilon}_{\mathbf{k}} + \sum_{\sigma'} \int \frac{d\mathbf{k}'}{(2\pi)^3} f_{\sigma\sigma'}(\mathbf{k}, \mathbf{k}') \delta n_{\mathbf{k}'\sigma'}. \tag{4.6}$$

Given that we are mainly interested in phenomena in the vicinity of the Fermi surface, we can linearize the quasi-particle dispersion as

$$\varepsilon_{\mathbf{k}} = \mu + \frac{k_F}{m^*}(|\mathbf{k}| - k_F) + o((|\mathbf{k}| - k_F)^2), \tag{4.7}$$

thus defining the *effective mass* as

$$\frac{1}{m^*} = \frac{1}{k_F} \frac{\partial \varepsilon_{\mathbf{k}}}{\partial \mathbf{k}}\bigg|_{|\mathbf{k}|=k_F}, \tag{4.8}$$

which is different from the "bare" mass m due to interaction effects that could in principle be calculated from a microscopic theory of the system.

It should be emphasized that quasi-particle and quasi-hole excitations are not necessarily the only elementary excitations in the interacting system. The adiabatic continuity hypothesis does not exclude the possibility of other elementary excitations of the real system which disappear when the interaction is reduced to zero.

[4] As far as equilibrium properties are concerned, Landau's theory has little quantitative predictive power because the crucial Landau parameters have actually to be determined from experiment. Nevertheless, it makes some important qualitative predictions, the most prominent being that even in the presence of interactions the low–temperature specific heat remains linear in temperature and that the spin susceptibility tends to a constant as $T \to 0$. The situation is different for non–equilibrium situations, where the existence of new phenomena, in particular *collective modes*, is quantitatively predicted. These modes are another kind of elementary excitations which, contrary to quasi-particles, involve a coherent motion of the whole system.

4.2 Microscopic Basis of Fermi Liquid Theory

Although Landau's Fermi liquid theory is a phenomenological theory, based on physical arguments, it translates naturally into the language of diagramatic many-body theory. The main goal of this microscopic approach to Fermi liquid theory is to show how the quasi-particle concept emerges from the single-particle Green function[5].

Let us first recall that the non-interacting system is described by the retarded Green's function (see also Section 2.3)

$$G^{0,R}(\mathbf{k},t) = \int_{-\infty}^{\infty} \frac{d\omega}{2\pi} \frac{e^{-i\omega t}}{\omega - \xi^0_{\mathbf{k}} + i0^+} = -i\theta(t) e^{-i\xi_{\mathbf{k}} t}, \tag{4.9}$$

where $\xi^0_{\mathbf{k}} = \mathbf{k}^2/(2m) - \mu$ is the usual free particle dispersion minus the chemical potential, while the corresponding spectral weight function is given by

$$A^0(\mathbf{k},\omega) = -\frac{1}{\pi} \operatorname{Im} G^{0,R}(\mathbf{k},\omega) = \delta(\omega - \xi^0_{\mathbf{k}}), \tag{4.10}$$

which is a Dirac peak located at the excitation energy $\xi^0_{\mathbf{k}}$.

Microscopically, when the interactions are adiabatically switched-on, we expect a shift and a broadening of the Dirac peak in the non-interacting spectral function (4.10). This peak represents the quasi-particle contribution, is located at the *quasi-particle excitation energy* $\xi_{\mathbf{k}}$ and has a width $\gamma_{\mathbf{k}} = 1/(2\tau_{\mathbf{k}})$, where $\tau_{\mathbf{k}}$ is *quasi-particle lifetime*. Moreover, we also expect the presence of a "featureless" *incoherent background* from the contribution of multi-particle excitations, which can extend to rather high energies but becomes small close to the Fermi surface. As shown in Figure 4.1, we deduce that the spectral weight function which defines a Fermi liquid can be written as

$$A(\mathbf{k},\omega) = \frac{Z_{\mathbf{k}}}{\pi} \frac{\gamma_{\mathbf{k}}}{(\omega - \xi_{\mathbf{k}})^2 + \gamma^2_{\mathbf{k}}} + A_{inc}(\mathbf{k},\omega), \tag{4.11}$$

where the quasi-particle peak (first term) assumes the form of a *Lorentzian distribution* with spectral weight $Z_{\mathbf{k}}$ ($0 \leq Z_{\mathbf{k}} \leq 1$), known as *quasi-particle residue*. The corresponding retarded Green's function is given by

$$G^R(\mathbf{k},\omega) = \int_{-\infty}^{\infty} d\omega' \frac{A(\mathbf{k},\omega')}{\omega - \omega' + i0^+} = \frac{Z_{\mathbf{k}}}{\omega - \xi_{\mathbf{k}} + i\gamma_{\mathbf{k}}} + G^R_{inc}(\mathbf{k},\omega), \tag{4.12}$$

and, by Fourier transforming to $(\mathbf{k},t)$ space, we obtains

$$G^R(\mathbf{k},t) = -iZ_{\mathbf{k}}\theta(t) e^{-\gamma_{\mathbf{k}} t} e^{-\xi_{\mathbf{k}} t} + G^R_{inc}(\mathbf{k},t). \tag{4.13}$$

Because $A_{inc}(\mathbf{k},\omega)$ has no sharp structure in the frequency, the incoherent part $G^R_{inc}(\mathbf{k},t)$ of the Green function decays quickly in time, and the long-time behavior

[5]For completeness, we just point out that the Landau function $f_{\sigma,\sigma'}(\mathbf{k},\mathbf{k}')$ admits a microscopic interpretation in terms of the *particle-hole vertex* function Γ_{ph}, but we will not discuss it in this thesis.

is dominated by the quasi-particle part. Therefore, for $|\xi_{\mathbf{k}}|^{-1} \ll t \ll \tau_{\mathbf{k}}$ one observes the oscillating behavior characteristic of an eigenstate of the Hamiltonian. Equation (4.13) confirms the interpretation of $\tau_{\mathbf{k}}$ as the lifetime of the quasi-particle. Furthermore, the oscillating part of the Green function is reduced by a factor $Z_{\mathbf{k}}$ in the interacting system. Thus, $Z_{\mathbf{k}}$ is a measure of the overlap between the particle state with momentum $\mathbf{k}$ and spin σ and the quasi-particle state with same momentum and spin; it can be seen as the fraction of bare particle contained in the quasi-particle.

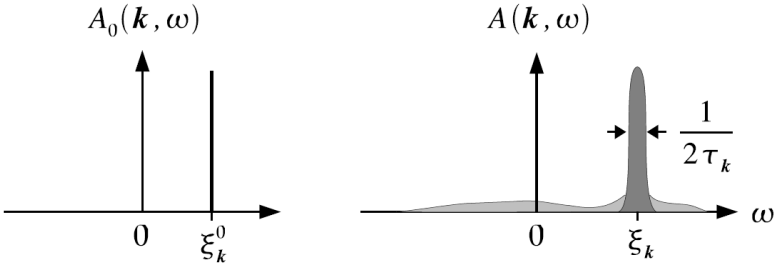

Figure 4.1: Spectral function in an ideal Fermi gas (left) and in a Fermi liquid (right). The dark shaded area shows the quasi-particle peak and the light shaded one the incoherent part of the spectrum. *Source*: reproduced from Ref. [90].

The existence of quasi-particles with reduced spectral weight has an important consequence for the momentum distribution function of the bare particles

$$n_{\mathbf{k}\sigma} = -i \int_{-\infty}^{\infty} \frac{d\omega}{2\pi} e^{i\omega 0^+} G^R(\mathbf{k},\omega) = \int_{-\infty}^{0} d\omega \; A(\mathbf{k},\omega). \tag{4.14}$$

When $\tau_{\mathbf{k}}^{-1} \ll |\xi_{\mathbf{k}}|$, the quasi-particle peak in $A(\mathbf{k},\omega)$ becomes sharper and sharper as we approach the Fermi surface and tends to $Z_{\mathbf{k}}\delta(\omega - \xi_{\mathbf{k}})$ for $\xi_{\mathbf{k}} \to 0$. Since the incoherent part of the spectral function varies smoothly with $\mathbf{k}$, it is continuous across the Fermi level. Therefore, a typical characteristic of a Fermi liquid is a sudden jump at k_F in the momentum distribution, exactly as in the non-interacting system, with magnitude given by the quasi-particle residue $\mathcal{Z} \equiv Z_{\mathbf{k}}|_{|\mathbf{k}|=k_F}$.

4.2.1 Self-Energy and Quasi-particle Properties

The quasi-particle properties, such as the excitation energies, residues, effective masses and lifetimes, can be related to the self-energy of the system. In the interacting system, the retarded Green's function and the spectral weight, introduced in Section 2.3, can be expressed in terms of the retarded self-energy as

$$G^R(\mathbf{k},\omega) = \frac{1}{\omega - \xi_{\mathbf{k}}^0 - \Sigma^R(\mathbf{k},\omega) + i0^+}, \tag{4.15}$$

$$A(\mathbf{k},\omega) = -\frac{1}{\pi} \frac{\operatorname{Im}\Sigma^R(\mathbf{k},\omega)}{(\omega - \xi_{\mathbf{k}}^0 - \operatorname{Re}\Sigma^R(\mathbf{k},\omega))^2 + (\operatorname{Im}\Sigma^R(\mathbf{k},\omega))^2}, \tag{4.16}$$

where the last expression holds only if $\operatorname{Im}\Sigma^R(\mathbf{k},\omega) \neq 0$, otherwise if $\operatorname{Im}\Sigma^R(\mathbf{k},\omega) = 0$ we have

$$A(\mathbf{k},\omega) = \delta(\omega - \xi_{\mathbf{k}}^0 - \operatorname{Re}\Sigma^R(\mathbf{k},\omega)). \tag{4.17}$$

Therefore, we readily get that the quasi-particle energy $\xi_{\mathbf{k}}$, i.e. the position of the maximum in the Lorentzian peak (4.11), is determined by the equation

$$\xi_{\mathbf{k}} = \xi^0_{\mathbf{k}} + \mathrm{Re}\,\Sigma^R(\mathbf{k}, \xi_{\mathbf{k}}), \tag{4.18}$$

if $\mathrm{Im}\,\Sigma^R(\mathbf{k}, \omega)$ varies weakly for $\omega \simeq \xi_{\mathbf{k}}$, i.e. $\partial_\omega \,\mathrm{Im}\,\Sigma^R(\mathbf{k}, \omega)|_{\omega=\xi_{\mathbf{k}}} = 0$. In particular, the chemical potential is obtained from $\xi_{k_F} = 0$, that is

$$\mu = \frac{k_F^2}{2m} + \Sigma^R(k_F, 0), \tag{4.19}$$

where we used the fact that $\Sigma^R(k_F, 0)$ is real at zero temperature [90]. Furthermore, by comparing (4.16) with (4.11), we immediately get the relation among the quasi-particle spectral width, the residue and the imaginary part of the retarded self-energy

$$\gamma_{\mathbf{k}} = -Z_{\mathbf{k}}\,\mathrm{Im}\,\Sigma^R(\mathbf{k}, \xi_{\mathbf{k}}). \tag{4.20}$$

If we now expand the retarded self-energy for $\omega \simeq \xi_{\mathbf{k}}$ as

$$\Sigma^R(\mathbf{k}, \omega) \simeq \mathrm{Re}\,\Sigma^R(\mathbf{k}, \xi_{\mathbf{k}}) + i\,\mathrm{Im}\,\Sigma^R(\mathbf{k}, \xi_{\mathbf{k}}) + (\omega - \xi_{\mathbf{k}}) \frac{\partial}{\partial \omega}\,\mathrm{Re}\,\Sigma(\mathbf{k}, \omega)\bigg|_{\omega=\xi_{\mathbf{k}}}, \tag{4.21}$$

use (4.18) and the expression

$$\omega - \xi^0_{\mathbf{k}} - \Sigma^R(\mathbf{k}, \omega) = \frac{\omega - \xi_{\mathbf{k}} + i\gamma_{\mathbf{k}}}{Z_{\mathbf{k}}}, \tag{4.22}$$

obtained by direct comparison with (4.12) and (4.15), we get the relation between the quasi-particle residue and the real part of the retarded self-energy

$$Z_{\mathbf{k}} = \left[1 - \frac{\partial}{\partial \omega}\,\mathrm{Re}\,\Sigma^R(\mathbf{k}, \omega)\bigg|_{\omega=\xi_{\mathbf{k}}}\right]^{-1}. \tag{4.23}$$

By requiring that the quasi-particle residue satisfies $0 \leq Z_{\mathbf{k}} \leq 1$, the condition

$$\frac{\partial}{\partial \omega}\,\mathrm{Re}\,\Sigma^R(\mathbf{k}, \omega)\bigg|_{\omega=\xi_{\mathbf{k}}} \leq 0, \tag{4.24}$$

naturally follows. We then differentiate (4.18) with respect to $\mathbf{k}$

$$\frac{\partial \xi_{\mathbf{k}}}{\partial \mathbf{k}} = \frac{\partial \xi^0_{\mathbf{k}}}{\partial \mathbf{k}} + \frac{\partial\,\mathrm{Re}\,\Sigma^R(\mathbf{k}, \xi_{\mathbf{k}})}{\partial \mathbf{k}} + \frac{\partial \xi_{\mathbf{k}}}{\partial \mathbf{k}} \frac{\partial\,\mathrm{Re}\,\Sigma^R(\mathbf{k}, \omega)}{\partial \omega}\bigg|_{\omega=\xi_{\mathbf{k}}}, \tag{4.25}$$

collect the derivative of $\xi_{\mathbf{k}}$ and use the definition of the effective mass (4.8) to get

$$\frac{1}{m^*} = \frac{\frac{1}{m} + \frac{1}{k_F}\frac{\partial}{\partial \mathbf{k}}\,\mathrm{Re}\,\Sigma^R(\mathbf{k}, 0)|_{|\mathbf{k}|=k_F}}{1 - \frac{\partial}{\partial \omega}\,\mathrm{Re}\,\Sigma^R(k_F, \omega)|_{\omega=0}}, \tag{4.26}$$

where we have set $\xi_{k_F} = 0$. Using the expression (4.23) for the quasi-particle residue, where $\mathcal{Z} = Z_{\mathbf{k}}|_{|\mathbf{k}|=k_F}$, we finally obtain the relation between the effective mass and the real part of the retarded self-energy

$$\frac{m}{m^*} = \mathcal{Z}\left[1 + \frac{m}{k_F}\frac{\partial}{\partial \mathbf{k}}\,\mathrm{Re}\,\Sigma^R(\mathbf{k}, 0)\bigg|_{|\mathbf{k}|=k_F}\right]. \tag{4.27}$$

4.3 Zero Temperature t-Matrix Approach

Until this point, within the t-matrix approximation, we worked exclusively in the normal phase at finite temperature but, as we have seen in Section 1.4, it may happen that a spin-imbalanced system remains in the normal phase also at $T = 0$. To formulate the theory also at zero temperature, we can take the limit $T \to 0$ (i.e. $\beta \to \infty$) in all relevant equations obtained within the finite temperature (Matsubara) formalism. However, we recall from Section 2.1 that the imaginary time τ at finite temperature is conventionally taken in the interval $(0, \beta)$, because of the periodicity (anti-periodicity) of the bosonic (fermionic) functions. Therefore, the naive implementation of its zero temperature limit would be to consider the $(0, \infty)$ interval, which is incorrect because it does not take into account the singularities for $\tau \to \beta^-$ (or equivalently for $\tau \to 0^-$) of some of the functions in the self-consistent cycle. While these singularities are taken into account at finite temperature thanks to the β-periodicity, they inevitably get lost in this naive version of the zero-temperature limit. Consequently, the interval to be considered in order to perform the correct limit is actually $(-\beta/2, \beta/2)$, which becomes $(-\infty, \infty)$ at zero temperature, so that both the singularities for $\tau \to 0^+$ and $\tau \to 0^-$ are taken into account. As a consequence, $\tau = 0$ is usually a point of discontinuity for a generic function of τ in the self-consistent cycle.

Following the above prescriptions for the $T = 0$ limit, discrete fermionic Matsubara frequencies $\omega_n = (2n + 1)\pi T$ or bosonic Matsubara frequencies $\Omega_\nu = 2\nu\pi T$ are thus replaced by continuous frequencies ω and Ω_ν along the imaginary axis, with the discrete sums $T\sum_n$ or $T\sum_\nu$ being replaced by integrals $\int_{-\infty}^{\infty} d\omega/(2\pi)$ and $\int_{-\infty}^{\infty} d\Omega/(2\pi)$. The advantage of working also at $T = 0$ with imaginary frequencies, rather than working with the *ground state formalism*, is that in this way one avoids the singularities (or nearly singularities) of the Green's functions calculated along the real frequency axis.

We can therefore rewrite the equations (3.77)-(3.80) for the Luttinger-Ward approach at $T = 0$ as

$$\mathcal{G}_\sigma(k) = \frac{1}{\mathcal{G}^0_\sigma(k)^{-1} - \Sigma_\sigma(k)}, \tag{4.28}$$

$$\Sigma_\sigma(k) = -\int \frac{dQ}{(2\pi)^4}\Gamma(Q)\mathcal{G}_{\bar{\sigma}}(Q - k), \tag{4.29}$$

$$\Gamma(Q) = -\frac{1}{2m_{red}/(4\pi a_F) + R_{pp}(Q)}, \tag{4.30}$$

$$R_{pp}(Q) = \int \frac{d\mathbf{k}}{(2\pi)^3}\left(\int_{-\infty}^{\infty} \frac{d\omega}{2\pi}\mathcal{G}_\uparrow(k + Q)\mathcal{G}_\downarrow(-k) - \frac{2m_{red}}{\mathbf{k}^2}\right), \tag{4.31}$$

where now we have used a different four-vector notation, with $k = (\mathbf{k}, \omega)$ and $Q = (\mathbf{Q}, \Omega)$. Similarly, the density equations in (3.44) become

$$n_\sigma = \int \frac{dk}{(2\pi)^4} e^{i\omega 0^+}\mathcal{G}_\sigma(k), \tag{4.32}$$

which can be properly inverted to find the chemical potentials μ_σ for the two species. However, in our numerical calculation it is more convenient to find μ_σ using (4.19),

which becomes

$$\mu_\sigma = \frac{k_{F\sigma}^2}{2m_\sigma} + \Sigma_\sigma(k_F, 0), \tag{4.33}$$

and checking that the expression (4.32) is always verified within a relative error of order 10^{-3} on the densities.

The details of the numerical procedures needed to implement the cycle of self-consistency at zero temperature must be properly generalized from the ones discussed in Appendix B. At zero temperature, one also needs to take into account a secondary subtraction scheme to deal with the quasi-particle contribution, which describes the sharp Fermi surface at $|\mathbf{k}| = k_{F\sigma}$ and the consequent oscillations at large $\mathbf{x}$ in the $(\mathbf{x}, \tau)$ representation [47]. Furthermore, considerations similar to those made in the Appendix C at T_c are required for working exactly at the critical polarization p_c.

4.3.1 Luttinger Theorem

While describing Fermi liquid theory in the previous sections, we made an implicit and crucial assumption: the Fermi momentum k_F is an *adiabatic invariant* when the interactions are turned on. Actually, this result is a direct consequence of a more general theorem, known as *Luttinger theorem*, when limited to isotropic systems. This theorem, originally derived by Luttinger in 1962 within perturbation theory at arbitrary order [95], states that the volume enclosed by the Fermi surface[6] of a normal Fermi gas at $T = 0$ is not altered by interaction, therefore it must remain the same as for the non-interacting gas. Indeed, in the isotropic case, it means that the radius of the Fermi sphere, that is $k_F = (3\pi^2 n)^{1/3}$, is not changed by interactions. This result is readily extended to a partially polarized Fermi liquid, in which one has two unchanged Fermi surfaces, namely $k_{F\sigma} = (6\pi^2 n_\sigma)^{1/3}$.

While the Luttinger theorem is valid for the exact theory, it is not guaranteed to hold in an approximate one. It is possible to prove analytically that, for the polarized Fermi gas, the theorem is still satisfied by the self-consistent t-matrix approach [96]. This is strictly related to the fact that the Luttinger-Ward approach is a conserving approximation, as discussed in 2.3.1. Therefore, the self-consistent t-matrix is the most suited approach for the description of the Fermi liquid phase, as it provides full control on the position of the Fermi surfaces for the two spin components. This important property is instead not shared by the non-self-consistent t-matrix approximation.

Just to give two concrete examples, Figure 4.2 shows the $T = 0$ momentum distributions $n_{\mathbf{k}\sigma} = \int_{-\infty}^{\infty} d\omega \; e^{i\omega 0^+} \mathcal{G}_\sigma(\mathbf{k}, \omega)$ for the mass-balanced system with polarization $p = 0.5$ at unitarity $(k_F a_F)^{-1} = 0$, calculated within the Luttinger-Ward approach and the non-self-consistent t-matrix approach. It is evident that the self-consistent t-matrix satisfies the Luttinger theorem by placing the Fermi steps exactly at $|\mathbf{k}| = k_{F\sigma}$, while the non-self-consistent t-matrix violates it for the minority component. Instead, Figure 4.3 shows the same distribution for the K-Dy mixture with polarization $p = -0.45$ at unitarity, calculated only within the Luttinger-Ward

[6] In the most general case, the Fermi surface is defined as the locus of discontinuities in the momentum distribution $n(\mathbf{k})$.

approach. As we can clearly see, the Luttinger theorem is still satisfied also for mass-imbalanced mixtures. This result, is a new contribution of this thesis.

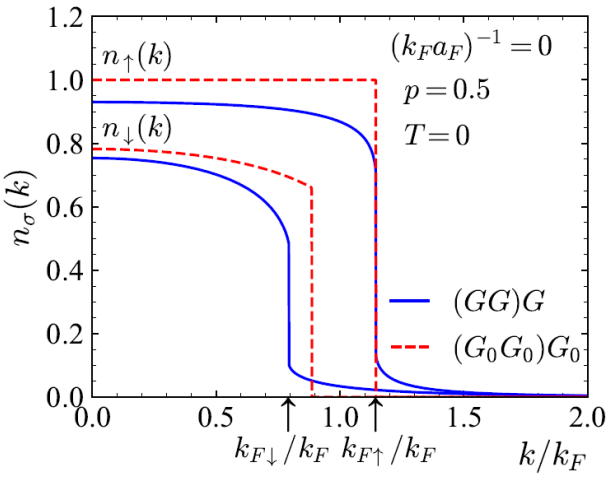

Figure 4.2: Momentum distributions $n_{\mathbf{k}\sigma}$ for the two spin components as a function of the momentum $k = |\mathbf{k}|$ (in units of the effective Fermi wave vector $k_F = (3\pi^2 n)^{1/3}$) at unitarity, polarization $p = 0.5$ and zero temperature, calculated within both the self-consistent t-matrix approach and the non-self-consistent t-matrix approach (denoted as $(GG)G$ and $(G_0G_0)G_0$ respectively). *Source*: reproduced from Ref. [47].

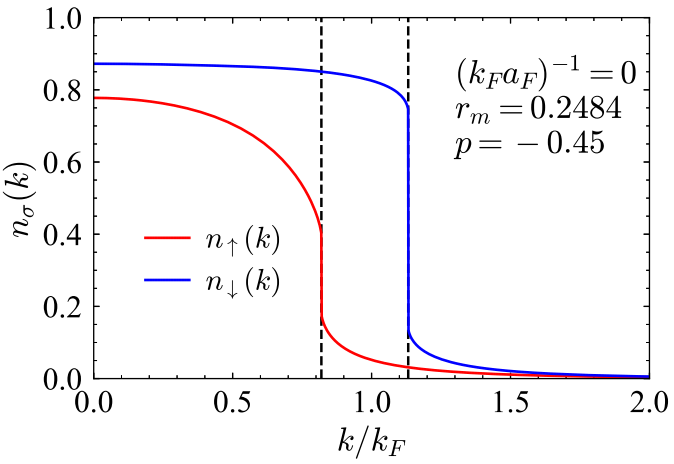

Figure 4.3: Momentum distributions $n_{\mathbf{k}\sigma}$ for the two spin components as a function of the momentum $k = |\mathbf{k}|$ (in units of the effective Fermi wave vector $k_F = (3\pi^2 n)^{1/3}$) at unitarity, polarization $p = -0.45$ and zero temperature, calculated within the self-consistent t-matrix approach for the K-Dy mixture. The two black dashed lines are located at the values of the Fermi momenta $k = k_{F\sigma}$.

4.3.2 Non-Fermi Liquid Behaviour at the QCP

Fermi liquid theory is considered one of the most successful theories in condensed matter physics, as it can describe the behavior of many metals or compounds in

terms of low-energy excitations of weakly interacting fermionic quasi-particles. However, in the last three decades, a variety of metals have been discovered which display thermodynamic and transport properties at low temperatures which are fundamentally different from those of the usual metallic systems which are well described by the Landau Fermi liquid theory. They have often been referred to as *singular* or *non-Fermi liquids* [97]. The most prominently discussed are the normal phase of high-temperature superconducting materials for a range of compositions near their highest T_c.

It has been known for a long time that Fermi liquid theory breaks down in the fluctuation regime of *classical phase transitions*. This breakdown occurs in a more substantial region of the phase diagram around the *quantum critical point* (QCP) of a *quantum phase transition* [98], where the transition temperature tends to zero as a function of some parameter.

In our diagrammatic approach at $T = 0$, we expect a QCP in correspondence to a critical polarization p_c for the second-order normal-to-superfluid transition, as identified by using the generalization of the Thouless criterion (see Section 3.2.1)

$$[\Gamma(\mathbf{Q} = \mathbf{Q}_0, \Omega = 0)|_{p=p_c}]^{-1} = 0, \tag{4.34}$$

where $\mathbf{Q}_0$ is the first pair wave vector at which $\Gamma(\mathbf{Q}, \Omega = 0)$ diverges coming from the normal phase. In particular, if $\mathbf{Q}_0 = 0$ the transition is toward a polarized homogeneous Sarma superfluid, while if $\mathbf{Q}_0 \neq 0$, the transition is toward a non-homogeneous FFLO superfluid. Therefore, by approaching the QCP coming from the *polaronic limit* (i.e. $p \simeq 1$), the quasi-particle description of the polarized ultracold Fermi gas may cease to be true, with a vanishing of the quasi-particle residues at the Fermi surfaces $\mathcal{Z}_\sigma$ and a corresponding divergence of the quasi-particle effective masses m^*_σ.

More precisely, within the self-consistent t-matrix, it is possible to prove analytically that a necessary condition for having a vanishing residue is that $\Gamma(\mathbf{Q}, \Omega = 0)$ diverges at finite pair-momentum $|\mathbf{Q_0}| > |k_{F\uparrow} - k_{F\downarrow}|$, therefore only in the case of a transition towards the FFLO phase and not towards the Sarma phase [47]. This breakdown at the FFLO QCP is quite expected because, generally speaking, one of the reasons why the residue can go to zero is the fact that the phase below the QCP becomes non-homogeneous, i.e. with some periodic structure in space due to a non-zero wave-vector $\mathbf{Q_0}$ [97].

For example, in Figure 4.4, we report the $T = 0$ momentum distributions $n_{\mathbf{k}\sigma}$ for the K-Dy mixture at the FFLO critical polarization $p_c = -0.60$, corresponding to a coupling $(k_F a_F)^{-1} = 1.072$, calculated within the Luttinger-Ward approach. As we can immediately see from this new result, the characteristic jumps at the Fermi momenta $k_{F\sigma}$, typical of a Fermi liquid (see Figure 4.3), disappear at the critical polarization for both the species. Therefore, these jumps at $|\mathbf{k}| = k_{F\sigma}$ in the momentum distributions are substituted by non-differentiable points at the same value, corresponding to a breakdown of the Fermi liquid theory at the QCP. As we discussed above, this effect is equivalent to a vanishing of the quasi-particle residues $\mathcal{Z}_\sigma = Z_{\mathbf{k}\sigma}|_{|\mathbf{k}|=k_{F\sigma}}$ at the FFLO QCP, which will be verified within our numerical calculations in Section 7.2.

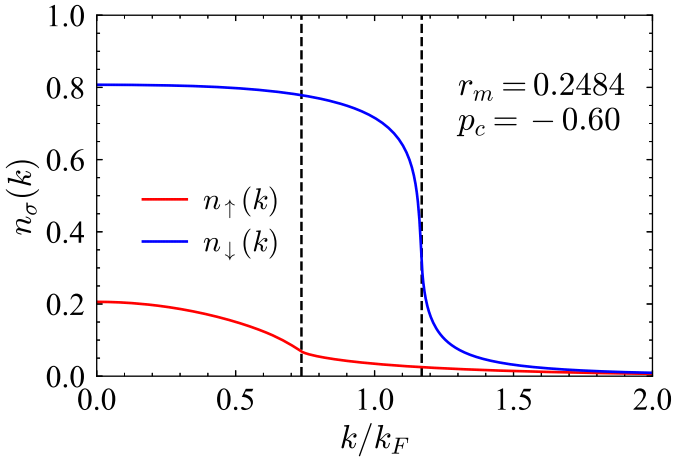

Figure 4.4: Momentum distributions $n_{\mathbf{k}\sigma}$ for the two spin components as a function of the momentum $k = |\mathbf{k}|$ (in units of the effective Fermi wave vector $k_F = (3\pi^2 n)^{1/3}$) at zero temperature and critical polarization $p_c = -0.60$, corresponding to a coupling $(k_F a_F)^{-1} = 1.072$, calculated within the self-consistent t-matrix approach for the K-Dy mixture. The two black dashed lines are located at the values of the Fermi momenta $k = k_{F\sigma}$.

Chapter 5

Experiments with Fermi-Fermi Mixtures

In this short chapter, we introduce some considerations on experiments with ultra-cold Fermi-Fermi mixtures, starting from the use of trapping potentials in experiments. We mainly focus on mass imbalanced systems and we discuss which mixtures have been or are currently being studied. This will be particularly useful to understand the choice of the mass ratios used in the numerical simulations, corresponding to the ^{40}K-^{161}Dy and ^{6}Li-^{53}Cr mixtures, presented in the following chapters.

5.1 Trapped Systems

As we have seen in Section 1.5, it is possible to tune the attractive interaction between two components of an ultra-cold Fermi gas, making the system to span all the BCS-BEC crossover. However, a crucial consideration is that ultra-cold gases require a trap to hold the neutral atoms together; only in this way they can be used as effective *quantum simulators*. In this regard, the *optical traps* are the most useful, because allow for an independent application of a magnetic field to tune a Fano-Feshbach resonance. Practically, these traps act on the atoms as an external potential proportional to the laser intensity, which has usually the shape of an inverted Gaussian. For many purposes, this can be approximated to an *anisotropic harmonic potential* of the form

$$V_\sigma(x,y,z) = \frac{1}{2} m_\sigma(\omega_{\sigma x}^2 x^2 + \omega_{\sigma y}^2 y^2 + \omega_{\sigma z}^2 z^2), \tag{5.1}$$

where the set of frequencies $(\omega_{\sigma x}, \omega_{\sigma y}, \omega_{\sigma z})$ are different for each fermionic component σ. For this reason, most of the experimental data so far available have been obtained within the trapping potential (5.1), which makes the system non-homogeneous.

To obtain a theoretical description of a system in the potential (5.1), one can adopt a *local density approximation* (LDA) approach. This consists in replacing the chemical potential μ_σ in all the t-matrix equations with a position-dependent chemical potential $\mu_\sigma(x,y,z) = \mu_\sigma^0 - V_\sigma(x,y,z)$, thereby obtaining a local Green's function $\mathcal{G}_\sigma(\mathbf{k}, \omega_n, \mu_\sigma(x,y,z))$. Therefore, this approach partitions the non-homogeneous trapped system into locally homogeneous regions with local densities $n_\sigma(x,y,z)$.

Without loss of generality, the original potential (5.1) is conveniently transformed into an *isotropic* harmonic potential through a simple rescaling of the spatial coordinates. More specifically, we consider the typical experimental situation where the trapping frequencies are taken to be $\omega_{\sigma x} = \omega_{\sigma y}$ and $\omega_{\sigma z} = \lambda_\sigma \omega_{\sigma x}$, so that the anisotropy is only along the z-axis. We also need the assumption $\lambda_\uparrow = \lambda_\downarrow \equiv \lambda$, which is met by the experiments in which both species are trapped by the same laser light. We can then rescale the variables as $(x, y, z) \to (x', y', z') = (\lambda^{-1/3}x, \lambda^{-1/3}y, \lambda^{2/3}z)$, such that the trapping potential becomes

$$V_\sigma(r') = \frac{1}{2} m_\sigma \bar{\omega}_\sigma^2 r'^2, \tag{5.2}$$

with $r' = \sqrt{x'^2 + y'^2 + z'^2}$ and $\bar{\omega}_\sigma = (\omega_{\sigma x}\omega_{\sigma y}\omega_{\sigma z})^{1/3} = \lambda^{1/3}\omega_{\sigma x}$. Accordingly, since the number of particles $N_\sigma = \int dx\, dy\, dz\, n_\sigma(x, y, z)$ is kept to be the same in the rescaling, we get the mapping $n_\sigma(x, y, z) = n'_\sigma(x', y', z')$.

For trapped systems, the coupling $(k_F^t a_F)^{-1}$ is expressed in terms of the effective Fermi wave-vector $k_F^t = \sqrt{4 m_{red} E_F^t}$, where $E_F^t = (\bar{\omega}_\uparrow \bar{\omega}_\downarrow)^{1/2}(3N)^{1/3}$ is the effective Fermi energy for the trapped system, with $N = N_\uparrow + N_\downarrow$. Another important quantity in trapped systems, which is usually used to express the position in the trap in dimensionless units, is the *Thomas-Fermi radius* R_{TF}. For balanced systems, it corresponds to the radius of the density profile of a non-interacting Fermi gas at zero temperature and is given by the condition $\frac{1}{2} m \bar{\omega}^2 R_{TF}^2 = E_F^t$.

In addition, the value of the critical temperature T_c depends on the position in the trap, that is, it is higher in the regions where the two local densities $n_\sigma(x, y, z)$ match better. For balanced systems, the central portion of the trap is where superfluidity is first established upon lowering the temperature from the normal phase. For imbalanced systems, in which the trapping frequencies are generally different for the two species, superfluidity can also occur in spherical shells where the local densities are better matched than in the center (also known as *shell superfluidity* [99]). However, quite generally, experimental physicists try to have the densities as matched as possible in the center in order to have an higher T_c, by modifying the trapping frequencies of the two species. Therefore, even for imbalanced systems, the latter is usually the most frequent situation.

Despite the experimental importance of harmonic traps, some quite recent experiments with balanced systems have been performed in a homogeneous box potential [100,101]. Moreover, it has been pointed out that, for the possible observation of FFLO phases or related effects, it would be better to use box-like traps, rather than harmonic traps [80]. This is because, in the latter case, a peak in the *"projected" pair-momentum distribution* $n_{pair}^{proj}(\mathbf{Q})$[1] at finite $\mathbf{Q}_0$ would be hard to be detected, due to the smearing produced by the trap average.

[1]The "projected" pair-momentum distribution $n_{pair}^{proj}(\mathbf{Q})$ corresponds to the momentum distribution of the molecules formed after a rapid sweep of the magnetic field to the BEC side of the crossover. This quantity is much more experimentally accessible than the pair susceptibility $\chi_{pair}(\mathbf{Q})$, introduced in Section 3.2.1. Anyhow, we expect that strong FFLO pairing fluctuations should result into a peak of $n_{pair}^{proj}(\mathbf{Q})$ at the same finite $\mathbf{Q}_0$ found for $\chi_{pair}(\mathbf{Q})$.

5.2 Experiments with Mass Balanced Systems

The original experimental observations on the BCS-BEC crossover, in the balanced case, were realized with trapped ultra-cold gases of fermionic ^{40}K [102] and ^{6}Li [103–105], using *broad* Fano-Feshbach resonances (see also Section 1.5.1). In brief, the typical procedure used to cool these gases of fermionic atoms to quantum degenerate temperatures[2] consists in an *evaporative cooling* in a *magnetic trap*, after a *laser cooling and trapping*[3]. For the final stage of evaporative cooling, the atoms are loaded into an *optical dipole trap* and, by lowering the depth of the optical trap, the atomic gas evaporates to temperatures far below the Fermi temperature.

Subsequently, these systems were investigated experimentally to study also the effects of a population imbalance [20, 21, 30, 31]. This is because, besides the tunability of the interaction, ultra-cold Fermi gases allow for a direct control of the population of the two fermionic components by choosing freely one of the two hyperfine states of the atom. A variable spin mixture of the two lowest hyperfine states is typically created by *radio frequency sweeps* (rf), where the relative number of the two states can be controlled by the rf power. States are sequentially and independently imaged in an optical trap by absorption. Analysis of these images provides measurement of the number of atoms in each state and thus the polarization.

5.3 Experiments with Mass Imbalanced Systems

The first attempts to realize a mass-imbalanced mixture were made with a ^{6}Li-^{40}K (lithium-potassium) mixture [106–108]. In these works, the quantum degenerate mixture is realized employing *sympathetic cooling*[4] of fermionic ^{6}Li and ^{40}K gases by an evaporatively cooled bosonic ^{87}Rb gas. Specifically, it was reported the observation of Feshbach resonances and the successful creation of ultra-cold bosonic heteronuclear molecules. However, it turns out that all resonances for s-wave scattering in this system are quite narrow, causing both practical and fundamental limitations for experimental applications, such as an interaction control practically limited by magnetic field uncertainties. Moreover, in Ref. [109], it was found the presence of *open decay channels*[5] for all the broader resonances, which means that atomic two-body collisions acquire an inelastic component. This implies two important consequences: firstly, this unavoidably limits the stability of an atomic Fermi-Fermi

[2]For an atomic gas, *quantum degeneracy* is established when the *de Broglie wavelength* $\lambda_{dB} = h/(mv)$ of particles becomes comparable to the average spacing between them $d = n^{-1/3}$, i.e. $\lambda_{dB} \gtrsim d$. For example, for a low density (dilute) gas we have $d \sim 1\mu$m and therefore, by using the classical relation $\frac{1}{2}k_BT = \frac{1}{2}mv^2$ from kinetic theory, we require a temperature $T \sim 100$ nK in order to achieve quantum degeneracy.

[3]It is interesting to notice that laser cooling works best on hydrogen-like atoms. This is why experimental physicists tend to laser cool mainly *alkali* atoms such as lithium (Li), sodium (Na), potassium (K), rubidium (Rb).

[4]Sympathetic cooling is a process in which particles of one type cool particles of another type. This technique is generally used to cool ions and atoms that cannot be cooled directly by laser cooling and it is most efficient when the mass/charge ratios of the sympathetic-cooled and laser-cooled atoms are similar.

[5]In a Feshbach resonance, if the closed channel can decay into open channels other than that in which the colliding pair is initially prepared, the situation is referred to as a *decaying resonance*.

mixture in the unitary regime and secondly, when Feshbach molecules are created via these decaying resonances, they will undergo spontaneous dissociation. In other words, from an experimental point of view, these two points imply short lifetimes (of the order of ~ 10 ms) for the Fermi-Fermi mixture, which make both the study of equilibrium properties and the production of a long-lived molecular BEC rather problematic.

In general, a large number of combinations could be selected to create a Fermi-Fermi mixture, from the variety of chemical elements that have been brought to quantum degeneracy with different experimental techniques. Indeed, in addition to alkali atoms, experimental physicists successfully brought to degeneracy many other atoms, such as chromium (Cr) and different *lanthanides* (dysprosium (Dy), erbium (Er) and ytterbium (Yb)), because of their large magnetic dipole moments which make them excellent candidates for quantum simulations of physical phenomena with long-range interactions. However, there are important criteria to follow, namely: a mass ratio above $r_m \equiv m_L/m_H = 0.0735$[6], tunable interactions and a collisional stability. Respecting these criteria, the possible combinations go down to the mixtures ^{40}K-^{161}Dy, ^{40}K-^{163}Dy, ^{40}K-^{167}Er and ^{6}Li-^{53}Cr [42].

The experimental investigation of the ^{40}K-^{161}Dy (potassium-dysprosium) mixture started quite recently in Innsbruck [42, 43]. The realization of this mixture in the quantum-degenerate regime was achieved by means of evaporative cooling of the dipolar dysprosium atoms together with sympathetic cooling of the potassium atoms. The specific choice of the K-Dy combination is related to its scattering spectrum, which is not chaotic but conveniently dense. Moreover, a very useful property of this mixture is the fact that the polarizability ratio of the two species in an infrared optical dipole trap nearly corresponds to its mass ratio ($r_m = 0.2484$). This allows one to easily match the Fermi surfaces of both species even in a harmonic trap, and thus to investigate pairing and superfluidity in the BCS-BEC crossover. In particular, it has been shown that the mixture presents a broad Feshbach resonance with a substantial suppression of inelastic losses, which is a key requirement for many experiments [43]. This makes it a promising candidate for a detailed analysis of the thermodynamic properties and the phase diagram of a mass-imbalanced system in the ongoing and near-future experiments.

In parallel, the ^{6}Li-^{53}Cr (lithium-chromium) mixture was successfully obtained experimentally in Florence [44], by realizing magneto-optically trapped Li-Cr clouds in the cold regime. This specific choice was motivated by the unique scattering properties of the Li-Cr system that cannot be obtained with any other atom-atom combination, and which open the way to many interesting possibilities. For example, the mass ratio $r_m = 0.1136$ is predicted to support one weakly bound Cr_2Li trimer state in the regime of strong Li-Cr repulsion, which may enable the resonant tuning of genuine few-body elastic interactions. Interestingly, although no predictions are currently available for the Feshbach resonances, the rich hyperfine and Zeeman

[6]The critical mass ratio $r_m = 0.0735$ is where the *Efimov effect* [110] occurs, i.e. the presence of an effective long-range three-body attraction in a system with nearly-resonant attractive short-range interaction, and the system becomes unstable. This instability happens because this effective interaction is mediated by a light atom moving back and forth between two heavy atoms, and it is strong enough to make the pairs to collapse [111, 112].

structure of these two atomic species, combined with the highly magnetic character of Cr atoms, is expected to yield rich resonance spectra. In this regard, it is also important to notice that even relatively narrow Feshbach resonances could guarantee a good collisional stability [44]. For these reasons, also this mixture seems to be a promising candidate for exploring the properties of mass imbalanced ultra-cold gases in the experiments, that are still going on.

Chapter 6

Numerical Results at Finite Temperature

In this chapter, we present the numerical results obtained within the Luttinger-Ward approach for different physical quantities at finite temperature. More precisely, we are going to discuss the results for the critical temperature T_c, the mean chemical potential μ and the imbalancing field h, the contact C and, in order to analyze the FFLO fluctuations, the pair susceptibility $\chi_{pair}(\mathbf{Q})$. We will focus on the temperature-coupling-polarization phase diagram for three different mass ratios, corresponding to a balanced mixture, a ^{40}K-^{161}Dy (potassium-dysprosium) mixture and a ^{6}Li-^{53}Cr (lithium-chromium) mixture. Moreover, the results for the chemical potential and the imbalancing field are compared with an analytical high-temperature limit of the t-matrix approach, which reduces to the virial expansion for a quantum gas in the high-T regime. The results for the two mass imbalanced mixtures are a new contribution of this thesis, and are compared with known results for a mass balanced mixture [46, 80, 113], which we have anyway reproduced for completeness.

6.1 Critical Temperature

One of the most important thermodynamic quantities, for standard BCS pairing, is the critical temperature for the superfluid transition T_c, which can be obtained from the Thouless criterion (3.45)

$$[\Gamma(\mathbf{Q}=0,\Omega_\nu=0)|_{T=T_c(p)}]^{-1}=0. \tag{6.1}$$

As already discussed in Section 3.2.1, we remark that our analysis at finite temperature focuses on a standard second-order normal-to-superfluid phase transition. Accordingly, it does not consider the occurrence of either phase separation related to a first-order normal-to-superfluid phase transition or a FFLO phase.

The results for the critical temperature T_c (in units of $E_F = k_F^2/(4m_{red})$) as a function of the coupling $(k_F a_F)^{-1}$ at zero polarization $p = 0$ are shown in Figure 6.1. The BCS and BEC temperatures, obtained in (3.33) and (3.59) respectively, are also reported in the figure for comparison (dashed lines). In the BEC limit $(k_F a_F)^{-1} \gg 1$, the Luttinger-Ward approach correctly recovers the condensation temperature for non-interacting composite bosons for each mass ratio considered.

Similarly, in the BCS limit $(k_F a_F)^{-1} \ll -1$, the mean-field critical temperature is recovered for all the mixtures here considered. For the Li-Cr mixture, we have not been able to go below the value $(k_F a_F)^{-1} = -1.8$, due to convergence problems in the numerical calculations.

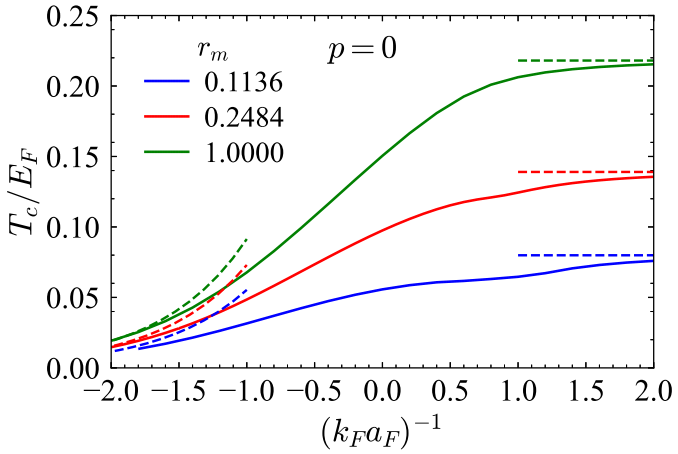

Figure 6.1: Critical temperature T_c (in units of the Fermi energy E_F) as a function of the coupling $(k_F a_F)^{-1}$ in the spin-balanced case $p = 0$. The dashed lines correspond to the BCS critical temperatures for $(k_F a_F)^{-1} < -1$ and the BEC critical temperatures of non-interacting composite bosons for $(k_F a_F)^{-1} > 1$. The mass ratios $r_m = (0.1136, 0.2484, 1.0000)$ correspond to the Li-Cr, K-Dy and balanced mixture, respectively.

The ratio T_c/E_F can also be obtained as a function of the polarization p, by fixing the coupling $(k_F a_F)^{-1}$, as shown in Figure 6.2 at unitarity. In this case the results were already obtained in a previous work [113] and are reproduced here for completeness. We notice that in the mass-balanced case the maximum of T_c/E_F occurs for equal densities ($p = 0$). For mass-imbalanced mixtures, however, the maximum occurs instead at $p > 0$, which corresponds to a majority of light atoms. In particular, one obtains $p_{max} = 0.0775$ for the K-Dy mixture and $p_{max} = 0.114$ for the Li-Cr mixture. Moreover, for the K-Dy mixture, on the $p < 0$ side the T_c curve decreases up to a point where it starts developing a re-entrance, in a similar way to what happens for the mass-balanced case (symmetric peak). As we have seen in Section 1.4, this re-entrant behavior is usually associated with a region of phase separation in the phase diagram, where the normal-superfluid phase transition becomes of first-order and the second-order curve for T_c is covered by this region. From mean-field calculations (see Figure 1.7 for example), one would expect in addition an FFLO phase to develop in this region of the phase diagram. For the Li-Cr mixture, on the other hand, convergence problems in the numerical calculations prevented exploring the low temperature region at negative polarization.

We conclude this section with an important consideration. In the previous figures, we see that the ratio T_c/E_F decreases monotonically for decreasing mass ratio $r_m = m_\uparrow/m_\downarrow$. Actually, at fixed heavier mass $m_\downarrow$, this is just an effect of the chosen normalization in terms of $E_F = (3\pi^2 n)^{2/3}/(4m_{red})$, since $E_F \to \infty$ for $r_m \to 0$. To remove this effect, we should consider the temperature in units of the Fermi energy

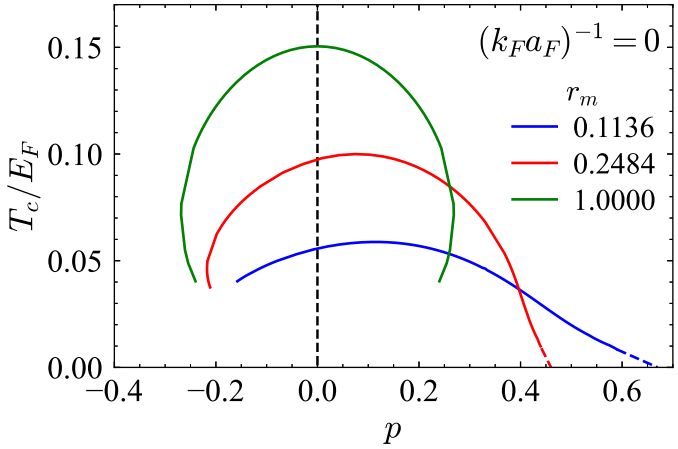

Figure 6.2: Critical temperature T_c (in units of the Fermi energy E_F) as a function of the polarization $p = (n_\uparrow - n_\downarrow)/n$ at unitarity. Following our conventions, $p > 0$ ($p < 0$) corresponds to the majority of the light (heavy) species. The mass ratios $r_m = (0.1136, 0.2484, 1.0000)$ correspond to the Li-Cr, K-Dy and balanced mixtures, respectively. *Source*: adapted from Ref. [113].

$E_{F\downarrow} = (6\pi^2 n_\downarrow)^{2/3}/(2m_\downarrow)$ of the heavy component. In this way, the ratio $T_c/E_{F\downarrow}$ is instead seen to increase for decreasing r_m. This also means that the value of p_{max}, referred to Figure 6.2, depends on the units used for normalizing T_c. When these units are in terms of $E_{F\downarrow}$ of the heavy component, we obtain $p_{max} = 0.166$ for the K-Dy mixture and $p_{max} = 0.204$ for the Li-Cr mixture. Otherwise, when the units are in terms of $E_{F\uparrow}$ of the light component, we obtain $p_{max} = -0.003$ for the K-Dy mixture and $p_{max} = 0.036$ for the Li-Cr mixture.

6.2 Chemical Potentials

Let us now consider the chemical potentials μ_σ, which are obtained by inverting the density equations in (3.44). In the following, rather than deal with $\mu_\uparrow$ and $\mu_\downarrow$, we will work with the mean chemical potential $\mu = (\mu_\uparrow + \mu_\downarrow)/2$ and the imbalancing field $h = (\mu_\uparrow - \mu_\downarrow)/2$, such that we easily recover the original μ and the trivial result $h = 0$ in the balanced case. In this section, we focus on these two quantities at unitarity $(k_F a_F)^{-1} = 0$ and low temperatures, i.e. $T < 1.2E_F$. However, it is important to notice that the numerical program initially requires two guess values for μ and h as input, which can be readily obtained within the high-temperature approximation discussed below.

In Figure 6.3, we report the temperature dependence of μ and h (in units of E_F) at unitarity, down to the critical temperature T_c, for three different values of the polarization $p = (-0.4, 0, 0.4)$. Notice that we have $h \neq 0$ even at zero polarization, if the mass ratio $r_m \neq 1$. This is because the chemical potentials μ_σ depends also on the masses m_σ, and not only on the densities n_σ. Moreover, we see that all the curves end up at the critical temperature T_c which depends on the chosen polarization p and mass ratio r_m, in agreement with the results discussed in Figure 6.2 above.

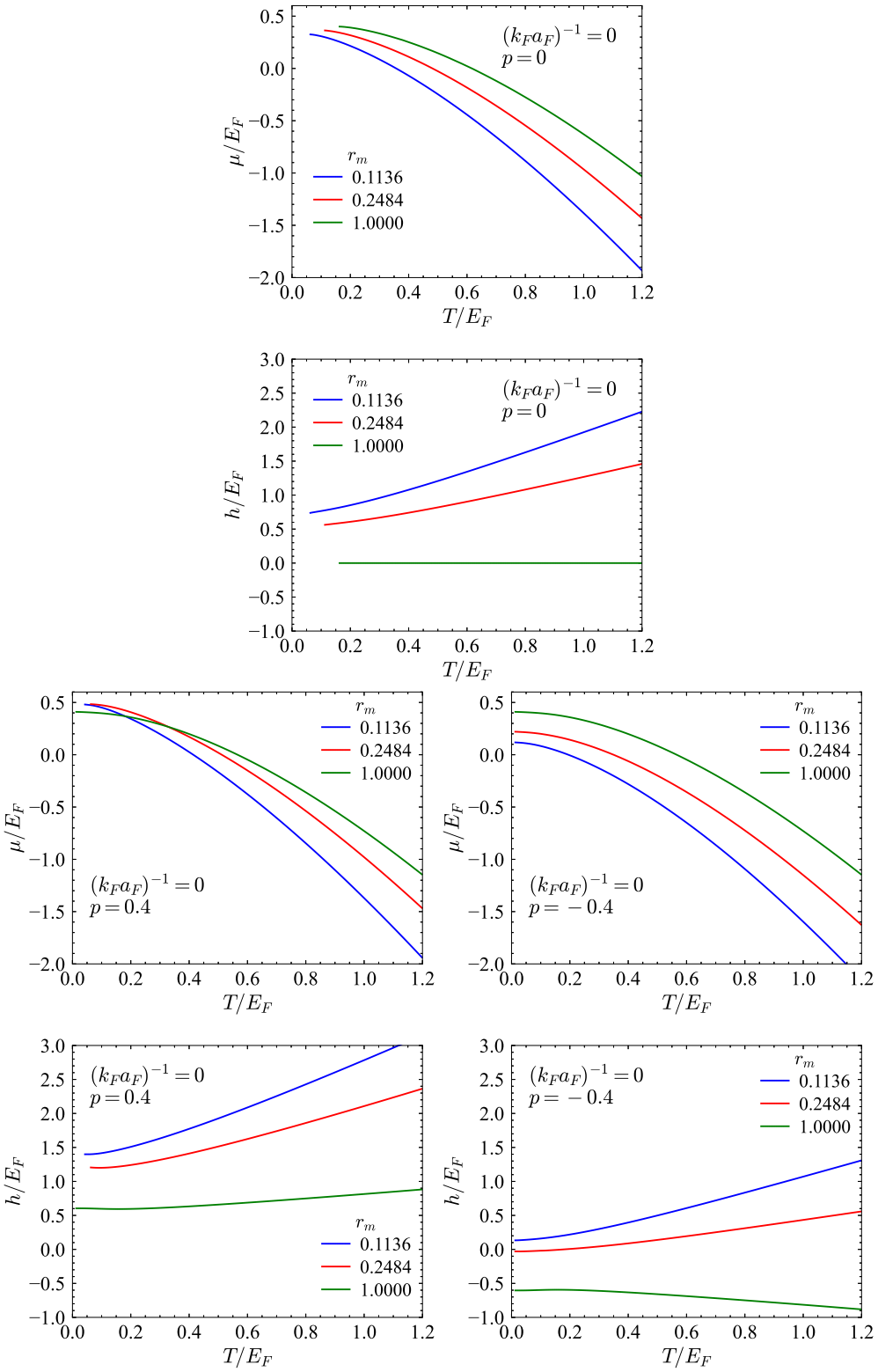

Figure 6.3: Mean chemical potential $\mu = (\mu_\uparrow + \mu_\downarrow)/2$ and imbalancing field $h = (\mu_\uparrow - \mu_\downarrow)/2$ as a function of the temperature T (both in units of the Fermi energy E_F) at unitarity, up to the critical temperature, for the polarization $p = (-0.4, 0, 0.4)$. The mass ratios $r_m = (0.1136, 0.2484, 1.0000)$ correspond to the Li-Cr, K-Dy and balanced mixtures, respectively.

6.2.1 High-temperature Limit

It is interesting to consider the high-temperature limit of the t-matrix approximation. We will show that it reduces to the quantum *virial expansion*[1] of Beth and Uhlenbeck [114], which means that it becomes exact in this limit [115]. This is naturally quite a satisfactory feature of this approximation and is also useful for providing initial values of μ and h in the numerical program[2].

We assume the temperature to be sufficiently high, such that the $z_\sigma = e^{\beta\mu_\sigma} \ll 1$, i.e. the *fugacity* is much smaller than one. In this limit, we can expand the equations for the particle densities n_σ in (3.44) since the self-energy Σ_σ is small with respect to $(\mathcal{G}^0_\sigma)^{-1}$, which contains the large energy scale μ_σ. We therefore have $n_\sigma = n^0_\sigma + \delta n_\sigma$, with

$$n^0_\sigma = \int \frac{d\mathbf{k}}{(2\pi)^3} f(\xi_{\mathbf{k}\sigma}) \simeq z_\sigma \left(\frac{m_\sigma T}{2\pi}\right)^{3/2} - z^2_\sigma \left(\frac{m_\sigma T}{4\pi}\right)^{3/2} \equiv n^0_{\sigma,1} + n^0_{\sigma,2}, \tag{6.2}$$

where $n^0_{\sigma,1}$ is the classical density for a free Fermi gas while $n^0_{\sigma,2}$ is the first correction to this value, and

$$\delta n_\sigma = \int \frac{d\mathbf{k}}{(2\pi)^3} \frac{1}{\beta} \sum_n \mathcal{G}^0_\sigma(k)^2 \Sigma_\sigma(k). \tag{6.3}$$

As we know from (3.78), the self-energy Σ_σ is defined in terms of the particle-particle propagator Γ which, for $z_\sigma \ll 1$, is replaced by its strong-coupling value Γ^{SC}_0 in 3.50. If we now consider the frequency sum

$$\begin{aligned} \frac{1}{\beta} \sum_n \frac{1}{i(\Omega_\nu - \omega_n) - \xi_{\mathbf{Q}-\mathbf{k}\bar{\sigma}}} \frac{1}{1 - a_F \sqrt{2m_{red}(\frac{\mathbf{Q}^2}{2m_B} - 2\mu - i\Omega_\nu)}} = \\ \oint_{\mathcal{C}} \frac{b(z)dz}{z - (i\omega_n + \xi_{\mathbf{Q}-\mathbf{k}\bar{\sigma}})} \frac{1}{1 - a_F \sqrt{2m_{red}(\frac{\mathbf{Q}^2}{2m_B} - 2\mu - z)}}, \end{aligned} \tag{6.4}$$

where the contour $\mathcal{C}$ surrounds the poles of the Bose function $b(z) = [e^{\beta z} - 1]^{-1}$ on the imaginary axis, we notice that we need to distinguish if $a_F < 0$, i.e. no bound states, or if $a_F > 0$. This is because, in the former case we have a contribution from the pole of $\mathcal{G}^0_{\bar{\sigma}}$ and one from the branch cut of Γ^{SC}_0, while in latter case we also have a contribution from the pole of Γ^{SC}_0.

Let us first discuss the case $a_F < 0$. For $z_\sigma \ll 1$, one can readily prove that the contribution from the cut is smaller than the one from the pole by a factor z_σ and

[1] The quantum virial expansion, alternatively referred to as *quantum cluster expansion*, is a standard method in quantum statistical mechanics which is practically useful for a dilute quantum gas. The basic idea is that, since we are dealing with a strongly correlated system at low temperatures, with increasing temperature the correlation between particles would become increasingly weak. Concretely, by Taylor-expanding $\Omega = -T \ln \mathcal{Z}$ in the fugacity, where $\mathcal{Z} = 1 + zZ_1 + z^2 Z_2 + \cdots$, the thermodynamic potential takes the form $\Omega = -TZ_1[z + b_2 z^2 + b_3 z^3 + \cdots]$, where b_n is referred to as the n-th virial coefficient. As shown by Beth and Uhlenbeck, the second virial coefficient for interacting Fermi gases can be expressed in terms of the phase shifts of a two-body scattering problem.

[2] The analytic derivation presented in this section is based on private notes by P. Pieri for the fully balanced case, here generalized to the mass and density imbalanced case.

can be neglected. We have then

$$\Sigma_\sigma(k) = -\int \frac{d\mathbf{Q}}{(2\pi)^3} \frac{e^{-\beta\xi_{\mathbf{Q}-\mathbf{k}\bar{\sigma}}}}{\frac{2m_{red}}{4\pi a_F} - \frac{(2m_{red})^{3/2}}{4\pi}\sqrt{\frac{\mathbf{Q}^2}{2m_B} - \xi_{\mathbf{Q}-\mathbf{k}\bar{\sigma}} - i\omega_n - 2\mu}}. \tag{6.5}$$

If we insert this quantity in the expression (6.3) for δn_σ and perform the sum over the Matsubara frequencies, we see that $k = |\mathbf{k}|$ is a cut-off when $k \gtrsim \sqrt{2m_\sigma T}$ and, similarly, the Boltzmann factor $e^{-\beta\xi_{\mathbf{Q}-\mathbf{k}\bar{\sigma}}}$ is a cut-off for $Q = |\mathbf{Q}|$. We can then neglect $(\mathbf{Q}-\mathbf{k})^2/2m_{\bar{\sigma}}$ and $\mathbf{Q}^2/2m_B$ in the denominator with respect to μ. This gives

$$\Sigma_\sigma(k) = \frac{n^0_{\bar{\sigma},1}}{\frac{2m_{red}}{4\pi a_F} - \frac{(2m_{red})^{3/2}}{4\pi}\sqrt{-i\omega_n - \mu_\sigma}}, \tag{6.6}$$

which can be inserted in the expression for δn_σ and, after an integration over k, we get

$$\delta n_\sigma = n^0_{\bar{\sigma},1}\frac{(2m_\sigma)^{3/2}}{8\pi}\frac{1}{\beta}\sum_n \frac{1}{\frac{2m_{red}}{4\pi a_F} - \frac{(2m_{red})^{3/2}}{4\pi}\sqrt{|\mu_\sigma| - i\omega_n}}\frac{1}{\sqrt{|\mu_\sigma| - i\omega_n}}. \tag{6.7}$$

The sum over the fermionic frequencies ω_n is transformed into an integral over frequency on a contour encircling the poles of the Fermi function, in analogy to what we have done in (6.4). This contour is then deformed into a clockwise contour $\mathcal{C}$ around the cut $[|\mu_\sigma|, \infty)$ of the square root. This gives, after some algebraic manipulations, the important result

$$\delta n_\sigma = n^0_{\bar{\sigma},1}\frac{2^{3/2}}{\pi}\left(\frac{m_\sigma}{2m_{red}}\right)^{3/2} z_\sigma F\left(\frac{\varepsilon_0}{T}\right), \tag{6.8}$$

where $\varepsilon_0 = (2m_{red}a_F^2)^{-1}$ is the binding energy, corresponding to a bound state if $a_F > 0$, while the function F is defined as

$$F(\alpha) = \int_0^\infty dx \frac{e^{-\alpha x^2}}{1+x^2}, \tag{6.9}$$

with $F(0) = \pi/2$. The expression (6.8) is just the Beth-Uhlenbeck result for our case. We have then, for $a_F < 0$ and $T \gg E_F$, the coupled equations

$$n_\sigma = z_\sigma\left(\frac{m_\sigma T}{2\pi}\right)^{3/2}\left[1 + \frac{2^{3/2}}{\pi}\left(\frac{m_{\bar{\sigma}}}{2m_{red}}\right)^{3/2} z_{\bar{\sigma}} F\left(\frac{\varepsilon_0}{T}\right) - \frac{1}{2^{3/2}}z_\sigma\right], \tag{6.10}$$

which can be solved analytically only by iteration, knowing that $z_\sigma \simeq (2\pi/(m_\sigma T))^{3/2} n_\sigma$ at leading order, and therefore gives the equations for the high-temperature chemical potentials of the two species

$$\mu_\sigma^{HT} = T\ln\left[\frac{\left(\frac{2\pi}{m_\sigma T}\right)^{3/2} n_\sigma}{1 + \frac{2^{3/2}}{\pi}\left(\frac{2\pi}{2m_{red}T}\right)^{3/2} n_{\bar{\sigma}} F\left(\frac{\varepsilon_0}{T}\right) - \frac{1}{2^{3/2}}\left(\frac{2\pi}{m_\sigma T}\right)^{3/2} n_\sigma}\right]. \tag{6.11}$$

It is important to notice that an exception occurs when we deal with a mass and spin-balanced system: in that case we would simply have a quadratic equation in z, instead of the two coupled equations in (6.10), which can be solved exactly.

We now pass to consider the case $a_F > 0$. The self-energy Σ_σ has also a contribution due to a pole in the particle-particle propagator Γ_0, which is given by

$$\Sigma_\sigma^B(k) = \frac{8\pi}{(2m_{red})^2 a_F} \int \frac{d\mathbf{Q}}{(2\pi)^3} \frac{b(\frac{\mathbf{Q}^2}{2m_B} - \mu_B)}{i\omega_n + \xi_{\mathbf{Q}-\mathbf{k}\bar{\sigma}} + \mu_B - \frac{\mathbf{Q}^2}{2m_B}}, \tag{6.12}$$

where we denoted $\mu_B = 2\mu + \varepsilon_0$. The Bose function in (6.12) restricts the range of Q to $Q \lesssim \sqrt{2m_B T}$. Since at high temperature one has $\beta|\mu_\sigma| \gg 1$, it then follows that $Q^2/(2m_B) \ll |\mu_\sigma|$. In addition, when integrating over $\mathbf{k}$ to calculate the densities, the relevant region of k contributing to the integral extends to k of the order of the large scale $\sqrt{2m_\sigma|\mu_\sigma|}$. We can thus consider $Q \ll k$, and thus set $\mathbf{Q} = 0$ everywhere in the denominator of (6.12) when calculating the densities. The corresponding contribution to the density is readily obtained as

$$\delta n_\sigma^B = \frac{8\pi n_B}{(2m_{red})^2 a_F} \frac{1}{\beta} \sum_n \int \frac{d\mathbf{k}}{(2\pi)^3} \frac{1}{(i\omega_n - \xi_{\mathbf{k}\sigma})^2} \frac{1}{i\omega_n + \xi_{-\mathbf{k}\bar{\sigma}} + \mu_B}, \tag{6.13}$$

where we defined $n_B = e^{\beta\mu_B}(m_B T/(2\pi))^{3/2}$. The double pole at $z = \xi_{\mathbf{k}\sigma}$ in the frequency sum yields a contribution which is suppressed by a factor z_σ. Therefore we remain with

$$\delta n_\sigma^B = n_B = e^{\beta\mu_B} \left(\frac{m_B T}{2\pi}\right)^{3/2}, \tag{6.14}$$

and, for $a_F > 0$ and $T \gg E_F$, the coupled equations in (6.10) become

$$n_\sigma = z_\sigma \left(\frac{m_\sigma T}{2\pi}\right)^{3/2} \left\{1 + \frac{2^{3/2}}{\pi} \left(\frac{m_{\bar{\sigma}}}{2m_{red}}\right)^{3/2} z_{\bar{\sigma}} \left[\pi e^{\beta\varepsilon_0} - F\left(\frac{\varepsilon_0}{T}\right)\right] - \frac{1}{2^{3/2}} z_\sigma\right\}. \tag{6.15}$$

For an arbitrary scattering length a_F, it is generally convenient to introduce the function

$$H\left(\frac{\varepsilon_0}{T}; a_F\right) = \pi e^{\beta\varepsilon_0}\theta(a_F) - \mathrm{sgn}(a_F) F\left(\frac{\varepsilon_0}{T}\right), \tag{6.16}$$

such that we get the generic expression for the high-temperature chemical potentials

$$\mu_\sigma^{HT} = T \ln\left[\frac{\left(\frac{2\pi}{m_\sigma T}\right)^{3/2} n_\sigma}{1 + \frac{2^{3/2}}{\pi}\left(\frac{2\pi}{2m_{red}T}\right)^{3/2} n_{\bar{\sigma}} H\left(\frac{\varepsilon_0}{T}; a_F\right) - \frac{1}{2^{3/2}}\left(\frac{2\pi}{m_\sigma T}\right)^{3/2} n_\sigma}\right], \tag{6.17}$$

which correctly recovers the classical value at leading order

$$\mu_\sigma^{cl} = T \ln\left[\left(\frac{2\pi}{m_\sigma T}\right)^{3/2} n_\sigma\right]. \tag{6.18}$$

As a check, in Figure 6.4 (above), we present the temperature dependence of μ and h at unitarity, calculated numerically within the t-matrix approach (Luttinger-Ward), together with the high-temperature expression in (6.17) and the classical

value in (6.18), for the K-Dy mixture and Li-Cr mixture at $p = 0.4$ and $p = -0.4$, respectively. Since the scales used in the plots for μ and h compress the differences, in the same figure (below) we reported the temperature dependence of $z_\uparrow z_\downarrow = e^{2\beta\mu}$ and $z_\uparrow / z_\downarrow = e^{2\beta h}$. We see that the high-$T$ expression (red dashed line) correctly overlaps the self-consistent t-matrix curve (black full line) at sufficiently high-temperatures, i.e. $T > E_F$, and greatly improves the classical result (blue dotted line).

6.3 Contact

The contact C can be obtained from the relation $C = (2m_{red}\Delta_\infty)^2$, where Δ^2_∞ is directly calculated from the particle-particle propagator Γ, using (3.71), as

$$\Delta^2_\infty = \int \frac{d\mathbf{Q}}{(2\pi)^3} \frac{1}{\beta} \sum_\nu e^{i\Omega_\nu 0^+} \Gamma(Q). \tag{6.19}$$

To check the internal consistency of the numerical program, one can verify that the contact calculated in this way coincides with the coefficient of the $\mathbf{k}^{-4}$ tail of the momentum distribution per spin component $n_\sigma(\mathbf{k})$, as in (1.35).

In Figure 6.5, we report the temperature dependence of C (in units of k_F^4) at unitarity, down to the critical temperature T_c, for three different values of the polarization $p = (-0.4, 0, 0.4)$. What is interesting here is the presence of a maximum in the curves for the spin-imbalanced systems, in particular only at $p < 0$ for the mass-imbalanced mixtures, i.e. majority of heavy species. From the definition of Tan's contact, discussed in Section 1.5.2, this means that there exists a temperature (greater than T_c) in the normal phase for which the pair correlation function for different species at short distances is maximal.

As we did for the chemical potentials μ_σ in the previous section, we can study the high-temperature behaviour also for the contact. Since for $T \gg E_F$ the mean chemical potential μ is large and negative, we are interested in

$$\Delta^2_\infty = \int \frac{d\mathbf{Q}}{(2\pi)^3} \int_{-\infty}^{\infty} d\omega \frac{1}{\pi} \mathrm{Im}\Gamma_0^{SC}(\mathbf{Q}, \omega + i0^+) b(\omega), \tag{6.20}$$

where $b(\omega) = [e^{\beta\omega} - 1]^{-1}$ is the Bose function.

Consider first the case $a_F < 0$, with no bound state. We have that $\mathrm{Im}\Gamma_0^{SC} \neq 0$ for $\omega > -2\mu + \mathbf{Q}^2/(2m_B)$ therefore, by setting $\omega = -2\mu + \mathbf{Q}^2/(2m_B) + x$, we have

$$\Delta^2_\infty = \int \frac{d\mathbf{Q}}{(2\pi)^3} \int_0^{\infty} dx \frac{1}{\pi} \mathrm{Im}\Gamma_0^{SC}\left(\mathbf{Q}, 2|\mu| + \frac{\mathbf{Q}^2}{2m_B} + x + i0^+\right) e^{-\beta\left(-2\mu + \frac{\mathbf{Q}^2}{2m_B} + x\right)}, \tag{6.21}$$

where we have replaced the function $b(\omega)$ with $e^{-\beta\omega}$, since $\beta\omega$ is large in the region where $\mathrm{Im}\,\Gamma_0^{SC} \neq 0$. We can therefore perform the integral over the momentum $\mathbf{Q}$ and, after a few algebraic passages, we get the important result

$$\Delta^2_\infty = z_\uparrow z_\downarrow \frac{T^2}{2\pi} \left(\frac{m_B}{m_{red}}\right)^{3/2} \left[1 - G\left(\frac{\varepsilon_0}{T}\right)\right], \tag{6.22}$$

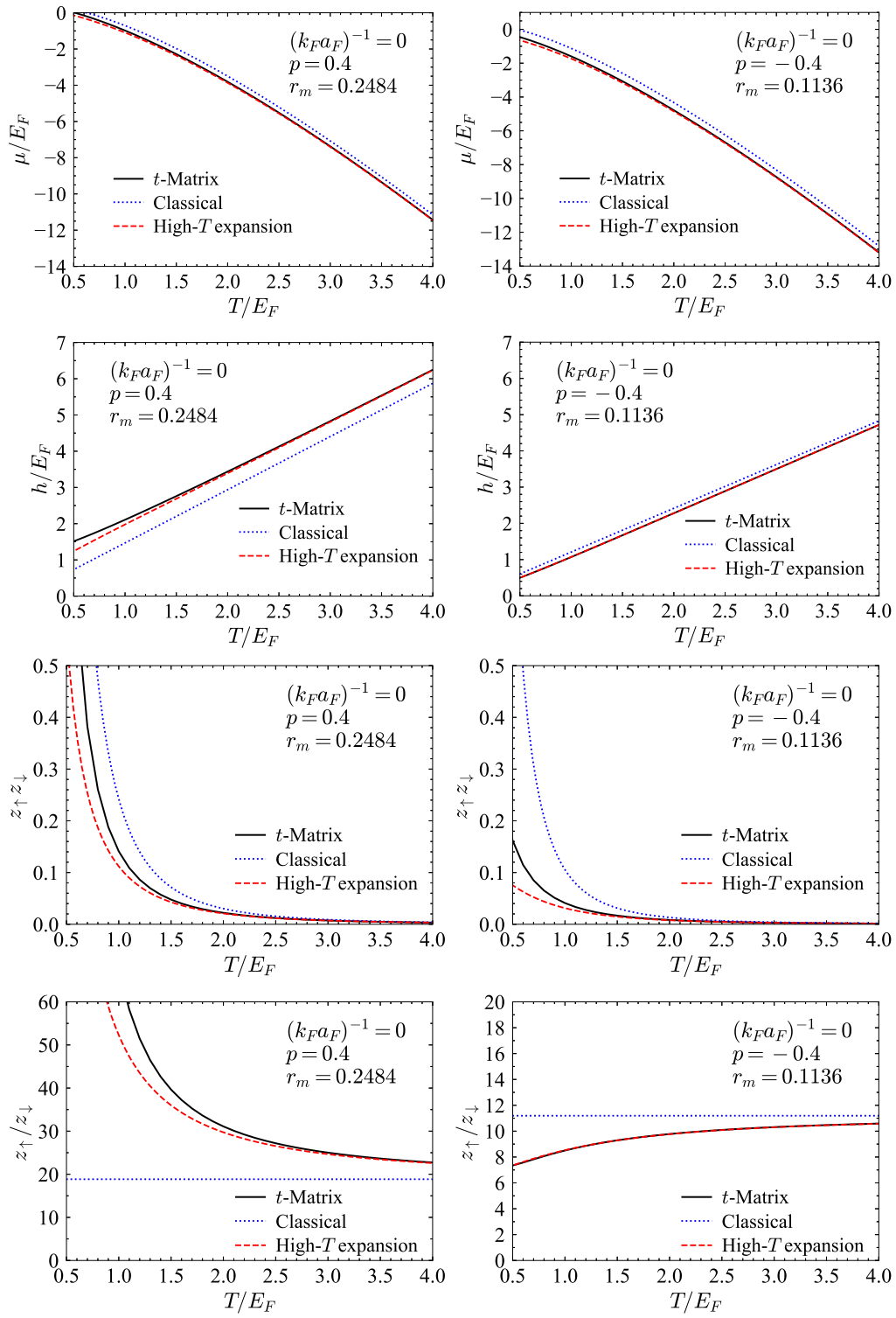

Figure 6.4: Above: mean chemical potential μ and imbalancing field h as a function of the temperature (both in units of the Fermi energy E_F) at unitarity for the K-Dy mixture at $p = 0.4$ (left) and Li-Cr mixture at $p = -0.4$ (right). The numerical data are compared with both the classical and high-temperature analytical expressions. Below: in order to show clearly the differences, the same results are presented in terms of the fugacities z_σ.

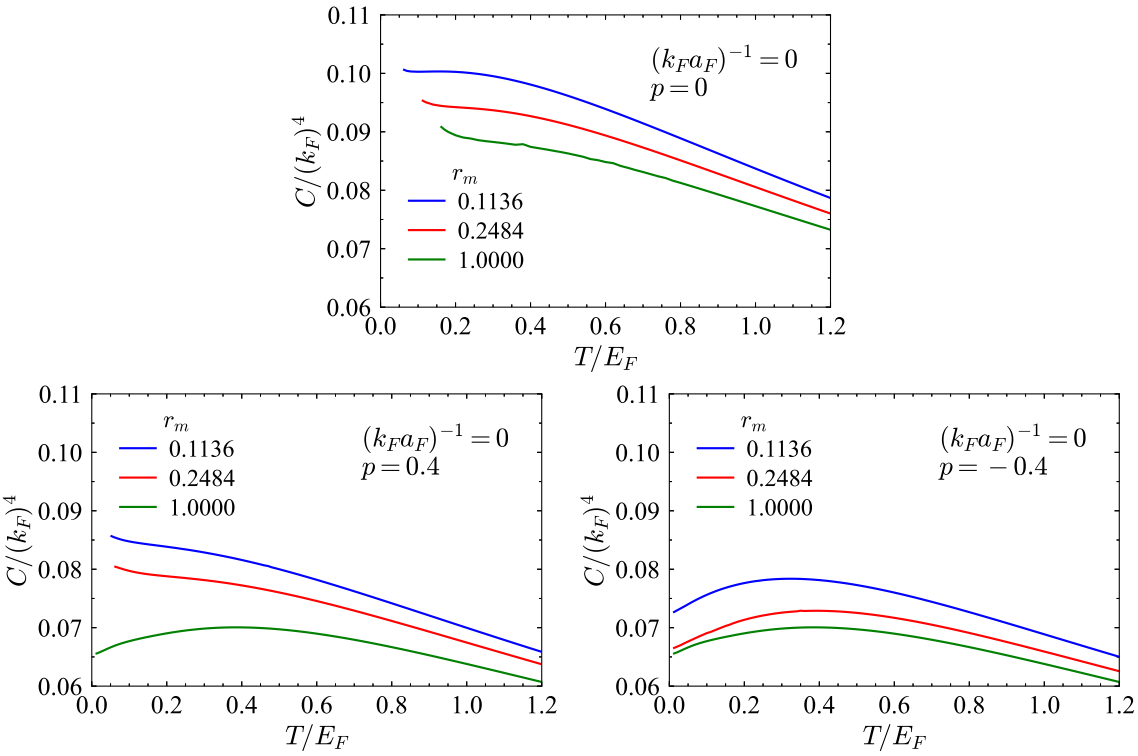

Figure 6.5: Contact C (in units of k_F^4) as a function of the temperature T (in units of the Fermi energy E_F) at unitarity, up to the critical temperature, for the polarization $p = (-0.4, 0, 0.4)$. The mass ratios $r_m = (0.1136, 0.2484, 1.0000)$ correspond to the Li-Cr, K-Dy and balanced mixtures, respectively.

where we used $e^{2\beta\mu} = z_\uparrow z_\downarrow$ and we introduced the function

$$G\left(\frac{\varepsilon_0}{T}\right) = \frac{2}{\sqrt{\pi}}\left(\frac{\varepsilon_0}{T}\right)^{1/2} F\left(\frac{\varepsilon_0}{T}\right), \tag{6.23}$$

with the function F defined in (6.9).

For $a_F > 0$, we also have a contribution due to the pole in the particle-particle propagator Γ_0, which is given by

$$(\Delta_\infty^B)^2 = z_\uparrow z_\downarrow e^{\beta\varepsilon_0}\left(\frac{m_B T}{2\pi}\right)^{3/2} \frac{8\pi}{(2m_{red})^2 a_F}. \tag{6.24}$$

To summarize, we have found that for $T \gg E_F$ and arbitrary scattering length a_F, we have

$$\Delta_\infty^2 = z_\uparrow z_\downarrow \frac{T^2}{2\pi}\left(\frac{m_B}{m_{red}}\right)^{3/2}\left[1 - G\left(\frac{\varepsilon_0}{T}\right)\right] + z_\uparrow z_\downarrow e^{\beta\varepsilon_0}\left(\frac{m_B T}{2\pi}\right)^{3/2} \frac{8\pi\theta(a_F)}{(2m_{red})^2 a_F}, \tag{6.25}$$

where the fugacities z_σ can be obtained from the high-temperature chemical potentials μ_σ in (6.17).

Exactly as we did before, we can compare the numerical results for the contact C at unitarity with those obtained using (6.25), both for the high-temperature result

for the chemical potentials (6.17) and classical result (6.18). This is done in Figure 6.6 for the K-Dy mixture at $p = 0.4$ and the Li-Cr mixture at $p = -0.4$. Also in this case, the contact obtained using high-T expression of the chemical potentials provides a better result than the same calculated using the classical chemical potentials. However, we see that for the K-Dy our approximation remains valid longer (going down from high T) than the one for the Li-Cr because, with the same T/E_F, the numerical error made in the product of the fugacities $z_\uparrow z_\downarrow$ is smaller.

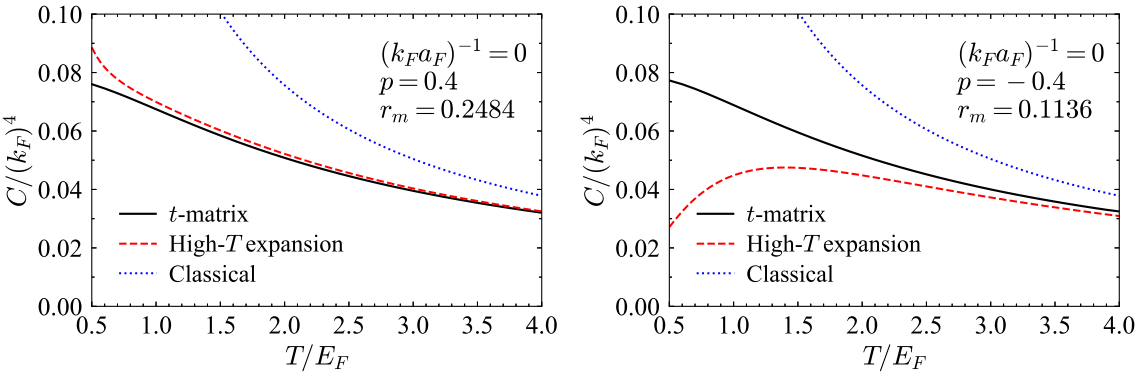

Figure 6.6: Contact (in units of k_F^4) as a function of the temperature (in units of the Fermi energy E_F) at unitarity for the K-Dy mixture at $p = 0.4$ (left) and Li-Cr mixture at $p = -0.4$ (right). The numerical data are compared with both the classical and high-temperature analytical expressions.

6.4 Pair Susceptibility and FFLO Fluctuations

As discussed in Section 3.2.1, even if we are not able to study the direct occurrence of a FFLO phase at finite temperature within the t-matrix approaches, we can still analyze the presence of strong FFLO fluctuations in the normal phase. In order to do this, we need to define the pair susceptibility $\chi_{pair}(\mathbf{Q})$, which describes the tendency of the Fermi gas in the normal phase towards the superfluid phase with pair momentum $\mathbf{Q}$, and to properly identify this quantity in our approximation.

Following the derivation of $\chi_{pair}(\mathbf{Q})$ presented in Ref. [80], we start with the grand-canonical Hamiltonian

$$\hat{K} = \sum_\sigma \int d\mathbf{x}\, \hat{\psi}^\dagger_\sigma(\mathbf{x}) \left(-\frac{\nabla^2}{2m_\sigma} - \mu_\sigma \right) \hat{\psi}_\sigma(\mathbf{x}) + v_0 \int d\mathbf{x}\, \hat{\psi}^\dagger_\uparrow(\mathbf{x}) \hat{\psi}^\dagger_\downarrow(\mathbf{x}) \hat{\psi}_\downarrow(\mathbf{x}) \hat{\psi}_\uparrow(\mathbf{x}), \quad (6.26)$$

where $\hat{\psi}_\sigma$ is a fermionic field operator and v_0 is the bare interaction strength, with $v_0 \to 0$ when the interaction is properly regularized using a_F in 3.29. We then add to the Hamiltonian (6.26) the symmetry-breaking term

$$\hat{H}_{ext} = -\int d\mathbf{x}\, \eta(\mathbf{x}) \hat{\varphi}(\mathbf{x}), \qquad \hat{\varphi}(\mathbf{x}) = \frac{1}{\sqrt{2}} \big(\hat{\Delta}(\mathbf{x}) + \hat{\Delta}^\dagger(\mathbf{x}) \big), \quad (6.27)$$

where $\eta(\mathbf{x})$ is a classical real field coupled to the gap operator $\hat{\Delta}(\mathbf{x}) = v_0 \hat{\psi}_\uparrow(\mathbf{x}) \hat{\psi}_\downarrow(\mathbf{x})$ and its hermitian conjugate. Within linear-response theory, the pair susceptibility

is obtained as the Fourier transform

$$\chi_{pair}(\mathbf{Q}) = \int d\mathbf{x}\, e^{-i\mathbf{Q}\cdot\mathbf{x}} \chi_{pair}(\mathbf{x}) \tag{6.28}$$

of the local functional derivative

$$\chi_{pair}(\mathbf{x}-\mathbf{x}') = \left.\frac{\delta\langle\hat{\varphi}(\mathbf{x})\rangle_\eta}{\delta\eta(\mathbf{x}')}\right|_{\eta=0}, \tag{6.29}$$

where $\langle\dots\rangle_\eta$ denotes grand-canonical thermal average containing the symmetry-breaking term in (6.27).

The expression (6.29) implies that a finite and weak probing field of the form $\eta(\mathbf{x}) = \eta\cos(\mathbf{Q}_0\cdot\mathbf{x})$ induces in the normal phase a gap parameter $\Delta_{\mathbf{Q}_0}(\mathbf{x}) \propto \chi_{pair}(\mathbf{Q}_0)\eta\cos(\mathbf{Q}_0\cdot\mathbf{x})$, thus signaling that $\chi_{pair}(\mathbf{Q})$ quantifies the tendency towards FFLO pairing. Therefore, evidence that the pair susceptibility becomes strongly peaked about a finite value $\mathbf{Q}_0$ can be considered as indicating the presence of strong FFLO pairing fluctuations in the normal phase.

The pair susceptibility $\chi_{pair}(\mathbf{x}-\mathbf{x}')$ can be related to an appropriate response function. This is done by calculating the functional derivative in (6.29) at finite η

$$\frac{\delta\langle\hat{\varphi}(\mathbf{x})\rangle_\eta}{\delta\eta(\mathbf{x}')} = \frac{\mathrm{Tr}[\frac{\delta e^{-\beta\hat{K}}}{\delta\eta(\mathbf{x}')}\hat{\varphi}(\mathbf{x})]}{\mathrm{Tr}[e^{-\beta\hat{K}}]} - \frac{\mathrm{Tr}[e^{-\beta\hat{K}}\hat{\varphi}(\mathbf{x})]}{\mathrm{Tr}[e^{-\beta\hat{K}}]}\frac{\mathrm{Tr}[\frac{\delta e^{-\beta\hat{K}}}{\delta\eta(\mathbf{x}')}]}{\mathrm{Tr}[e^{-\beta\hat{K}}]}, \tag{6.30}$$

using the operator identity

$$e^{(\hat{A}+\delta\hat{A})s} = e^{\hat{A}s}\big[1 + \int_0^s ds' e^{-\hat{A}s'}\delta\hat{A}e^{-\hat{A}s'} + \cdots\big], \tag{6.31}$$

to linear order in $\delta\hat{A}$ [80]. If we then introduce the following *temperature response function*

$$\mathcal{D}(\mathbf{x}\tau,\mathbf{x}'\tau') = \langle T_\tau[\hat{\Delta}(\mathbf{x},\tau)\hat{\Delta}^\dagger(\mathbf{x}',\tau')]\rangle_{\eta=0}, \tag{6.32}$$

after some algebraic manipulations, we get

$$\chi_{pair}(\mathbf{x}-\mathbf{x}') = \int_0^\beta d\tau\, \mathcal{D}(\mathbf{x}-\mathbf{x}',\tau) = \mathcal{D}(\mathbf{x}-\mathbf{x}',\Omega_\nu=0), \tag{6.33}$$

which becomes $\chi_{pair}(\mathbf{Q}) = \mathcal{D}(\mathbf{Q},\Omega_\nu=0)$ in Fourier space.

In our diagrammatic approach, the simplest physically meaningful approximation for $\mathcal{D}(\mathbf{Q},\Omega_\nu)$ results by summing the series of non-self-consistent ladder diagrams, yielding $\mathcal{D}(\mathbf{Q},\Omega_\nu) = \Gamma_0(\mathbf{Q},\Omega_\nu)$, which justifies the result given at the end of Section 3.2.1. However, in our improved description of an imbalanced Fermi gas within the self-consistent t-matrix, is natural to identify the pair susceptibility as

$$\chi_{pair}(\mathbf{Q}) = \Gamma(\mathbf{Q},\Omega_\nu=0). \tag{6.34}$$

In Figure 6.7, we present the results for the dimensionless pair susceptibility $\chi_{pair}(\mathbf{Q})2m_{red}k_F$ at unitarity for two values of polarization $p = (-0.4, 0.4)$. From these results one sees that the pair susceptibility gets strongly enhanced about a

finite momentum $\mathbf{Q}_0$ of order $|k_{F\uparrow} - k_{F\downarrow}|$ as the temperature is progressively lowered, thereby signaling the presence of strong FFLO fluctuations in the normal phase. Moreover, consistently with what has been discussed at the end of Section 1.4.1, we see that the FFLO phase is suppressed for $p > 0$, i.e. when the light species is the majority. However it seems that, the more the mass ratio $r_m = m_\uparrow/m_\downarrow$ decreases, the more the FFLO effects are confined to lower temperatures. Exactly as we said at the end of Section 6.1, this is just an artifact due to our choice of the normalization in terms of E_F. Indeed, from the point of view of experimental feasibility, what matters is the ratio $T/E_{F\downarrow}$, which becomes much higher. For example, at $p = -0.4$ the value $T/E_F = 0.01$ becomes $T/E_{F\downarrow} = (0.039, 0.020, 0.008)$ for the Li-Cr, K-Dy and balanced mixtures, respectively.

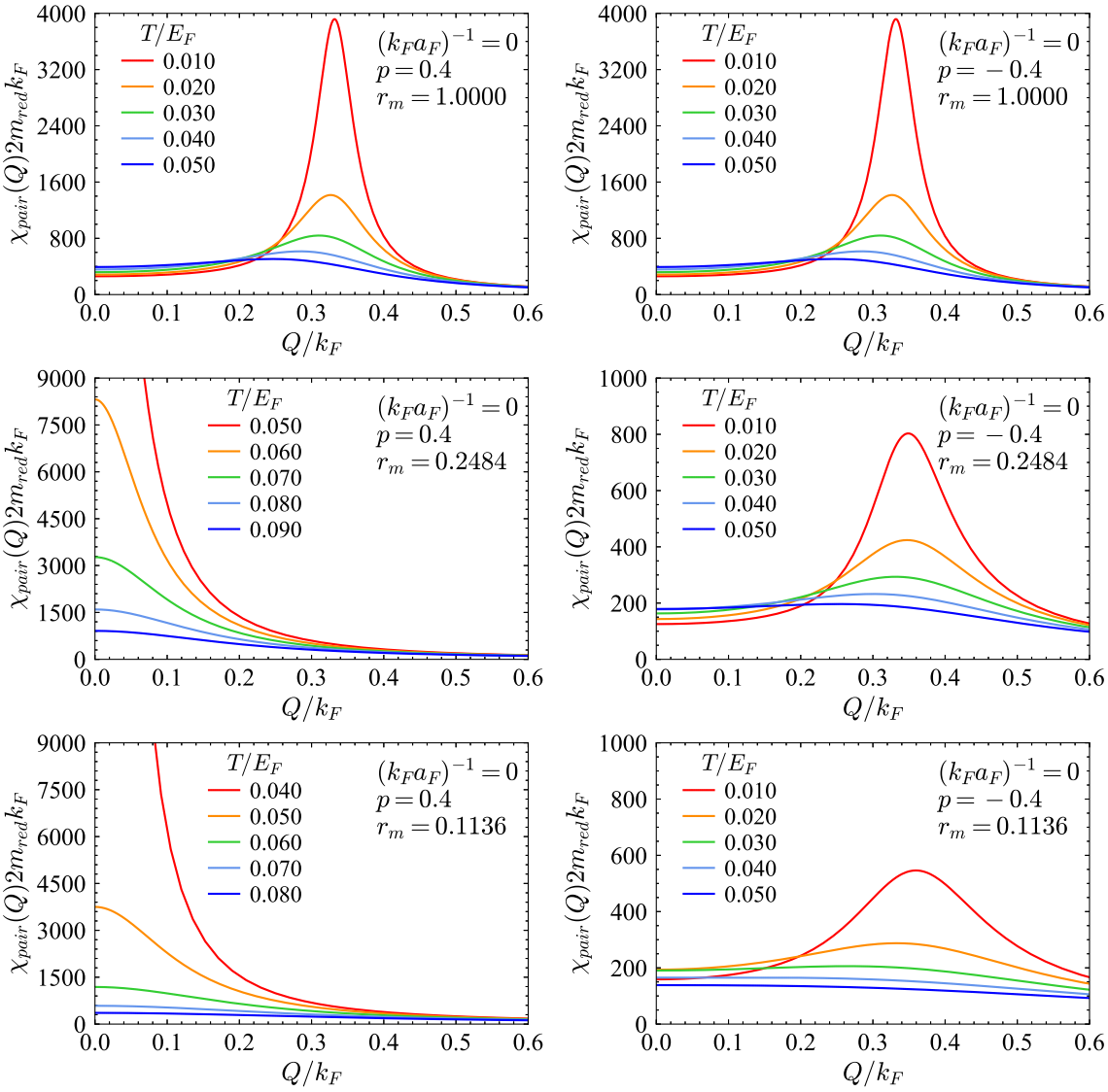

Figure 6.7: Pair susceptibility $\chi_{pair}(\mathbf{Q})$ (in units of $(2m_{red}k_F)^{-1}$) at unitarity vs pair momentum $Q = |\mathbf{Q}|$ (in units of k_F) at various temperatures for two different values of polarization $p = 0.4$ (left) and $p = -0.4$ (right). The three different mass ratios r_m correspond to the balanced (top), K-Dy (middle) and Li-Cr (bottom) mixtures.

Chapter 7

Numerical Results at Zero Temperature

In this chapter, we present the numerical results obtained within the Luttinger-Ward approach at zero temperature. First of all, we discuss the results for the $T = 0$ phase diagram (coupling-polarization), focusing on three different mass ratios, corresponding to a balanced mixture, a ^{40}K-^{161}Dy (potassium-dysprosium) mixture and a ^{6}Li-^{53}Cr (lithium-chromium) mixture. The evolution towards a non-Fermi liquid behaviour at the quantum critical point (QCP) is investigated by analyzing the quasi-particle residues and effective masses in function of the polarization. Finally, we present some results for the Matsubara self-energies, which can be connected to the low frequency behaviour of the spectral weight functions at the Fermi surface. The results for the two mass imbalanced mixtures are a new contribution of this thesis, while the results for the mass balanced mixture were already obtained in Ref. [47], anyway reproduced here for completeness.

7.1 Zero Temperature Phase Diagram

As discussed in Section 4.3.2, The critical polarization p_c for the second-order normal-to-superfluid transition is determined by the generalized Thouless criterion (4.34)

$$[\Gamma(\mathbf{Q} = \mathbf{Q}_0, \Omega = 0)|_{p=p_c}]^{-1}, \tag{7.1}$$

where, if $\mathbf{Q}_0 = 0$, the transition is towards a Sarma superfluid, while if $\mathbf{Q}_0 \neq 0$, the transition is towards a FFLO superfluid. Indeed, we recall that the FFLO transition line can be correctly found only at zero temperature in our diagrammatic approach, because the divergence in the self-energy discussed in Section 3.2.1 becomes integrable only in the $T = 0$ limit.

In Figure 7.1, we present the critical polarization p_c as a function of the coupling $(k_F a_F)^{-1}$ at $T = 0$, within the zero temperature Luttinger-Ward approach, for three different mass ratios $r_m = m_\uparrow/m_\downarrow$. In all the diagrams, we can identify three phases: a normal Fermi liquid phase (N), a homogeneous polarized superfluid (Sarma) and an inhomogeneous superfluid (FFLO). They all meet at two different *Lifshitz points* (LP), generally defined as tricritical points among a disordered phase, a spatially uniform ordered phase and a spatially modulated ordered phase [116].

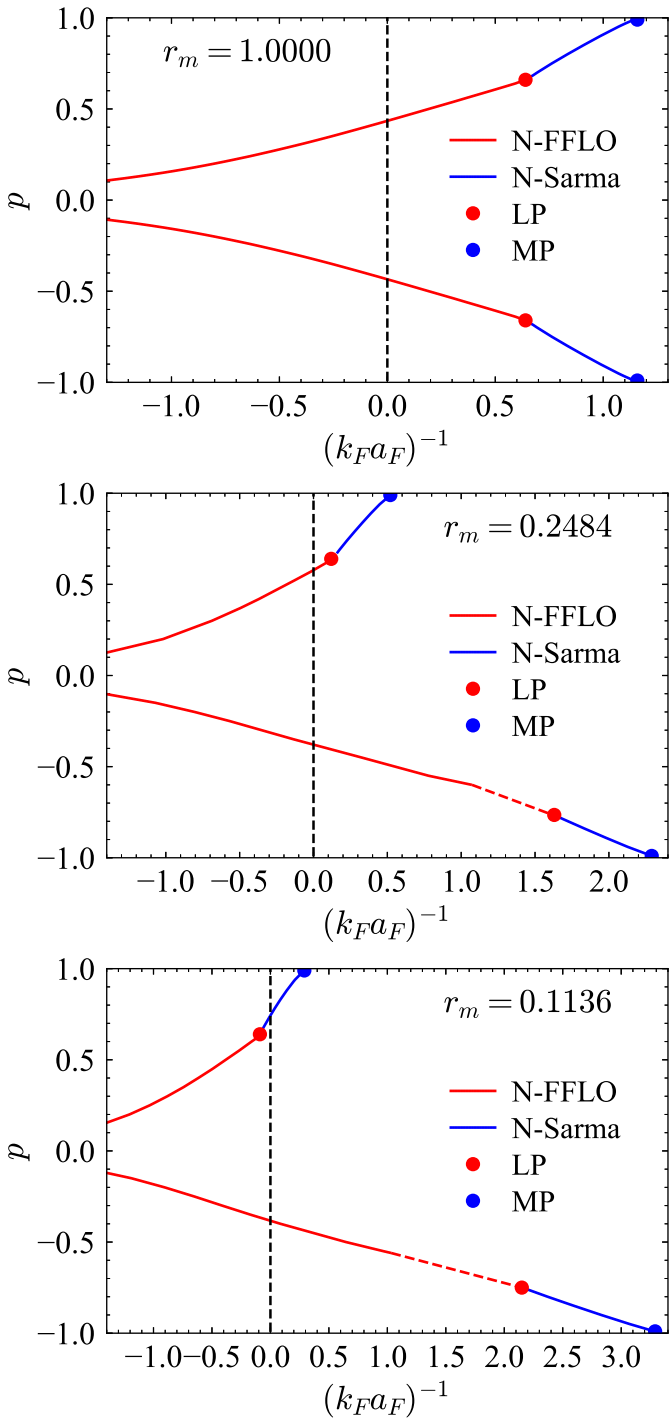

Figure 7.1: Polarization-vs-coupling phase diagram of the imbalanced ultra-cold Fermi gas at zero temperature, for the mass-balanced (above), K-Dy (middle) and Li-Cr mixtures (below). The diagrams are calculated within the self-consistent t-matrix approach, considering only the second order phase transitions from the normal (N) phase towards a FFLO superfluid (red line) or a Sarma superfluid (blue line). LP is the Lifshitz point while MP is the polaron-to-molecule transition point.

Notice that the presence of two Lifshitz points is related to an asymmetric situation in the polarization line due to a mass imbalance in the system. Indeed, for the mass-balanced mixture, the Lifshitz points are symmetrical and, in our approach, they are found at $((k_F a_F)_L^{-1}, p_L) = [(0.643, 0.658), (0.643, -0.658)]$. Instead, for the K-Dy mixture we have found $((k_F a_F)_L^{-1}, p_L) = [(0.106, 0.638), (1.627, -0.765)]$, while for the Li-Cr mixture $((k_F a_F)_L^{-1}, p_L) = [(-0.096, 0.629), (2.154, -0.749)]$. On the left of the Lifshitz points, the phase transition (red line) is between the normal (N) and the FFLO phase and slowly approaches $p = 0$ in weak-coupling $(k_F a_F)^{-1} \ll -1$. On its right, instead, the phase transition (blue line) is between the normal (N) and the Sarma phase and ends up in the *polaron-to-molecule transition points* (MP). These points are found at $(k_F a_F)_M^{-1} = [1.17, 1.17]$ for the mass-balanced mixture, $(k_F a_F)_M^{-1} = [0.54, 2.36]$ for the K-Dy mixture and $(k_F a_F)_M^{-1} = [0.29, 3.34]$ for the Li-Cr mixture. Unfortunately, for the mass-imbalanced systems at $p < 0$, we have not been able to complete the normal-FFLO transition line due to convergence problems in our numerical calculations. Despite this, we are still able to define the Lifshitz point as the final point in the normal-Sarma transition line, and therefore to obtain an extrapolation of the missing data.

Notably, for the mass-balanced system, the transition at unitarity $(k_F a_F)^{-1} = 0$ is still of FFLO kind at a critical polarization $p_c = 0.434$, in contrast to what is found in mean-field. For later convenience, we report the value $p_c = 0.776$, corresponding to the coupling $(k_F a_F)^{-1} = 0.8$. Moreover, for the K-Dy and Li-Cr mixtures at unitarity, we get $p_c = [0.578, -0.379]$ and $p_c = [0.743, -0.388]$, respectively.

The most important result of this analysis is a pure enlargement of the FFLO region when the system is mass-imbalanced with a majority of the heavy species, i.e. $p < 0$ following our convention. This is consistent with what has been discussed at the end of Section 1.4.1, within a mean-field approach. However, to be sure of this consideration, one has to check if the presence of a mass-imbalance in the system does not also imply a shift to the right of the strong-coupling limit in the phase diagram. This is done by evaluating the ratio $-\mu/(2\varepsilon_0)$ at the Lifshitz point with $p < 0$, where $\varepsilon_0 = (2m_{red} a_F^2)^{-1}$ is the binding energy of the bound state between two fermions of different species while $\mu = (\mu_\uparrow + \mu_\downarrow)/2$ is the mean chemical potential. Indeed, as discussed in Section 1.3, we expect that in the $(k_F a_F)^{-1} \gg 1$ limit this ratio approaches to one. From our calculations, we get $\mu_L/E_F = -2.89$ for the D-Ky mixture and $\mu_L/E_F = -4.99$ for the Li-Cr mixture, therefore $-\mu_L/(2\varepsilon_0) \equiv (k_F a_F)^2 \mu_L/E_F \simeq 1.09$ for the K-Dy and $-\mu_L/(2\varepsilon_0) \simeq 1.08$ for the Li-Cr. This means that the strong-coupling limit is not shifted with respect to the mass-balanced case.

At the QCP in the strong-coupling limit, one also expects that the ratio $|h|/(2\varepsilon_0)$ is of the order of one, where $h = (\mu_\uparrow - \mu_\downarrow)/2$ is the imbalancing field, while it increases in the normal phase and decreases in the superfluid phase. This happens because the presence of a sufficiently strong external field destroys the fermion pairs and hinders superfluidity also at $T = 0$. Indeed, at the Lifshitz points with negative polarization, we get $h_L/(2\varepsilon_0) \simeq 1.17$ for the K-Dy mixture and $h_L/(2\varepsilon_0) \simeq 1.11$ for the Li-Cr mixture.

7.2 Quasi-particle Residues and Effective Masses

In this section, we characterize the evolution of the Fermi liquid phase from the polaronic limit ($p \simeq 1$) to the superfluid QCP ($p = p_c$) at zero temperature in terms of the quasi particle residues at the Fermi surface $\mathcal{Z}_\sigma$ and effective masses m^*_σ.

First of all, it is necessary to generalize the results presented in Section 4.2.1, which are obtained in terms of the retarded self-energy, by extending the quasi-particle picture to the Matsubara formalism. Indeed, the expressions (4.23) and (4.27) (properly generalized to an imbalanced system) can also be obtained from the self-energies calculated on the imaginary axis. In order to do this, we substitute ω with $i\omega$ in the upper complex plane in (4.22), thus we get

$$i\omega - \xi^0_{\mathbf{k}\sigma} - \Sigma_\sigma(\mathbf{k}, \omega) = \frac{i\omega - \xi_{\mathbf{k}\sigma} + i\gamma_{\mathbf{k}\sigma}}{Z_{\mathbf{k}\sigma}}, \tag{7.2}$$

where now $\Sigma_\sigma(\mathbf{k}, \omega)$ is the Matsubara self-energy. We therefore expand the self-energy near the origin of the complex plane $i\omega = 0$ for $|\mathbf{k}| = k_{F\sigma}$ (since $\gamma_{k_{F\sigma}\sigma} = 0$ and $\xi_{k_{F\sigma}\sigma} = 0$)

$$\Sigma_\sigma(\mathbf{k}, \omega) \simeq \Sigma_\sigma(\mathbf{k}, 0) + i\omega \frac{\partial}{\partial(i\omega)} \operatorname{Im} \Sigma_\sigma(\mathbf{k}, \omega)\Big|_{i\omega=0}, \tag{7.3}$$

and, by inserting (7.3) in (7.2), we obtain the desired expression for the quasi-particle residues at the Fermi surface

$$\mathcal{Z}_\sigma = \left[1 - \frac{\partial}{\partial\omega} \operatorname{Im} \Sigma_\sigma(k_{F\sigma}, \omega)\Big|_{\omega=0}\right]^{-1}. \tag{7.4}$$

With algebraic manipulations similar to those made in Section 4.2.1, the inverse of the effective masses can be obtained from the relation

$$\frac{m_\sigma}{m^*_\sigma} = \mathcal{Z}_\sigma \left[1 + \frac{m_\sigma}{k_{F\sigma}} \frac{\partial}{\partial \mathbf{k}} \Sigma_\sigma(\mathbf{k}, 0)\Big|_{|\mathbf{k}|=k_{F\sigma}}\right]. \tag{7.5}$$

Figure 7.2 shows the evolution of the quasi-particle residues (7.4) and the inverse effective mass ratio (7.5) for the mass-balanced system in the normal phase as a function of the polarization $p > 0$, for two characteristic couplings $(k_F a_F)^{-1} = (0, 0.8)$. In the polaronic limit ($p \simeq 1$), the majority component is completely non-interacting, so $\mathcal{Z}_\uparrow = 1$ and and $m/m^*_\uparrow = 1$. The minority component, instead, is dressed by the majority atoms through the attractive interaction, and forms a quasi-particle (*attractive polaron*), with $\mathcal{Z}_\downarrow < 1$ and $m/m^*_\downarrow < 1$. By reducing p, the effects of the attractive interaction become stronger for both spin components, and the values of $\mathcal{Z}_\sigma$ and m/m^*_σ monotonically decrease. As discussed in Section 4.3.2, at the QCP the nature of the superfuid phase strongly influences the behavior of the quasi-particles: in the case of a FFLO phase, i.e. $(k_F a_F)^{-1} = 0$, the quasi-particle residues vanish and the effective masses diverge, while in the case of a Sarma phase, i.e. $(k_F a_F)^{-1} = 0.8$, they all remain finite, albeit strongly reduced with respect to the polaronic limit. The vanishing of quasi-particle residues and the divergence of the effective masses at a FFLO QCP correspond to a complete breakdown of the quasi-particle description of the Fermi liquid phase.

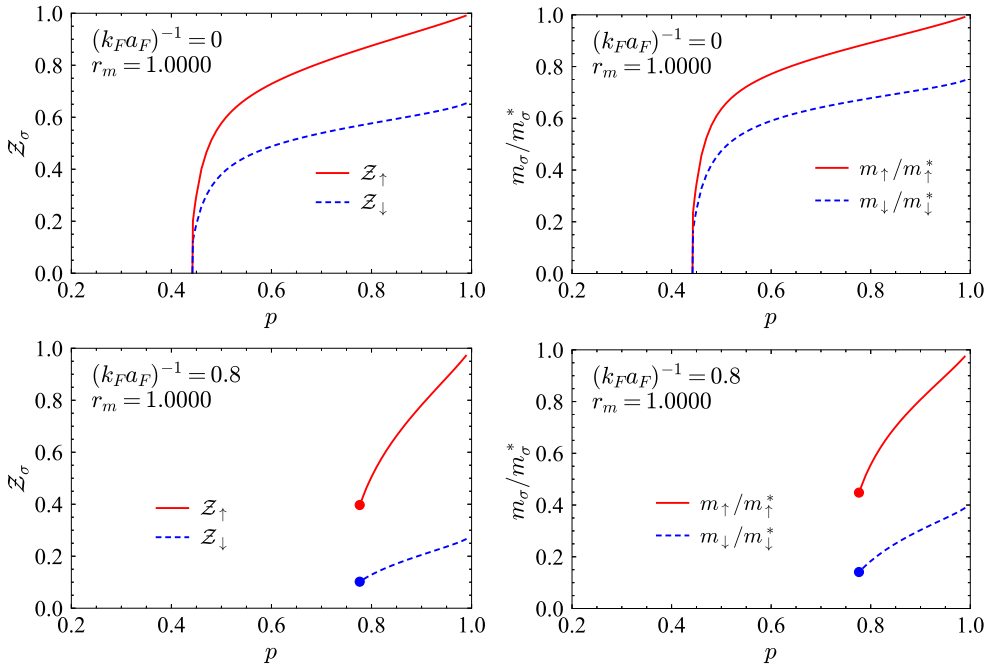

Figure 7.2: Quasi-particle residues $\mathcal{Z}_\sigma$ (left) and inverse effective mass ratio m/m_σ^* (right) for the two spin components as a function of the polarization $p > 0$ for the mass-balanced system at the couplings $(k_F a_F)^{-1} = 0$ (above) and $(k_F a_F)^{-1} = 0.8$ (below). *Source*: adapted from Ref. [47].

Figure 7.3 reports the same evolution at unitarity for the K-Dy and Li-Cr mixtures, for negative values of polarization $p < 0$ (majority of heavy species). Also in this case, the breakdown of the Fermi liquid theory at the FFLO QCP is evident, with a vanishing of Z_σ and m_σ/m_σ^* at the values of the critical polarization consistent with the results discussed in Section 7.1. At the negative polaronic limit ($p \simeq -1$), corresponding to a completely non-interacting system of heavier fermions, one can see that value of the quasi-particle residue for the minority component $\mathcal{Z}_\uparrow < 1$ decreases by reducing the mass ratio of the Fermi mixture $r_m = m_\uparrow/m_\downarrow$. The same consideration also applies for the ratio m_σ/m_σ^*. In particular, we obtain $\mathcal{Z}_\uparrow = 0.594$ and $m_\uparrow/m_\uparrow^* = 0.732$ for the K-Dy mixture, while $\mathcal{Z}_\uparrow = 0.473$ and $m_\uparrow/m_\uparrow^* = 0.515$ for the Li-Cr mixture.

It is also interesting to evaluate, for the two mass-imbalanced mixtures, the *polaron energy* in the polaronic limit at unitarity, given by the ratio $\mu_\uparrow/E_{F\downarrow}$ if $p \simeq -1$ (i.e. light polaron). We get $\mu_\uparrow/E_{F\downarrow} = -1.616$ and $\mu_\uparrow/E_{F\downarrow} = -3.269$ for the Li-Cr mixture, both very different from the same value in the mass-balanced case, $\mu_\uparrow/E_{F\downarrow} = -0.677$. This means that the absolute value of the light polaron energy becomes larger as the mass ratio $r_m = m_\uparrow/m_\downarrow$ decreases. Moreover, we also recover the trivial result $\mu_\downarrow/E_{F\downarrow} = 1$ for both the mixtures at $p \simeq -1$, consistently with the value of the chemical potential for a non-interacting Fermi gas at $T = 0$.

The previous results for the mass-imbalanced systems can be compared with the Diagrammatic Monte Carlo (DMC) values in the polaronic limit at unitarity [117]. It has been found that, for the K-Dy mixture, $\mathcal{Z}_\uparrow = 0.735$ and $\mu_\uparrow/E_{F\downarrow} = -2.61$ while, for the Li-Cr mixture, $\mathcal{Z}_\uparrow = 0.680$ and $\mu_\uparrow/E_{F\downarrow} = -1.49$. One sees that,

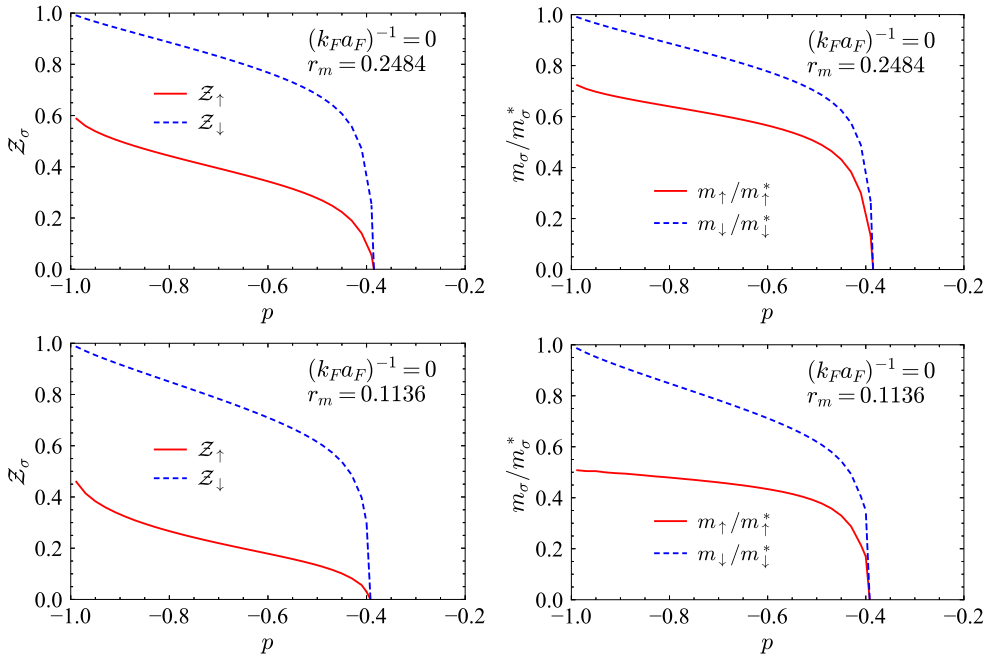

Figure 7.3: Quasi-particle residues $\mathcal{Z}_\sigma$ (left) and inverse effective mass ratio m/m^*_σ (right) for the two spin components as a function of the polarization $p < 0$ for the mass-imbalanced systems at unitarity $(k_F a_F)^{-1} = 0$. the mass ratios $r_m = (0.2484, 0.1136)$ correspond to the K-Dy (above) and the Li-Cr mixtures (below), respectively.

if we consider the DMC results as a benchmark, the fully self-consistent t-matrix approach slightly overestimates the effects of interaction with the majority species. This consideration obviously holds also in the mass-balanced case where, according to the DMC results, $\mathcal{Z}_\uparrow = 0.760$ and $\mu_\uparrow/E_{F\downarrow} = -0.615$.

7.3 Matsubara Self-Energies

From the expression (7.4), we see that the vanishing of the quasi-particle residues $\mathcal{Z}_\sigma$ at the FFLO QCP requires the derivative of $\mathrm{Im}\,\Sigma_\sigma(k_{F\sigma}, \omega)$ with respect to ω to diverge at $\omega = 0$. It is interesting to see how this non-Fermi liquid behavior is reached by progressively reducing the polarization and thus approaching the QCP.

In Figure 7.4, we show the evolution with polarization $(p < 0)$ of $\mathrm{Im}\,\Sigma_\sigma(k_{F\sigma}, \omega)$ for both spin components in the K-Dy mixture at unitarity. We can see that, for $\omega \simeq 0$, the Fermi liquid linear behavior $\mathrm{Im}\,\Sigma_\sigma(k_{F\sigma}, \omega) \simeq (1 - 1/\mathcal{Z})\omega$ is gradually replaced by a square-root behavior at the FFLO QCP. Specifically, we find a robust fit of the data at low ω given by

$$\mathrm{Im}\,\Sigma_\sigma(k_{F\sigma}, \omega) = -C_\sigma \sqrt{\omega}, \tag{7.6}$$

where C_σ is a real positive constant. Notice that, consistently with the finding of a finite residue, along the N-Sarma critical line $\mathrm{Im}\,\Sigma_\sigma(k_{F\sigma}, \omega)$ remains linear with ω.

In Figure 7.5, we report the evolution with polarization $(p < 0)$ in the K-Dy mixture at unitarity for the quantities $\mathrm{Re}\,\Delta\Sigma_\sigma(k_{F\sigma}, \omega) = \mathrm{Re}[\Sigma_\sigma(k_{F\sigma}, \omega) - \Sigma_\sigma(k_{F\sigma}, 0)]$.

Also in this case, we find a square root behaviour at low ω of the form

$$\mathrm{Re}\,\Sigma_\sigma(k_{F\sigma},\omega) = \Sigma_\sigma(k_{F\sigma},0) + B_\sigma\sqrt{\omega}, \tag{7.7}$$

where B_σ is a real positive constant and we used the fact that the self-energies $\Sigma_\sigma(k_{F\sigma},0)$ are real.

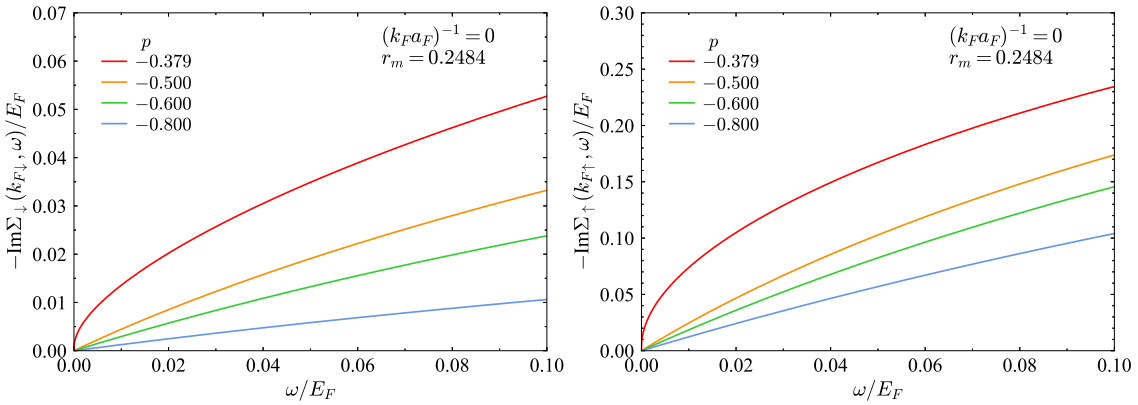

Figure 7.4: Imaginary part of self-energies $\Sigma_\sigma(k_{F\sigma},\omega)$ (in units of $E_F = k_F^2/(4m_{red})$) at the Fermi surface as a function of the frequency on the imaginary axis ω at $T=0$ and unitarity for the K-Dy mixture. The value $p=-0.379$ corresponds to the critical polarization p_c at unitarity.

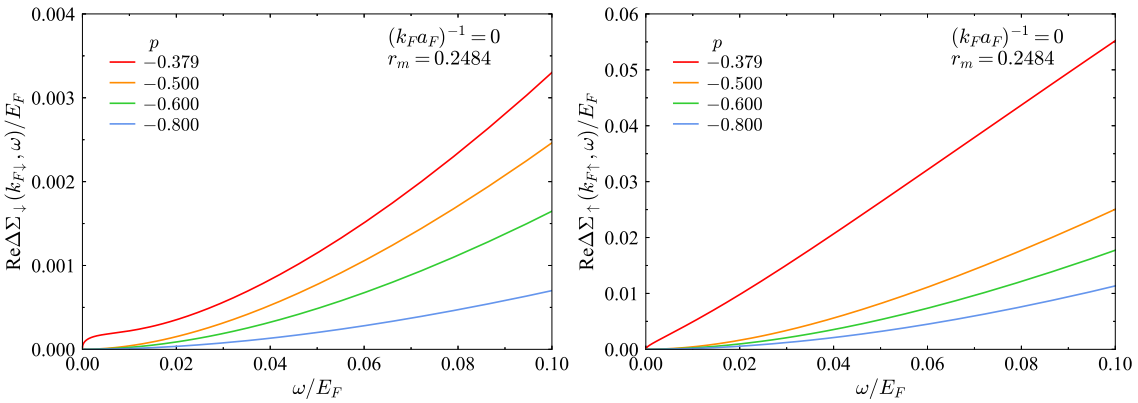

Figure 7.5: Real part of $\Delta\Sigma_\sigma(k_{F\sigma},\omega) = \Sigma_\sigma(k_{F\sigma},\omega) - \Sigma_\sigma(k_{F\sigma},0)$ (in units of $E_F = k_F^2/(4m_{red})$) at the Fermi surface as a function of the frequency on the imaginary axis ω at $T=0$ and unitarity for the K-Dy mixture. The value $p=-0.379$ corresponds to the critical polarization p_c at unitarity.

The square-root behavior which we have found for both $\mathrm{Im}\,\Sigma_\sigma$ and $\mathrm{Re}\,\Delta\Sigma_\sigma$ can be connected to the low frequency behaviour of the spectral weight functions $A_\sigma(k_{F\sigma},\omega)$ at the FFLO QCP. This is quite interesting because we can still get some information on the spectral weight functions from the imaginary-time formalism, although a complete knowledge of these quantities is achieved only after a numerical analytic continuation, as discussed in Section 2.3.1. We start by noticing that the expressions

(7.6) and (7.7), after the analytical continuation in the upper complex plane $i\omega \to \omega + i0^+$, allow us to get the small frequency behaviour of the retarded self-energies

$$\Sigma_\sigma^R(k_{F\sigma},\omega) = \Sigma_\sigma(k_{F\sigma},0) + [B_\sigma - C_\sigma \mathrm{sgn}(\omega)]\sqrt{\frac{|\omega|}{2}} - i[C_\sigma + B_\sigma \mathrm{sgn}(\omega)]\sqrt{\frac{|\omega|}{2}}, \quad (7.8)$$

for frequencies $\omega \to 0$. Notice that the physical condition $\mathrm{Im}\,\Sigma_\sigma^R \leq 0$ requires $B_\sigma \leq C_\sigma$, a condition which we found to be always satisfied by our fittings. This expression, plugged in the Dyson equation (4.28) to get the retarded Green's functions $G_\sigma^R(k_{F\sigma},\omega)$, together with the expression (4.33), yields

$$A_\sigma^{(QCP)}(k_{F\sigma},\omega) = \frac{D_{\sigma\pm}}{|\omega|^{1/2}}, \quad (7.9)$$

where the coefficient $D_{\sigma\pm}$ depends on the sign of the frequency ω, and is given by

$$D_{\sigma\pm} = \frac{1}{\sqrt{2}\pi}\frac{C_\sigma + B_\sigma \mathrm{sgn}(\omega)}{B_\sigma^2 + C_\sigma^2}. \quad (7.10)$$

It is clear that the behaviour in (7.9) is very different from the Fermi liquid behaviour at $|\mathbf{k}| = k_{F\sigma}$, given by $A_\sigma(k_{F\sigma},\omega) = \mathcal{Z}_\sigma\delta(\omega)$, as discussed in Section 4.2. This means that the spectral weight functions $A_\sigma(\mathbf{k},\omega)$, as well as containing important dynamical properties of the system, also present a direct evidence of the non-Fermi liquid behavior at the FFLO QCP.

Moreover, the behaviour (7.9) at the QCP can be connected to the *dynamical critical exponent* z[1] of the *dynamic pair susceptibility* $\chi_{pair}(\mathbf{Q},\Omega) \equiv \Gamma(\mathbf{Q},\Omega)$, obtained by generalizing the expression (6.34). It has been verified numerically [47] that, on the positive imaginary frequency axis for $|\mathbf{Q}| \simeq Q_0$ and $i\Omega \simeq 0$, one has

$$\chi_{pair}(\mathbf{Q},\Omega) \simeq \frac{(2m_{red}k_F)^{-1}}{\epsilon + b(|\mathbf{Q}| - Q_0)^2 - (d_1 + id_2)i\Omega}, \quad (7.11)$$

where the parameters ϵ,b,d_1,d_2 are all real and positive, and ϵ vanishes at the QCP. By performing the analytic continuation $i\Omega \to \Omega + i0^+$ to the real axis, and introducing the *coherence length* $\xi = \sqrt{b/\epsilon}$[2], we obtain the scaling form for the dynamical pairing susceptibility

$$\tilde{\chi}_{pair}(\mathbf{Q},\Omega;\xi) = \frac{\xi^2}{2m_{red}k_F b}\Phi_0[(|\mathbf{Q}| - Q_0)\xi, m_1\Omega\xi^2], \quad (7.12)$$

where $m_1 = (d_1 + id_2)/b$ is a non-universal complex constant and Φ_0 is a universal *scaling function*. From this expression, we see that the real frequency Ω scales with the inverse of a *coherence time* $\xi_t \sim \xi^2$ i.e. the dynamical critical exponent is $z = 2$.

[1] It is known that, near second order (continuous) phase transitions, many static physical quantities show *power law* behaviours described by different exponents, known as *critical exponents*. However, critical singularities also occur in dynamic properties, such as multi-time correlation functions, responses to time-dependent perturbations and transport coefficients. In particular, the characteristic time t_{char} of a system diverges with the *correlation length* ξ as $t_{char} \propto \xi^z$, where z is the *dynamical critical exponent* [118].

[2] The *phase coherence length* ξ is the length associated with the spatial fluctuations of the superfluid order parameter [119]. It represents the correlation length for our theory.

Quite generally, at QCPs where the quasi-particle residue vanishes, the spectral weight functions for $|\mathbf{k}| \simeq k_{F\sigma}$ and $\omega \simeq 0$ should have the scaling form [47] [120]

$$A_{\sigma}^{(QCP)}(\mathbf{k},\omega) = \frac{c_{0\sigma}}{|\omega|^{1/z}} F_0\left[\frac{c_{1\sigma}\omega}{||\mathbf{k}| - k_{F\sigma}|^z}\right], \tag{7.13}$$

where F_0 is a universal scaling function, $c_{0\sigma}$ and $c_{1\sigma}$ are non-universal constants. By taking the limit $|\mathbf{k}| \to k_{F\sigma}$ in (7.13), we recover (7.9), with $D_{\sigma\pm} = c_{0\sigma}F(\pm\infty)$. We thus conclude that, also in this case, the dynamical critical exponent is $z = 2$.

Conclusions and Perspectives

In this thesis, we have presented a theoretical study of the properties of a mass-imbalanced and polarized ultra-cold Fermi gas in the normal phase throughout the BCS-BEC crossover. In particular, we focused on two different mass-imbalanced systems: ^{40}K-^{161}Dy (potassium-dysprosium) mixture and ^{6}Li-^{53}Cr (lithium-chromium) mixture. The study has been performed by means of a many-body diagrammatic approach based on the t-matrix approximation, where only ladder diagrams with repeated particle-particle interactions are retained. More specifically, the calculations have been implemented using the Luttinger-Ward approach, or fully self-consistent t-matrix, obtained by replacing all the bare propagators $\mathcal{G}^0_\sigma$ with dressed propagators $\mathcal{G}_\sigma$ in the t-matrix self-energy diagrams.

At finite temperature, the analysis of the system was carried out by calculating different thermodynamic quantities: the critical temperature T_c, the chemical potentials for the two species μ_σ, the Tan's contact C and the pair susceptibility $\chi_{pair}(\mathbf{Q})$. We have shown that the latter is used to study the presence of strong FFLO fluctuations in the normal phase, which are precursors of an exotic Fulde-Ferrell-Larkin-Ovchinnikov (FFLO) phase, an inhomogeneous superfluid characterized by a finite center-of-mass momentum of the fermionic pairs. In this regard, we have found that the FFLO phase in mass-imbalanced systems is suppressed when the majority of the species is the lighter one. Moreover, we have also considered the high-temperature limit of the t-matrix approximation, which reduces to the virial expansion for a quantum gas and thus becomes exact in this limit. This is naturally quite a satisfactory feature of this approximation and is also useful for providing initial guess values of the chemical potentials in our numerical calculations.

At zero temperature, for large polarization and not too strong interactions, we have seen that the mixtures still remain in the normal phase, because an imbalance between the two spin populations works against pairing and superfluidity. In this region, the system is well described by the Landau theory of Fermi liquids, which however breaks down at the FFLO quantum critical point (QCP). In this case, to obtain the numerical results, it was essential to employ a $T = 0$ formulation of the fully self-consistent t-matrix approach, so that the FFLO quantum critical line could be correctly identified. This version, which still works with frequencies on the imaginary axis, has been shown to satisfy the Luttinger theorem and correctly describe the Fermi surfaces over which the fermionic quasi-particles are defined. A relevant result in the coupling-polarization phase diagram for the mass-imbalanced mixtures, is a pure enlargement of the FFLO region with a majority of the heavy species, without any shift to the right of the strong-coupling limit. The evolution of the Fermi liquid normal phase towards a non-Fermi liquid behaviour has been

investigated by studying the quasi-particle residues and effective masses, ranging in polarization from the polaronic limit to the superfluid QCP. We found that the Fermi liquid description in terms of quasi-particles remains valid at the QCP towards the homogeneous polarized phase (Sarma phase), while at the FFLO QCP we found instead a complete breakdown of the quasi-particle description, characterized by the vanishing of the quasi-particle residues, the divergence of the quasi-particle effective masses and an anomalous $\sim \omega^{1/2}$ frequency dependence of the real and imaginary parts of the Matsubara self-energies at the Fermi surface. This square-root behaviour allowed us to find the form of the spectral weight functions at the FFLO QCP, in the low frequency limit at the Fermi surface, which is found to be very different from the standard behaviour of a Fermi liquid. This result is consistent with a scaling at the QCP with dynamical critical exponent $z = 2$.

As a perspective, it would be interesting to have a complete knowledge of the spectral weight functions for a mass and spin-imbalanced system, which is achieved only after a numerical analytic continuation. This is usually performed by means of the Padè approximants, using a recursive algorithm developed by Serene in 1977 [121]. Although this simple algorithm is already a powerful tool for the analytic continuation, it is known in the literature that, in practice, the procedure is quite sensitive to the numerical errors in the input values on the imaginary axis, to the extent that sometimes defects appear in the spectral function, distorting it and even making it acquire negative values. To mitigate this issue, it is possible to consider an average over multiple analytic continuations performed with different sets of points on the imaginary axis, discarding the analytic continuations which give negative functions. Actually, in a very recent work by Fei et al. [122], it was proposed an alternative method for the analytic continuation that makes use of Nevanlinna functions, a set complex functions analytical in the open upper half plane with a non-negative imaginary part. Within this interesting method, the spectral weight functions are guaranteed to be intrinsically positive. Finally, to explore in more details the properties of imbalanced ultra-cold Fermi gases, it would be very intriguing to extend our formalism to describe the superfluid phase and to study the system at different dimensionalities, in particular in 2D, where a Berezinskii-Kosterlitz-Thouless transition (BKT) from bound vortex-antivortex pairs at low temperatures to unpaired vortices and anti-vortices at some critical temperature can occur.

Appendix A

Haussmann's Fourier Transforms

Here we describe the numerical procedure developed by Haussmann [85, 86] to compute the Fourier transforms, as in (3.81) and (3.82), for the Green's function $\mathcal{G}$ and the particle-particle propagator Γ, respectively. This powerful method is a good alternative to the standard fast Fourier transform (FFT), which requires a constant step width, since it receives as input any grid of points. However, to get this freedom of choice we need to pay a price: numerical efficiency.

The numerical work can be considerably reduced by exploiting the rotational symmetry of the system, which implies that the functions to be transformed depend only on the absolute values of $\mathbf{k}$, $\mathbf{Q}$ and $\mathbf{x}$ (i.e. we can analytically perform an integration over the angles). Thus, the Fourier transformations (3.81) and (3.82) become effectively two-dimensional and we need a one-dimensional continuous Fourier transformation for transforming the functions in the variables $k, Q \leftrightarrow x$ and $\tau \to \omega_n, \Omega_\nu$, plus a discrete Fourier transformation for transforming the functions in the variables $\omega_n, \Omega_\nu \to \tau$[1].

A.1 Continuous Fourier Transformation

We need to evaluate quantities in the form

$$f(k) = \int_{x_{min}}^{x_{max}} dx\, e^{ikx} f(x) \approx \lim_{\Delta x \to 0} \sum_{x=x_{min}}^{x_{max}} \Delta x\, e^{ikx} f(x), \tag{A.1}$$

where x is a discrete variable with constant step width Δx and the sum is a *trapezoid sum* (i.e. the first and last term are multiplied by a factor 1/2). We assume that the function values are known in a finite subset of $N+1$ distinct points x_j such that they cover the whole interval between x_{min} and x_{max}, i.e. $x_{min} = x_0 < x_1 < \cdots < x_N = x_{max}$, distributed on a generic grid. Notice that, in general, the choice of the points depends on the characteristics of the function to be transformed. For example, we can use a *logarithmic grid* given by

$$x_j = \gamma^{-1} \sinh(\gamma \Delta x j), \tag{A.2}$$

[1]Some analytical expressions for the discrete Fourier transformations are reproduced from private notes by M. Pini.

where γ is a numerical parameter which determines the distribution of points on the grid, or an *equally-spaced grid*, i.e. $x_j = x_0 + j\Delta x$, but also a combination of the previous two.

Consequently, we can divide the sum in (A.1) into a sum of N trapezoid sums

$$\sum_{x=x_{min}}^{x_{max}} \Delta x\, e^{ikx} f(x) = \sum_{j=0}^{N-1} \Big\{ \sum_{x=x_j}^{x_{j+1}} \Delta x\, e^{ikx} f(x) \Big\}, \tag{A.3}$$

and we assume that the function $f(x)$ can be approximated for $x \in [x_j, x_{j+1}]$ by a *cubic spline polynomial*

$$f(x) = a_j + b_j(x - x_j) + c_j(x - x_j)^2 + d_j(x - x_j)^3, \tag{A.4}$$

where the spline coefficients a_j, b_j, c_j and d_j can be calculated numerically. By inserting the spline polynomial into (A.3), we find that the trapezoid sums can be evaluated analytically, obtaining

$$f(k) = \sum_{j=0}^{N-1} \big\{ a_j I_j^{(0)}(k) + b_j I_j^{(1)}(k) + c_j I_j^{(2)}(k) + d_j I_j^{(3)}(k) \big\}, \tag{A.5}$$

where

$$I_j^{(n)}(k) = e^{ikx_j} \left(-i\frac{\partial}{\partial k} \right)^n \left[\frac{\Delta x}{2i} \cot\left(\frac{k\Delta x}{2} \right) [e^{ik(x_{j+1}-x_j)} - 1] \right]. \tag{A.6}$$

The continuous limit is easily obtained by taking $\Delta x \to 0$ in the previous expression, i.e. $\Delta x/(2i)\cot(k\Delta x/2) \to 1/(ik)$.

The expression (A.5) is good for small values of k ($|kx_j| \lesssim 1$ for all $j = 0, \ldots, N$), since it does not have any divergence for $k \to 0$. However, for large values of k it is better to use an alternative formula obtained from the properties of the spline interpolation. Indeed, since a cubic spline function and its two derivatives are continuous by construction, we easily get the continuity conditions

$$\begin{aligned} f(x_{j+1}) &= a_j + b_j(x_{j+1} - x_j) + c_j(x_{j+1} - x_j)^2 + d_j(x_{j+1} - x_j)^3 = a_{j+1}, \\ f'(x_{j+1}) &= b_j + 2c_j(x_{j+1} - x_j) + 3d_j(x_{j+1} - x_j)^2 = b_{j+1}, \\ f''(x_{j+1}) &= 2c_j + 6d_j(x_{j+1} - x_j) = 2c_{j+1}, \end{aligned} \tag{A.7}$$

which may be used to regroup the terms in (A.5). As a result, we get the alternative expression

$$\begin{aligned} f(k) = J^{(0)}(k)[e^{ikx_N} a_N - e^{ikx_0} a_0] + J^{(1)}(k)[e^{ikx_N} b_N - e^{ikx_0} b_0] \\ + J^{(2)}(k)[e^{ikx_N} c_N - e^{ikx_0} c_0] + J^{(3)}(k) \sum_{j=0}^{N-1} [(e^{ikx_{j+1}} - e^{ikx_j}) d_j], \end{aligned} \tag{A.8}$$

where

$$J^{(n)}(k) = \left(-i\frac{\partial}{\partial k} \right)^n \left[\frac{\Delta x}{2i} \cot\left(\frac{k\Delta x}{2} \right) \right], \tag{A.9}$$

which is still well defined in the continuous limit $\Delta x \to 0$. The functions (A.9) diverge for $k \to 0$ as $J^{(n)}(k) \sim |k|^{-(n+1)}$ and, for this reason, the alternative formula

(A.8) can be applied numerically only for large values of k ($|kx_j| \gtrsim 1$ for all $j = 0, \ldots, N$). In practice, we use a combination of both formulas (A.5) and (A.8) such that we obtain a special numerical Fourier transformation which is stable and reliable.

A.2 Discrete Fourier Transformation

The previous procedure can be applied also to a Fourier series

$$f(\tau) = \frac{1}{\beta} \sum_{\nu} e^{-i\omega_\nu \tau} f(\omega_\nu), \tag{A.10}$$

where the Matsubara frequencies ω_ν can be either bosonic or fermionic. We assume for simplicity that $f(\omega_\nu) = f(-\omega_\nu)^*$, i.e. $f(\tau)$ is a real function, such that we can rewrite the series as

$$f(\tau) = \frac{1}{\beta} f(\omega_\nu = 0) + \frac{2}{\beta} \mathrm{Re} \left[\sum_{\nu>0} e^{-i\omega_\nu \tau} f(\omega_\nu) \right], \tag{A.11}$$

where the first term is present only in the bosonic case. In this way, we have to calculate the sum only for positive frequencies, i.e. $\nu > 0$. Also in this case, we take into account distinct and ordered Matsubara frequencies ω_j, sampled on a generic grid. For example, a good choice for the fermionic frequencies on a logarithmic scale is given by

$$\omega_j = \frac{2\pi}{\beta} \mathrm{nint}\left(\frac{\sinh(\gamma j)}{\gamma} \right) + \frac{\pi}{\beta}, \tag{A.12}$$

where $\mathrm{nint}(\ldots)$ is the nearest integer function, while for an equally-spaced grid we have $\omega_j = j\Delta\omega + \pi/\beta$, where $\Delta\omega = 2\pi/\beta$ is the difference between two neighboring frequencies.

Now we have to evaluate numerically the quantity in the square brackets in (A.11), which can be expressed as a sum of $N-1$ sums

$$\sum_{\nu=\nu_{min}}^{\nu_{max}} e^{-i\omega_\nu \tau} f(\omega_\nu) \equiv \sum_{\omega=\omega_{min}}^{\omega_{max}} e^{-i\omega\tau} f(\omega) = \sum_{j=1}^{N-1} \left\{ \sum_{\omega=\omega_j}^{\omega_{j+1}} e^{-i\omega\tau} f(\omega) \right\}, \tag{A.13}$$

with $\omega_{min} = \omega_1 < \omega_2 < \cdots < \omega_N = \omega_{max}$. Notice that, unlike the continuous case, we do not have any trapezoid sum here. We can now perform the cubic spline approximation for $\omega \in [\omega_j, \omega_{j+1}]$

$$f(\omega) = a_j + b_j(\omega - \omega_j) + c_j(\omega - \omega_j)^2 + d_j(\omega - \omega_j)^3, \tag{A.14}$$

which allows to evaluate analytically the sums inside the curly brackets in (A.13), obtaining an expression for small values of τ that is identical to (A.5), where now

$$I_j^{(n)}(\tau) = e^{-i\omega_j\tau} \left(i\frac{\partial}{\partial\tau} \right)^n \left[\frac{1 - e^{-i(\omega_{j+1}-\omega_j)\tau}}{1 - e^{-i\Delta\omega\tau}} \right]. \tag{A.15}$$

In the same way, we can get an alternative formula identical to (A.8), which can be applied only for large values of τ, with the modified J-functions given by

$$J^{(n)}(\tau) = \left(i\frac{\partial}{\partial\tau} \right)^n \left[\frac{1}{e^{-i\Delta\omega\tau} - 1} \right]. \tag{A.16}$$

Appendix B

Achievement of Self-consistency at Finite Temperature

Here we present in detail the numerical procedures that are needed to implement the cycle of self-consistency, presented in Figure 3.5, in the Luttinger-Ward approach at finite temperature. This appendix is the direct generalization to the imbalanced case of Appendix A in Ref. [46]. Consistently with the numerical programs, all the expressions reported in this appendix are given in dimensionless units, such that wave vectors are in units of the *effective* Fermi momentum $k_F = (3\pi^2 n)^{1/3}$, with $n = n_\uparrow + n_\downarrow$, and energies (as well as temperatures, since $k_B = 1$) in units of the Fermi energy $E_F = k_F^2/(2m)$[1]. The parameter m is simply substituted by $2m_{red}$ for mass imbalanced systems. Accordingly, the single-particle propagator $\mathcal{G}_\sigma(\mathbf{k}, \omega_n)$ is in units of E_F^{-1}, the self-energy $\Sigma_\sigma(\mathbf{k}, \omega_n)$ in units of E_F and the particle-particle propagator $\Gamma(\mathbf{Q}, \Omega_\nu)$ in units of $(mk_F)^{-1}$. In addition, we use the symbol $v = (k_F a_F)^{-1}$ for the coupling.

B.1 Transforming from $\mathcal{G}_\sigma(\mathbf{k}, \omega_n)$ to $\mathcal{G}_\sigma(\mathbf{x}, \tau)$

The Fourier transform of the single-particle fermionic propagator $\mathcal{G}$ can be done in two steps, namely

$$\mathcal{G}_\sigma(\mathbf{k}, \omega_n) \to \mathcal{G}_\sigma(\mathbf{k}, \tau) \to \mathcal{G}_\sigma(\mathbf{x}, \tau), \tag{B.1}$$

hence a discrete transformation followed by a continuous one.

First of all, we recall that the dressed Green's function $\mathcal{G}(\mathbf{k}, \omega_n)$ for large frequencies behaves like the free propagator

$$\mathcal{G}_\sigma(\mathbf{k}, \omega_n) \underset{\omega_n \to \infty}{\simeq} \mathcal{G}_\sigma^0(\mathbf{k}, \omega_n) = \frac{1}{i\omega_n - \xi_{\mathbf{k}\sigma}}, \tag{B.2}$$

where $\xi_{\mathbf{k}\sigma} = \gamma_\sigma \mathbf{k}^2 - \mu_\sigma$, with $\gamma_\sigma = m/m_\sigma$. We can therefore calculate numerically the Fourier series from ω_n to τ of the difference $\Delta\mathcal{G}_\sigma(\mathbf{k}, \omega_n) = \mathcal{G}_\sigma(\mathbf{k}, \omega_n) - \mathcal{G}_\sigma^0(\mathbf{k}, \omega_n)$,

[1] Notice that these choices are just conventions that easily generalize the case of a balanced system. For example, another possible choice is to consider the Fermi momentum $k_{F\sigma} = (6\pi^2 n_\sigma)^{1/3}$ and the Fermi energy $E_{F\sigma} = k_{F\sigma}^2/(2m_\sigma)$ referring to the heavier species.

which is easier to obtain since it converges for large frequencies as $\Delta\mathcal{G}_\sigma(\mathbf{k},\omega_n) \sim \omega_n^{-5/2}$. Then we add to this result the quantity $\mathcal{G}^0_\sigma(\mathbf{k},\tau)$, which it is known analytically in the form

$$\mathcal{G}^0_\sigma(\mathbf{k},\tau) = e^{-\xi_{\mathbf{k}\sigma}\tau}(f(\xi_{\mathbf{k}\sigma})-1), \tag{B.3}$$

as we can easily check from (2.24) with $\tau > 0$, where $f(\xi_{\mathbf{k}\sigma})$ is the Fermi function.

In the second step, it is convenient to split the expression B.3 in two parts

$$\begin{aligned} \mathcal{G}^0_{\sigma,n}(\mathbf{k},\tau) &= f(\xi_{\mathbf{k}\sigma})e^{-\xi_{\mathbf{k}\sigma}\tau}, \\ \mathcal{G}^0_{\sigma,a}(\mathbf{k},\tau) &= -e^{-\xi_{\mathbf{k}\sigma}\tau}, \end{aligned} \tag{B.4}$$

such that $\mathcal{G}^0_\sigma(\mathbf{k},\tau) = \mathcal{G}^0_{\sigma,n}(\mathbf{k},\tau) + \mathcal{G}^0_{\sigma,a}(\mathbf{k},\tau)$, where the subscripts n and a mean that the term has to be numerically and analytically transformed, respectively. Therefore, we can compute the analytical Fourier transform, which is given by

$$\mathcal{G}^0_{\sigma,a}(\mathbf{x},\tau) = -\frac{e^{\mu_\sigma\tau}e^{-\mathbf{x}^2/(4\gamma_\sigma\tau)}}{8(\pi\gamma_\sigma\tau)^{3/2}}, \tag{B.5}$$

which in the limit $\tau \to 0^+$ is a representation of the Dirac delta function $\delta(\mathbf{x})$. This term describes the singular behaviour for $(\mathbf{x},\tau) \to 0^+$, not only in the free case but also for the dressed propagator. It is thus convenient to work with the difference $\tilde{\Delta}\mathcal{G}_\sigma(\mathbf{k},\tau) = \mathcal{G}_\sigma(\mathbf{k},\tau) - \mathcal{G}^0_{\sigma,a}(\mathbf{k},\tau)$, which can be readily Fourier transformed numerically. The desired function $\mathcal{G}_\sigma(\mathbf{x},\tau)$ is obtained by adding (B.5) to $\tilde{\Delta}\mathcal{G}_\sigma(\mathbf{x},\tau)$.

B.2 Transforming from $\Gamma(\mathbf{Q},\Omega_\nu)$ to $\Gamma(\mathbf{x},\tau)$

The Fourier transform of the particle-particle propagator Γ can done be in two steps, namely

$$\Gamma(\mathbf{Q},\Omega_\nu) \to \Gamma(\mathbf{Q},\tau) \to \Gamma(\mathbf{x},\tau), \tag{B.6}$$

exactly as we did above for the fermionic propagator $\mathcal{G}$.

We begin by noticing that, for large frequencies, the particle-particle propagator $\Gamma(\mathbf{Q},\Omega_\nu)$ behaves like its non-self-consistent counterpart in the strong-coupling limit, i.e. Γ_0^{SC} in (3.50), that in dimensionless units reads

$$\Gamma(\mathbf{Q},\Omega_\nu) \underset{\Omega_\nu\to\infty}{\simeq} \Gamma_0^{SC}(\mathbf{Q},\Omega_\nu) = -\frac{4\pi}{v - \sqrt{\gamma_\uparrow\gamma_\downarrow\frac{\mathbf{Q}^2}{4} - \mu + i\frac{\Omega_\nu}{2}}}, \tag{B.7}$$

where $\mu = (\mu_\uparrow + \mu_\downarrow)/2$. However, using $\Gamma_0^{SC}(\mathbf{Q},\Omega_\nu)$ as the reference function to be subtracted in the Fourier transform may lead to problems, because for $\Omega_\nu = 0$ this function shows a pole at $|\mathbf{Q}| = 2\sqrt{(v^2+\mu)/(\gamma_\uparrow\gamma_\downarrow)}$ for $v > 0$. Since we are interested only in taking care of the large-frequency behavior of $\Gamma(\mathbf{Q},\Omega_\nu)$, we are led to introduce the new reference function $\tilde{\Gamma}_0^{SC}(\mathbf{Q},\Omega_\nu) = \Gamma_0^{SC}(\mathbf{Q},\Omega_\nu) - \Gamma_0^{SC}(\mathbf{Q},0)$. Although the Fourier transform of $\tilde{\Gamma}_0^{SC}(\mathbf{Q},\Omega_\nu)$ cannot be calculated analytically, it can be computed with limited effort by writing it as an integral over the complex plane

$$\tilde{\Gamma}_0^{SC}(\mathbf{Q},\tau) = \frac{1}{\beta}\sum_\nu e^{-i\Omega_\nu\tau}\tilde{\Gamma}_0^{SC}(\mathbf{Q},\Omega_\nu) = \frac{1}{2\pi i}\oint_{\mathcal{C}} dz \frac{e^{z\tau}}{e^{\beta z}-1}\tilde{\Gamma}_0^{SC}(\mathbf{Q},z), \tag{B.8}$$

where the contour $\mathcal{C}$ surrounds the poles of the Bose function $(e^{\beta z}-1)^{-1}$ on the imaginary axis. Here, the function $\tilde{\Gamma}_0^{SC}(\mathbf{Q},z)$ has a branch cut along the negative real axis starting at $z_c = 2(\mu - \gamma_\uparrow\gamma_\downarrow\mathbf{Q}^2/4)$, as well as a pole at $z_p = 2v^2 + z_c$ when $v > 0$. The integral (B.8) then reduces to the calculation of an integral along the branch cut and of the residue of the pole, and can accordingly be split in the following way

$$\tilde{\Gamma}_0^{SC}(\mathbf{Q},\tau) = \Gamma_{0,n}^{SC}(\mathbf{Q},\tau) + \Gamma_{0,a}^{SC}(\mathbf{Q},\tau) + \Gamma_{0,res}^{SC}(\mathbf{Q},\tau) - T\,\mathrm{Re}[\Gamma_0^{SC}(\mathbf{Q},0)], \tag{B.9}$$

where the first two terms (to be numerically and analytically Fourier transformed, respectively) are contributed by the branch cut while the third term by the pole.

The first term in (B.9), for $z_c \leq 0$, can be cast in the form

$$\Gamma_{0,n}^{SC}(\mathbf{Q},\tau) = \frac{8\sqrt{2}e^{z_c\tau}}{\sqrt{\tau}}\int_0^\infty dx \frac{e^{-x^2}x^2}{(e^{-\beta(z_c-x^2/\tau)}-1)(x^2+2\tau v^2)}, \tag{B.10}$$

and, for $z_c > 0$, in the form

$$\begin{aligned}\Gamma_{0,n}^{SC}(\mathbf{Q},\tau) = {} & \frac{8\sqrt{2}e^{z_c\tau}}{\sqrt{\tau}}\int_{\sqrt{\tau(z_c-z_0)}}^\infty dx \frac{e^{-x^2}x^2}{(e^{-\beta(z_c-x^2/\tau)}-1)(x^2+2\tau v^2)} \\ & + 8\sqrt{\frac{2}{\tau}}\int_0^{\sqrt{\tau(z_c-z_0)}} dx \frac{1}{e^{-\beta(z_c-x^2/\tau)}-1}\left(\frac{e^{z_c\tau-x^2}x^2}{x^2+2\tau v^2} - \frac{x\sqrt{z_c}}{z_p\sqrt{\tau}}\right) \\ & + \frac{4\sqrt{2z_c}}{z_p}\left(z_0 - z_c - T\ln\left|\frac{e^{-\beta z_c}-1}{e^{-\beta z_0}-1}\right|\right),\end{aligned} \tag{B.11}$$

where z_0 is a negative real number (typically we take $z_0 = -2T$).

The second term in (B.9) has the semi-analytic form

$$\Gamma_{0,a}^{SC}(\mathbf{Q},\tau) = 4\sqrt{2\pi}\,c(\tau,v)\frac{e^{2\mu\tau}e^{-\gamma_\uparrow\gamma_\downarrow\mathbf{Q}^2\tau/2}}{\sqrt{\tau}}, \tag{B.12}$$

where the coefficient $c(\tau,v)$ is given by

$$c(\tau,v) = \frac{2}{\sqrt{\pi}}\int_0^\infty dx \frac{x^2e^{-x^2}}{x^2+2\tau v^2}, \tag{B.13}$$

with $c(\tau,v) \to 1$ for $\tau \to 0^+$ or $v = 0$. The term (B.12) admits also an analytic Fourier transform from $\mathbf{Q}$ to $\mathbf{x}$, given by

$$\Gamma_{0,a}^{SC}(\mathbf{x},\tau) = \frac{2c(\tau,v)e^{\mu\tau}e^{-\mathbf{x}^2/(2\gamma_\uparrow\gamma_\downarrow\tau)}}{(\gamma_\uparrow\gamma_\downarrow)^{3/2}\pi\tau^2}. \tag{B.14}$$

It is possible to show that this is the leading term of the singular behavior of the full $\Gamma(\mathbf{x},\tau)$ for $(\mathbf{x},\tau) \to 0^+$ throughout all the BCS-BEC crossover.

The third term in (B.9) is given by

$$\Gamma_{0,res}^{SC}(\mathbf{Q},\tau) = -\theta(v)\frac{16\pi v e^{z_p\tau}}{e^{\beta z_p}-1}, \tag{B.15}$$

and one can show that the divergence of this term at $z_p = 0$ is exactly compensated by the fourth term in (B.9), in such a way that $\tilde{\Gamma}_0^{SC}(\mathbf{Q}, \tau)$ is always a smooth function of $\mathbf{Q}$.

At this point, to obtain $\Gamma(\mathbf{Q}, \tau)$, we can calculate numerically the Fourier transform of the difference $\Delta\Gamma(\mathbf{Q}, \Omega_\nu) = \Gamma(\mathbf{Q}, \Omega_\nu) - \tilde{\Gamma}_0^{SC}(\mathbf{Q}, \Omega_\nu)$, and then add to it $\tilde{\Gamma}_0^{SC}(\mathbf{Q}, \tau)$. Finally, to obtain $\Gamma(\mathbf{x}, \tau)$, we Fourier transform the difference function $\tilde{\Delta}\Gamma(\mathbf{Q}, \tau) = \Gamma(\mathbf{Q}, \tau) - \Gamma_{0,a}^{SC}(\mathbf{Q}, \tau)$ and then add to it $\Gamma_{0,a}^{SC}(\mathbf{x}, \tau)$.

B.3 Transforming from $\Sigma_\sigma(\mathbf{x}, \tau)$ to $\Sigma_\sigma(\mathbf{k}, \omega_n)$

Also in this case, the Fourier transform of the self-energy Σ is done in two steps, namely

$$\Sigma_\sigma(\mathbf{x}, \tau) \to \Sigma_\sigma(\mathbf{k}, \tau) \to \Sigma_\sigma(\mathbf{k}, \omega_n), \tag{B.16}$$

where now the transformations are in the reversed direction with respect to the previous cases. This is because, from the relation

$$\Sigma_\sigma(\mathbf{x}, \tau) = -2\Gamma(\mathbf{x}, \tau)\mathcal{G}_{\bar{\sigma}}(-\mathbf{x}, -\tau) \equiv 2\Gamma(\mathbf{x}, \tau)\mathcal{G}_{\bar{\sigma}}(\mathbf{x}, \beta - \tau), \tag{B.17}$$

once $\mathcal{G}_{\bar{\sigma}}(\mathbf{x}, \tau)$ and $\Gamma(\mathbf{x}, \tau)$ are known, $\Sigma_\sigma(\mathbf{x}, \tau)$ is also known. In the expression (B.17) we have a factor 2 due to the use of dimensionless units, while in the second line we have used the spatial isotropy and the anti-periodicity of the fermionic propagator to write Σ_σ in an alternative form. Since both $\mathcal{G}_{\bar{\sigma}}(\mathbf{x}, \tau)$ and $\Gamma(\mathbf{x}, \tau)$ are strongly peaked for $(\mathbf{x}, \tau) \to 0^+$, we expect the singular behavior of $\Sigma_\sigma(\mathbf{x}, \tau)$ to be captured by the expressions $\Sigma_\sigma^{(+)}(\mathbf{x}, \tau) \simeq 2\Gamma(\mathbf{x}, \tau)\mathcal{G}_{\bar{\sigma}}(0, \beta^-)$ and $\Sigma_\sigma^{(-)}(\mathbf{x}, \tau) \simeq 2\Gamma(0, \beta^-)\mathcal{G}_{\bar{\sigma}}(\mathbf{x}, \beta - \tau)$ in the limit $(\mathbf{x}, \tau) \to (0, 0^+)$ and $(\mathbf{x}, \tau) \to (0, \beta^-)$, respectively. Out of these two terms, $\Sigma_\sigma^{(+)}$ is the dominant one because $\Gamma(\mathbf{x}, \tau)$ is more strongly peaked than $\mathcal{G}_{\bar{\sigma}}(\mathbf{x}, \tau)$ in the limit $\tau \to 0^+$ (see the expressions in (B.14) and (B.5), therefore $\Sigma_\sigma^{(-)}$ is a sub-leading contribution.

At this point, we consider the difference $\Delta\Sigma_\sigma(\mathbf{x}, \tau) = \Sigma_\sigma(\mathbf{x}, \tau) - \Sigma_\sigma^{(+)}(\mathbf{x}, \tau)$, where we write

$$\Sigma_\sigma^{(+)}(\mathbf{x}, \tau) = -2n_{\bar{\sigma}} \frac{e^{-\mathbf{x}^2/(2\gamma_\uparrow\gamma_\downarrow\tau)}}{(\gamma_\uparrow\gamma_\downarrow)^{3/2}\pi\tau^2}. \tag{B.18}$$

Here, we have approximated Γ with the analytic result in (B.14) with $c(\tau, v) \to 1$ and $e^{\mu\tau} \to 1$, since we are interested only in the leading behavior of $\Sigma_\sigma^{(+)}$ for $(\mathbf{x}, \tau) \to 0^+$, and used $n_{\bar{\sigma}} = -2\mathcal{G}_{\bar{\sigma}}(0, \beta^-)$ for the fermionic density $n_{\bar{\sigma}}$ (in dimensionless units). This expression has the further advantage that its Fourier transform can be obtained analytically in terms of the *error function*, in the form

$$\Sigma_\sigma^{(+)}(\mathbf{k}, \omega_n) = -8\pi n_{\bar{\sigma}} \frac{\mathrm{erf}(\sqrt{\beta(\gamma_\uparrow\gamma_\downarrow\mathbf{k}^2 - 2i\omega_n)/2})}{\sqrt{\gamma_\uparrow\gamma_\downarrow\mathbf{k}^2 - 2i\omega_n}}. \tag{B.19}$$

Once the difference $\Delta\Sigma_\sigma(\mathbf{x}, \tau)$ has been numerically Fourier transformed (first from $\mathbf{x}$ to $\mathbf{k}$ and then from τ to ω_n) according to the above prescriptions to obtain $\Delta\Sigma_\sigma(\mathbf{k}, \omega_n)$, we can add to it the analytic expression (B.19) and obtain the desired function $\Sigma_\sigma(\mathbf{k}, \omega_n)$.

Appendix C

Convergence Optimization near T_C

Here we discuss the procedures that we have adopted to achieve optimal convergence toward self-consistency within the Luttinger-Ward approach. This appendix is the direct generalization to the imbalanced case of Appendix B in Ref. [46]. An optimization procedure in achieving convergence is especially required when the temperature approaches T_c, to the extent that this approach become intrinsically unstable when one uses the straightforward iterative procedure sketched in Figure (3.5).

C.1 Need of an Optimization Procedure

The fully self-consistent equations (3.77)-(3.80) can be written in a compact way as a functional equation for the self-energy Σ_σ, in the form

$$\Sigma_\sigma(k) = \mathcal{F}[\Sigma_\sigma(p)](k), \tag{C.1}$$

because once Σ_σ is known, we can readily obtain $\mathcal{G}_\sigma$ and Γ in the previous equations. Suppose that $\Sigma^{sol}_\sigma(k)$ is the self-consistent solution to (C.1) which the iterative method is expected to reach. At a generic iterative step i towards self-consistency, the self-energy Σ^i_σ deviates from the solution by a quantity $\delta\Sigma^i_\sigma$, i.e.

$$\Sigma^i_\sigma(k) = \Sigma^{sol}_\sigma(k) + \delta\Sigma^i_\sigma(k). \tag{C.2}$$

The functional equation (C.1) can be linearized around Σ^{sol}_σ, provided we are close enough to the self-consistent solution, to write

$$\begin{aligned}\Sigma^{sol}_\sigma(k) + \delta\Sigma^i_\sigma(k) &= \mathcal{F}[\Sigma^{i-1}_\sigma(p)](k) \\ &\simeq \Sigma^{sol}_\sigma(k) + \sum_\lambda \int dp \left[\frac{\delta\mathcal{F}[\Sigma_\sigma(p)](k)}{\delta\Sigma_\lambda(p)}\right]_{sol} \delta\Sigma^{i-1}_\lambda(p),\end{aligned} \tag{C.3}$$

where the integral over p contains both an integral over the wave vector $\mathbf{p}$ and a sum over the Matsubara frequency ω_n. This provides a relation for the distance $\delta\Sigma$ from the self-consistent solution between the steps $i-1$ and i

$$\delta\Sigma^i_\sigma(k) = \sum_\lambda \int dp \left[\frac{\delta\mathcal{F}[\Sigma_\sigma(p)](k)}{\delta\Sigma_\lambda(p)}\right]_{sol} \delta\Sigma^{i-1}_\lambda(p). \tag{C.4}$$

In our numerical calculations $\Sigma_\sigma(k)$ is calculated on a k-grid of points, therefore $\delta\Sigma$ can be regarded as a vector which is acted upon by the functional derivative matrix $[\delta F/\delta\Sigma]_{sol}$. The convergence of the iterative procedure, from $i-1$ to i and so on, is then governed by the behavior of this matrix, which can be rewritten in the form

$$\frac{\delta\mathcal{F}[\Sigma_\lambda(p)](k)}{\delta\Sigma_\sigma(p)} = \sum_\mu \frac{\delta\mathcal{F}[\Sigma_\sigma(p)](k)}{\delta\mathcal{G}_\mu(p)} \frac{\delta\mathcal{G}_\mu(p)}{\delta\Sigma_\lambda(p)}. \tag{C.5}$$

Using (3.77), the factor on the right is given by

$$\frac{\delta\mathcal{G}_\mu(p)}{\delta\Sigma_\lambda(p)} = \delta_{\mu\lambda}\mathcal{G}_\lambda(p)^2, \tag{C.6}$$

while the factor on the left can be calculated by recalling that, using (3.78) and (C.1), we have

$$\mathcal{F}[\Sigma_\sigma(p)](k) = \Sigma_\sigma(k) = -\int dQ\, \Gamma(Q)\mathcal{G}_{\bar\sigma}(Q-k), \tag{C.7}$$

yielding

$$\frac{\delta\mathcal{F}[\Sigma_\sigma(p)](k)}{\delta\mathcal{G}_\mu(p)} = -\delta_{\mu\bar\sigma}\Gamma(p+k) - \int dQ\, \frac{\delta\Gamma(Q)}{\delta\mathcal{G}_\mu(p)}\mathcal{G}_{\bar\sigma}(Q-k). \tag{C.8}$$

In this expression, the functional derivative of the particle-particle propagator $\Gamma(Q)$ can be obtained from (3.79)

$$\frac{\delta\Gamma(Q)}{\delta\mathcal{G}_\mu(p)} = -\Gamma(Q)^2\frac{\delta R_{pp}(Q)}{\delta\mathcal{G}_\mu(p)}, \tag{C.9}$$

where the functional derivative of the renormalized particle-particle bubble $R_{pp}(Q)$ is obtained from (3.80)

$$\frac{\delta R_{pp}(Q)}{\delta\mathcal{G}_\mu(p)} = \mathcal{G}_{\bar\mu}(Q-p). \tag{C.10}$$

Grouping all the above results together and splitting $\delta\Sigma^i_\sigma$ in two terms for later convenience, i.e. $\delta\Sigma^i_\sigma(k) = \delta\Sigma^i_{\sigma,1}(k) + \delta\Sigma^i_{\sigma,2}(k)$, we obtain

$$\delta\Sigma^i_{\sigma,1}(k) = -\int dp\, \mathcal{G}_{\bar\sigma}(p)^2\Gamma(p+k)\delta\Sigma^{i-1}_{\bar\sigma}(p), \tag{C.11}$$

$$\delta\Sigma^i_{\sigma,2}(k) = \sum_\lambda \int dp\, \mathcal{G}_\lambda(p)^2 \int dQ\, \Gamma(Q)^2\mathcal{G}_{\bar\sigma}(Q-k)\mathcal{G}_{\bar\lambda}(Q-p)\delta\Sigma^{i-1}_\lambda(p). \tag{C.12}$$

Suppose now that $T = T_c$. The Thouless criterion 3.45 implies that the particle-particle propagator $\Gamma(Q)$ shows a pole for $Q = 0$, such that we expect $\Gamma(Q)$ to be strongly peaked in the vicinity of $Q = 0$. The expressions (C.11) and (C.12) can be then simplified by setting to zero the arguments of the particle-particle propagators in the smooth functions that multiply them. For the term C.11 we thus have

$$\begin{aligned}\delta\Sigma^i_{\sigma,1}(k) &\simeq -\mathcal{G}_{\bar\sigma}(-k)^2\delta\Sigma^{i-1}_{\bar\sigma}(-k)\int dp\,\Gamma(p+k)\\ &= -C\,\mathcal{G}_{\bar\sigma}(-k)^2\delta\Sigma^{i-1}_{\bar\sigma}(-k),\end{aligned} \tag{C.13}$$

where C is the contact according to (3.71). This term poses no problem to the convergence, since the quantity that multiplies $\Sigma^{i-1}_{\bar{\sigma}}(-k)$ is finite. For the term (C.12) we instead obtain

$$\delta\Sigma^{i}_{\sigma,2}(k) \simeq \sum_{\lambda} \mathcal{G}_{\bar{\sigma}}(-k) \int dQ\, \Gamma(Q)^2 \int dp\, \mathcal{G}_{\lambda}(p)^2 \mathcal{G}_{\bar{\lambda}}(-p) \delta\Sigma^{i-1}_{\lambda}(p), \tag{C.14}$$

where the factor $\int dQ\, \Gamma(Q)^2$ is infrared divergent at $T = T_c$, because for the term with zero frequency we have $\Gamma(\mathbf{Q}, \Omega_\nu = 0) \sim \mathbf{Q}^{-2}$ when $\mathbf{Q} \to 0$ at $T = T_c$.

This divergence represents a problem for the convergence of the iterative algorithm, because it implies that the step i is bound to run infinitely away from it, no matter how close the step $i-1$ might be to the self-consistent solution. Depending on how much $\Gamma(Q)$ is peaked in $Q = 0$, this problem can affect the convergence of the iterative algorithm also for temperatures $T \gtrsim T_c$.

C.2 Optimization for $T > T_c$

There exists a simple method to make the iterative approach (C.4) converge for $T \gtrsim T_c$, although it cannot converge at exactly $T = T_c$. It consists in redefining the iterative steps in terms of the weighted sum

$$\Sigma^{i}_{\sigma}(k) = \alpha \mathcal{F}[\Sigma^{i-1}_{\sigma}(p)](k) + (1-\alpha)\Sigma^{i-1}_{\sigma}(k), \tag{C.15}$$

where the weight factor α ranges between 0 and 1. This method is used to reduce the effects of the divergence and to reach the converge sufficiently close to T_c. Nevertheless, the method fails upon approaching T_c, because smaller and smaller values of α are needed for obtaining convergence. Notice also that a smaller value of α implies that more iterative steps are required for convergence. In the numerical program, we found that a good choice for the weight factor is $\alpha \propto [\Gamma(\mathbf{Q} = 0, \Omega_\nu = 0)]^{-1/2}$, which updates and decreases automatically at each iteration, by lowering the temperature. In practice, before it becomes numerically too demanding, this method can conveniently be used down to temperatures for which $(T - T_c)/T_c \simeq 1\%$.

C.3 Optimization for $T = T_c$

Exactly at $T = T_c$, we can rely on a different method that avoids the convergence problem discussed above. We begin by fixing the values n_σ of the densities and a guess value T_g/E_F for the temperature in units of the Fermi energy, as well as the ratios μ/T_g and h/T_g, where $\mu = (\mu_\uparrow + \mu_\downarrow)/2$ and $h = (\mu_\uparrow - \mu_\downarrow)/2$. Next, we replace the particle-particle propagator in (3.79) with the following quantity

$$\tilde{\Gamma}(Q)^{-1} = R_{pp}(Q) - R_{pp}(Q = 0), \tag{C.16}$$

in such a way that $\tilde{\Gamma}(Q = 0)^{-1} = 0$ by construction, i.e. the Thouless criterion is always satisfied, no matter what was the initial guess temperature.

At this point one can proceed and perform the iterative procedure toward self-consistency, with $\Gamma(Q)$ replaced by $\tilde{\Gamma}(Q)$. Once self-consistency has been achieved

with this modified set of equations, one can obtain the modified density as $\tilde{n}_\sigma = -2\tilde{\mathcal{G}}_\sigma(\mathbf{x}=0,\tau=\beta^-)$, and the modified scattering length $\tilde{a}_F$ from the expression

$$\frac{1}{\tilde{a}_F} = -\frac{4\pi}{2m_{red}}\tilde{R}_{pp}(Q=0), \tag{C.17}$$

where $\tilde{R}_{pp}$ is obtained from (3.80) with $\tilde{\mathcal{G}}_\sigma$ replacing $\mathcal{G}_\sigma$. This result follows directly from the Thouless criterion corresponding to the modified density $\tilde{n}_\sigma$.

Finally, in terms of $\tilde{n} = \tilde{n}_\uparrow + \tilde{n}_\downarrow$ one obtains the modified Fermi wave vector $\tilde{k}_F$ and the modified Fermi energy $\tilde{E}_F$. The desired value of the critical temperature is then obtained by

$$\frac{T_c}{E_F} = \frac{T_g}{E_F}\frac{E_F}{\tilde{E}_F}, \tag{C.18}$$

while the corresponding coupling value is given by

$$\frac{1}{k_F a_F} = \frac{1}{\tilde{k}_F \tilde{a}_F} = -\frac{4\pi\tilde{R}_{pp}(Q=0)}{2m_{red}k_F}\frac{k_F}{\tilde{k}_F}. \tag{C.19}$$

This method avoids the convergence problem discussed above for the iterative procedure. Specifically, for the functional derivative of $\tilde{\Gamma}(Q)$ with respect to $\tilde{\mathcal{G}}_\mu(p)$ one obtains

$$\begin{aligned}\frac{\delta\tilde{\Gamma}(Q)}{\delta\tilde{\mathcal{G}}_\mu(p)} &= -\tilde{\Gamma}(Q)^2\frac{\delta(\tilde{R}_{pp}(Q) - \tilde{R}_{pp}(Q=0))}{\delta\tilde{\mathcal{G}}_\mu(p)} \\ &= -\tilde{\Gamma}(Q)^2[\tilde{\mathcal{G}}_{\bar{\mu}}(Q-p) - \tilde{\mathcal{G}}_{\bar{\mu}}(-p)],\end{aligned} \tag{C.20}$$

while the corresponding variation of the self-energy related to this functional derivative then becomes

$$\begin{aligned}\delta\tilde{\Sigma}_2^i(k) = \sum_\lambda \int dp\, \tilde{\mathcal{G}}_\lambda(p)^2 \int dQ\, \tilde{\Gamma}(Q)^2\tilde{\mathcal{G}}_{\bar{\sigma}}(Q-k) \\ \times [\tilde{\mathcal{G}}_{\bar{\lambda}}(Q-p) - \tilde{\mathcal{G}}_{\bar{\lambda}}(-p)]\delta\tilde{\Sigma}_\lambda^{i-1}(p).\end{aligned} \tag{C.21}$$

Comparing this result with C.12, one notice that the singular behavior of $\tilde{\Gamma}(Q)$ for $Q \to 0$ is now suppressed by the presence of the factor $[\tilde{\mathcal{G}}_{\bar{\lambda}}(Q-p) - \tilde{\mathcal{G}}_{\bar{\lambda}}(-p)]$. This feature makes it possible to reach convergence exactly at $T = T_c$ without the need for the weighted sum in (C.15), with a limited number of iterations.

Bibliography

[1] H. K. Onnes, *The resistance of pure mercury at helium temperatures*, Commun. Phys. Lab. Univ. Leiden **12**, 120 (1911).

[2] F. London, H. London, *The Electromagnetic Equations of the Supraconductor*, Proceedings of the Royal Society of London A **149**.866, 71 (1935).

[3] V. L. Ginzburg, L.D. Landau, *On the theory of superconductivity*, Zh. Eksp. Teor. Fiz. **20**, 1064 (1950).

[4] J. Bardeen, L. N. Cooper, J. R. Schrieffer, *Theory of Superconductivity*, Phys. Rev. **108**, 1175 (1957).

[5] L. P. Gor'kov, *Microscopic derivation of the Ginzburg—Landau equations in the theory of superconductivity*, Zh. Eksp. Teor. Fiz. **36**, 1364 (1959).

[6] M. R. Schafroth, S. T. Butler, J. M. Blatt, *Quasi-chemical equilibrium model for superconductivity*, Helv. Phys. Acta **30**, 93 (1957).

[7] D. M. Eagles, *Possible Pairing without Superconductivity at Low Carrier Concentrations in Bulk and Thin-film Superconducting Semiconductors*, Phys. Rev. **186**, 456 (1969).

[8] A. J. Leggett, *Diatomic molecules and Cooper pairs*, in: A. Pekalski, R. Przystawa (Eds.), *Modern trends in the theory of condensed matter*, Lecture Notes in Physics **115**, Springer-Verlag, Berlin, 13 (1980).

[9] P. Nozières, S. Schmitt-Rink, *Bose Condensation in an Attractive Fermion Gas: From Weak to Strong Coupling Superconductivity*, J. Low Temp. Phys. **59**, 195 (1985).

[10] M. Randeria, J. M. Duan, L. Y. Shieh, *Bound states, Cooper pairing, and Bose condensation in two dimensions*, Phys. Rev. Lett. **62**, 981 (1989).

[11] M. Randeria, J. M. Duan, L.Y. Shieh, *Superconductivity in a two-dimensional Fermi gas: Evolution from Cooper pairing to Bose condensation*, Phys. Rev. B **41**, 327 (1990).

[12] R. Micnas, J. Ranninger, S. Robaszkiewicz, *Superconductivity in narrow-band systems with local non retarded attractive interactions*, Rev. Modern Phys. **62**, 113 (1990).

[13] M. Randeria, N. Trivedi, A. Moreo, R. T. Scalettar, *Pairing and spin gap in the normal state of short coherence length superconductors*, Phys. Rev. Lett. **69**, 2001 (1992).

[14] M. Drechsler, W. Zwerger, *Crossover from BCS-superconductivity to Bose-condensation*, Ann. Phys. **504**, 15 (1992).

[15] R. Haussmann, *Crossover from BCS superconductivity to Bose-Einstein condensation: A self-consistent theory*, Z. Phys. B **91**, 291 (1993).

[16] F. Pistolesi, G. C. Strinati, *Evolution from BCS superconductivity to Bose condensation: Role of the parameter* $k_F\xi$, Phys. Rev. B **49**, 6356 (1994).

[17] M. Casas, J. M. Getino, M. de Llano, A. Puente, R.M. Quick, H. Rubio, D.M. van der Walt, *BCS-Bose model of exotic superconductors: Generalized coherence length*, Phys. Rev. B **50**, 15945 (1994).

[18] M. Baldo, U. Lombardo, P. Schuck, *Deuteron formation in expanding nuclear matter from a strong coupling BCS approach*, Phys. Rev. C **52**, 975 (1995).

[19] M. Inguscio, W. Ketterle, C. Salomon (Eds.), *Ultra-Cold Fermi Gases*, in: Proceedings of the International School of Physics "Enrico Fermi" **164**, IOS Press, Amsterdam (2007).

[20] M. W. Zwierlein, A. Schirotzek, C. H. Schunck, W. Ketterle, *Fermionic superfluidity with imbalanced spin populations*, Science **311**, 492 (2006).

[21] G. B. Partridge, W. Li, R. I. Kamar, Y. Liao, R. G. Hulet, *Pairing and phase separation in a polarized Fermi gas*, Science **311**, 503 (2006).

[22] G. Sarma, *On the Influence of a Uniform Exchange Field acting on the Spins of the Conduction Electrons in a Superconductor*, J. Phys. Chem. Solids **24**, 1029 (1963).

[23] P. Fulde, R. A. Ferrell, *Superconductivity in a strong spin-exchange field*, Phys. Rev. **135**, A550 (1964).

[24] A. I. Larkin, Y. N. Ovchinnikov, *Nonuniform state of superconductors*, Sov. Phys. JETP **20**, 762 (1965); Zh. Eksp. Teor. Fiz. **47**, 1136 (1964).

[25] R. Lortz, Y. Wang, A. Demuer, P. H. M. Böttger, B. Bergk, G. Zwicknagl, Y. Nakazawa, J. Wosnitza, *Calorimetric Evidence for a Fulde-Ferrell-Larkin-Ovchinnikov Superconducting State in the Layered Organic Superconductor* κ-(BEDT-TTF)$_2$Cu(NCS)$_2$, Phys. Rev. Lett. **99**, 187002 (2007).

[26] G. Koutroulakis, H. Kühne, J. A. Schlueter, J. Wosnitza, S. E. Brown, *Microscopic Study of the Fulde-Ferrell-Larkin- Ovchinnikov State in an All-Organic Superconductor*, Phys. Rev. Lett. **116**, 067003 (2016).

[27] J. Wosnitza, *FFLO states in layered organic superconductors*, Ann. Phys. (Berlin) **530**, 1700282 (2018).

[28] C. Cho, J. H. Yang, N. F. Q. Yuan, J. Shen, T. Wolf, R. Lortz, *Thermodynamic Evidence for the Fulde-Ferrell-Larkin-Ovchinnikov State in the* KFe_2As_2 *Superconductor*, Phys. Rev. Lett. **119**, 217002 (2017).

[29] Y. Liao, A. S. C. Rittner, T. Paprotta, W. Li, G. B. Partridge, R. G. Hulet, S. K. Baur, E. J. Mueller, *Spin-imbalance in a one-dimensional Fermi gas*, Nature **467**, 567 (2010).

[30] Y. Shin, C. H. Schunck, A. Schirotzek, W. Ketterle, *Phase diagram of a two-component Fermi gas with resonant interactions*, Nature **451**, 689 (2008).

[31] B. A. Olsen, M. C. Revelle, J. A. Fry, D. E. Sheehy, R. G. Hulet, *Phase diagram of a strongly interacting spin imbalanced Fermi gas*, Phys. Rev. A **92**, 63616 (2015).

[32] J. Wang, Y. Che, L. Zhang, Q. Chen, *Enhancement effect of mass imbalance on Fulde-Ferrell-Larkin-Ovchinnikov type of pairing in Fermi-Fermi mixtures of ultracold quantum gases*, Sci. Rep. **7**, 39783 (2017).

[33] G. C. Strinati, P. Pieri et al., *The BCS–BEC Crossover: from Ultra-cold Fermi Gases to Nuclear Systems*, Phys. Rep. **738**, 1 (2018).

[34] W. Zwerger (Ed.), *The BCS-BEC Crossover and the Unitary Fermi Gas*, Lecture Notes in Physics **863**, Springer-Verlag, Berlin, Heidelberg (2012).

[35] V. M. Galitskii, *The energy spectrum of a non-ideal Fermi gas*, Sov. Phys. JETP **7**, 104 (1958); Zh. Eksp. Teor. Fiz. **34**, 151 (1958).

[36] M. J. H. Ku, A. T. Sommer, L. W. Cheuk, and M. W. Zwierlein, *Revealing the superfluid lambda transition in the universal thermodynamics of a unitary Fermi gas*, Science **335**, 563 (2012).

[37] W. Zwerger, *Strongly interacting Fermi gases*, in: *Quantum Matter at Ultralow Temperatures*, M. Inguscio, W. Ketterle, S. Stringari G. Roati (Eds.), Proceedings of the International School of Physics "Enrico Fermi" **191**, 63, IOS Press, Amsterdam (2016).

[38] C. Carcy, S. Hoinka, M. G. Lingham, P. Dyke, C. C. N. Kuhn, H. Hu, C. J. Vale, *Contact and sum rules in a near-uniform Fermi gas at unitarity*, Phys. Rev. Lett. **122**, 203401 (2019).

[39] B. Mukherjee, P. B. Patel, Z. Yan, R. J. Fletcher, J. Struck, M. W. Zwierlein, *Spectral response and contact of the unitary Fermi gas*, Phys. Rev. Lett. **122**, 203402 (2019).

[40] S. Jensen, C. N. Gilbreth, Y. Alhassid, *Contact in the unitary Fermi gas across the superfluid phase transition*, Phys. Rev. Lett. **125**, 043402 (2020).

[41] L. Rammelmuller, Y. Hou, J. E. Drut, J. Braun, *Pairing and the spin susceptibility of the polarized unitary Fermi gas in the normal phase*, Phys. Rev. A **103**, 43330 (2021).

[42] C. Ravensbergen, V. Corre, E. Soave, M. Kreyer, E. Kirilov, R. Grimm, *Production of a degenerate Fermi-Fermi mixture of dysprosium and potassium atoms*, Phys. Rev. A **98**, 63624 (2018).

[43] C. Ravensbergen, E. Soave, V. Corre, M. Kreyer, B. Huang, E. Kirilov, R. Grimm, *Resonantly interacting Fermi-Fermi mixture of* ^{161}Dy *and* ^{40}K, Phys. Rev. Lett. **124**, 203402 (2020).

[44] E. Neri, A. Ciamei, C. Simonelli, I. Goti, M. Inguscio, A. Trenkwalder, and M. Zaccanti, *Realization of a cold mixture of fermionic chromium and lithium atoms*, Phys. Rev. A **101**, 63602 (2020).

[45] M. Pini, P. Pieri, G. C. Strinati, *Fermi gas throughout the BCS-BEC crossover: Comparative study of t-matrix approaches with various degrees of self-consistency*, Phys. Rev. B **99**, 94502 (2019).

[46] M. Pini, *Strong correlations in the normal phase of an attractive Fermi gas*, PhD thesis, University of Camerino (2020).

[47] M. Pini, P. Pieri, G. C. Strinati, *Evolution of an attractive polarized Fermi gas from the polaronic limit to the superfluid quantum critical point*, to be published.

[48] J. R. Schrieffer, *Theory of Superconductivity*, Benjamin, New York (1964).

[49] P. Ring, P. Schuck, *The Nuclear Many Body Problem*, Springer-Verlag, Berlin (1980).

[50] C. Pethick, H. Smith, *Bose–Einstein Condensation in Dilute Gases*, 2nd ed., Cambridge University Press (2008).

[51] N. N. Bogoliubov. *On the theory of superfluidity*, J. Phys. (USSR) **11** ,23 (1947).

[52] N. Andrenacci, A. Perali, P. Pieri and G. C. Strinati, *Density-induced BCS to Bose-Einstein crossover*, Phys. Rev. B **60**.17, 12410 (1999).

[53] C. A. R. Sá de Melo, M. Randeria, J. R. Engelbrecht, *Crossover from BCS to Bose Superconductivity: Transition Temperature and Time-dependent Ginzburg-Landau theory*, Phys. Rev. Lett. **71**, 3202 (1993).

[54] Q. Chen, J. Stajic, S. Tan, K. Levin, *BCS-BEC crossover: From High Temperature Superconductors to Ultracold Superfluids*, Phys. Rep. **412**, 1 (2005).

[55] M. Randeria, *Pre-pairing for Condensation*, Nature Phys. **6**, 561 (2010).

[56] A. M. Clogston, *Upper Limit for the Critical Field in Hard Superconductors*, Phys. Rev. Lett. **9**, 266 (1962).

[57] B. S. Chandrasekhar, *A Note on the Maximum Critical field of High-field Superconductors*, Appl. Phys. Lett. **1**, 7 (1962).

[58] U. Lombardo, P. Nozières, P. Schuck, H. J. Schulze, A. Sedrakian, *Transition from BCS pairing to Bose-Einstein condensation in low-density asymmetricnuclear matter*, Phys. Rev. C **64**, 064314 (2001).

[59] J. J. Kinnunen et al., *The Fulde–Ferrell–Larkin–Ovchinnikov state for ultracold fermions in lattice and harmonic potentials: a review*, Reports on Progress in Physics **81**, 046401 (2018).

[60] S. Takada, T. Izuyama, *Superconductivity in a molecular field. I*, Progr. Theoret. Phys. **41**, 635 (1969).

[61] F. Chevy, C. Mora, *Ultra-cold polarized Fermi gases*, Rep. Progr. Phys. **73**, 112401 (2010).

[62] D. T. Son, M. A. Stephanov, *Phase diagram of a cold polarized Fermi gas*, Phys. Rev. A **74**, 013614 (2006).

[63] M. Iskin, C. A. R. Sá de Melo, *Two-species fermion mixtures with population imbalance*, Phys. Rev. Lett. **97**, 100404 (2006).

[64] K. B. Gubbels, M. W. J. Romans, H. T. C. Stoof, *Sarma phase in trapped unbalanced Fermi gases*, Phys. Rev. Lett. **97**, 210402 (2006).

[65] D. E. Sheehy, L. Radzihovsky, *BEC-BCS crossover, phase transitions and phase separation in polarized resonantly-paired superfluids*, Ann. Phys. **322**, 1790 (2007).

[66] P. Pieri, G. C. Strinati, *Trapped fermions with density imbalance in the Bose-Einstein condensate limit*, Phys. Rev. Lett. **96**, 150404 (2006).

[67] C. Chin, R. Grimm, P. Julienne, E. Tiesinga, *Feshbach resonances in ultracold gases*, Rev. Mod. Phys. **82**, 1225 (2010).

[68] S. Simonucci, P. Pieri, G. C. Strinati, *Broad vs. narrow Fano-Feshbach resonances in the BCS-BEC crossover with trapped Fermi atoms*, Europhys. Lett. **69**, 713 (2005).

[69] S. Tan, *Energetics of a strongly correlated Fermi gas*, Ann. Phys. **323**, 2952 (2008).

[70] S. Tan, *Large momentum part of a strongly correlated Fermi gas*, Ann. Phys. **323**, 2971 (2008).

[71] S. Tan, *Generalized virial theorem and pressure relation for a strongly correlated Fermi gas*, Ann. Phys. **323**, 2987 (2008).

[72] A. L. Fetter, J. D. Walecka, *Quantum Theory of Many-Particle Systems*, McGraw-Hill, New York (1971).

[73] P. Pieri, L. Pisani, G. C. Strinati, *Pairing fluctuation effects on the single-particle spectra for the superconducting state*, Phys. Rev. Lett. **92**, 110401 (2004).

[74] H. T. C. Stoof, K. B. Gubbels, D. B.M. Dickerscheid, *Ultracold Quantum Fields*, Springer, Berlin (2009).

[75] J. R. Taylor, *Scattering Theory*, Dover Publications, New York (2000).

[76] H. Caldas, C. W. Morais, A. L. Mota, *Phase transition in asymmetrical superfluids: Equal Fermi surfaces*, Phys. Rev. D **72**, 045008 (2005).

[77] L.P. Gor'kov, T. K. Melik-Barkhudarov, *Contribution to the theory of superconductivity in an imperfect Fermi gas*, Sov. Phys. JETP **13**, 1018 (1961).

[78] D. J. Thouless, *Perturbation theory in statistical mechanics and the theory of superconductivity*, Ann. Phys. **10**, 553 (1960).

[79] Y. Ohashi, *On the Fulde-Ferrell State in spatially isotropic superconductors*, J. Phys. Soc. Japan **71**, 2625 (2002).

[80] M. Pini, P. Pieri, G. C. Strinati, *Strong Fulde-Ferrell Larkin-Ovchinnikov pairing fluctuations in polarized Fermi systems*, Phys. Rev. Research **3**, 43068 (2021).

[81] V. N. Popov, *Functional Integrals and Collective Excitations*, Cambridge Univ. Press, Cambridge (1987).

[82] A. Perali, P. Pieri, G. C. Strinati, C. Castellani, *Pseudogap and spectral function from superconducting fluctuations to the bosonic limit*, Phys. Rev. B **66**, 24510 (2002).

[83] T. Kashimura, R.Watanabe, Y. Ohashi, *Spin susceptibility and fluctuation corrections in the BCS-BEC crossover regime of an ultracold Fermi gas*, Phys. Rev. A **86**, 43622 (2012).

[84] J. M. Luttinger, J. C. Ward, *Ground-State Energy of a Many-Fermion System*, Phys. Rev. **118**, 1417 (1960).

[85] R. Haussmann, *Properties of a Fermi liquid at the superfluid transition in the crossover region between BCS superconductivity and Bose-Einstein condensation*, Phys. Rev. B **49**, 12975 (1994).

[86] R. Haussmann, W. Rantner, S. Cerrito, W. Zwerger, *Thermodynamics of the BCS-BEC crossover*, Phys. Rev. A **75**, 023610 (2007).

[87] G. Baym, L. P. Kadanoff, *Conservation laws and correlation functions*, Phys. Rev. **124**, 287 (1961).

[88] G. Baym, *Self-consistent approximations in many-body systems*, Phys. Rev. **127**, 1391 (1962).

[89] H. J. Schulz, G. Cuniberti, P. Pieri, *Fermi liquids and Luttinger liquids*, in: *Field Theories for low-dimensional condensed matter systems*, Springer, Berlin, 9 (2000).

[90] N. Dupuis, *Notes on the many-body problem*, Lab. Phys. Theor. Mat. Con., Sorbonne University, Chapter 4 (2019).

[91] P. Coleman, *Introduction to Many Body Physics*, Cambridge University Press (2016).

[92] L. D. Landau, *The theory of a Fermi liquid*, Zh. Eksp. Teor. Fiz. **30**, 1058 (1956).

[93] L. D. Landau, *Oscillations in a Fermi liquid*, Zh. Eksp. Teor. Fiz. **32**, 59 (1957).

[94] P. Nozières, *Theory of Interacting Fermi Systems*, Benjamin, New York (1964).

[95] J. M. Luttinger, *Fermi surface and some simple equilibrium properties of a system of interacting fermions*, Phys. Rev. **119**, 1153 (1960).

[96] P. Pieri, G. C. Strinati, *Luttinger theorem and imbalanced Fermi systems*, Eur. Phys. J. B **90**, 68 (2017).

[97] C. M. Varma, Z. Nussinov, W. Van Saarloos, *Singular or non-Fermi liquids*, Phys. Rep. **361**, 267 (2002).

[98] S. Sachdev, *Quantum Phase Transitions*, Cambridge University Press, Cambridge (1999).

[99] G.D. Lin, W. Yi, L. M. Duan, *Superfluid shells for trapped fermions with mass and population imbalance*, Phys. Rev. A **74**, 31604 (2006).

[100] B. Mukherjee, Z. Yan, P. B. Patel, Z. Hadzibabic, T. Yefsah, J. Struck, M. W. Zwierlein, *Homogeneous atomic Fermi gases*, Phys. Rev. Lett. **118**, 123401 (2017).

[101] Z. Yan, P. B. Patel, B. Mukherjee, R. J. Fletcher, J. Struck, M. W. Zwierlein, *Boiling a Unitary Fermi liquid*, Phys. Rev. Lett. **122**, 93401 (2019).

[102] M. Greiner, C. A. Regal, D. S. Jin, *Emergence of a molecular Bose-Einstein condensate from a Fermi gas*, Nature **426**, 537 (2003).

[103] S. Jochim, M. Bartenstein, A. Altmeyer, G. Hendl, S. Riedl, C. Chin, J. Hecker Denschlag, R. Grimm, *Bose-Einstein condensation of molecules*, Science **302**, 2101 (2003).

[104] S. Jochim, M. Bartenstein, A. Altmeyer, G. Hendl, C. Chin, J. Hecker Denschlag, R. Grimm, *Pure gas of optically trapped molecules created from fermionic atoms*, Phys. Rev. Lett. **91**, 240402 (2003).

[105] M. W. Zwierlein, C. A. Stan, C. H. Schunck, S. M. F. Raupach, S. Gupta, Z. Hadzibabic, W. Ketterle, *Observation of Bose-Einstein condensation of molecules*, Phys. Rev. Lett. **91**, 250401 (2003).

[106] M. Taglieber, A. C. Voigt, T. Aoki, T. W. Hänsch, K. Dieckmann, *Quantum degenerate two-species Fermi-Fermi mixture coexisting with a Bose-Einstein condensate*, Phys. Rev. Lett. **100**, 10401 (2008).

[107] E. Wille, F. M. Spiegelhalder, G. Kerner, D. Naik, A. Trenkwalder, G. Hendl, F. Schreck, R. Grimm, T. G. Tiecke, J. T. M. Walraven, S. J. J. M. F. Kokkelmans, E. Tiesinga, P. S. Julienne, *Exploring an ultracold Fermi-Fermi mixture: interspecies Feshbach resonances and scattering properties of* ^{6}Li *and* ^{40}K, Phys. Rev. Lett. **100**, 053201 (2008).

[108] A. C. Voigt, M. Taglieber, L. Costa, T. Aoki, W. Wieser, T. W. H¨ansch, K. Dieckmann, *Ultracold heteronuclear Fermi-Fermi molecules*, Phys. Rev. Lett. **102**, 20405 (2009).

[109] D. Naik, A. Trenkwalder, C. Kohstall, F. M. Spiegelhalder, M. Zaccanti, G. Hendl, F. Schreck, R. Grimm, T. M. Hanna, P.S. Julienne, *Feshbach resonances in the* ^{6}Li-^{40}K *Fermi-Fermi mixture: elastic versus inelastic interactions*, Eur. Phys. J. D **65**, 55 (2011).

[110] V. Efimov, *Energy levels arising from resonant two-body forces in a three-body system*, Phys. Lett. B **33**, 563 (1970).

[111] D. S. Petrov, C. Salomon, G. V. Shlyapnikov, *Diatomic molecules in ultracold Fermi gases-novel composite bosons*, J. Phys. B: At., Mol. Opt. Phys. **38**, S645 (2005).

[112] P. Naidon, S. Endo, *Efimov Physics: a review*, Rep. Prog. Phys. **80**, 56001 (2017).

[113] M. Pini, P. Pieri, R. Grimm, G. C. Strinati, *Beyond-mean-field description of a trapped unitary Fermi gas with mass and population imbalance*, Physical Review A **103**.2, 23314 (2021) (2021).

[114] E. Beth, G. Uhlenbeck, *The quantum theory of the non-ideal gas II. Behaviour at low temperatures*, Physica **4**, 915 (1937).

[115] R. Combescot, X. Leyronas, M. Yu. Kagan, *Self-consistent theory for molecular instabilities in a normal degenerate Fermi gas in the BEC-BCS crossover*, Phys. Rev. A **73**, 23618 (2006).

[116] P. M. Chaikin, T. C. Lubensky, *Principles of Condensed Matter Physics*, Cambridge University Press, Cambridge (1995).

[117] P. Kroiss, L. Pollet, *Diagrammatic Monte Carlo study of a mass-imbalanced Fermi-polaron system*, Phys. Rev. B **91**, 144507 (2015).

[118] B. I. Halperin, *Theory of dynamic critical phenomena*, Physics Today **72**.2, 42 (2019).

[119] F. Pistolesi, G. C. Strinati, *Evolution from BCS superconductivity to Bose condensation: Calculation of the zero-temperature phase coherence length*, Phys. Rev. B **53**, 15168 (1996).

[120] T. Senthil, *Critical Fermi surfaces and non-Fermi liquid metals*, Phys. Rev. B **78**, 35103 (2008).

[121] H. J. Vidberg, J. W. Serene, *Solving the Eliashberg equations by means of N-point Padé approximants*, J. Low Temp. Phys. **29**, 179 (1977).

[122] J. Fei, C. Yeh, E. Gull, *Nevanlinna Analytical Continuation*, Phys. Rev. Lett. **126**, 56402 (2021).

Ringraziamenti

Penso sia doveroso dedicare uno spazio a tutti coloro che mi sono stati vicini, non solo durante la scrittura di questo elaborato, ma in tutto questo percorso di crescita personale e professionale. Sono già riuscito a scamparla una volta, evitando i ringraziamenti nella tesi triennale con la scusa «Va beh tanto tra due anni c'è un'altra laurea!», ma questa volta non si fugge. Scherzi a parte, ci tengo molto a scrivere queste righe, pur non essendo bravo in queste cose, prometto quindi di fare del mio meglio.

In primis, un ringraziamento speciale al mio relatore prof. Pierbiagio Pieri, per la sua immensa pazienza, per i suoi indispensabili consigli, per le conoscenze trasmesse durante tutto il percorso di stesura dell'elaborato. Il suo costante appoggio si è rivelato fondamentale anche per riuscire ad ottenere l'agognato posto di dottorato a Padova. A tal proposito, ringrazio inoltre il prof. Armando Bazzani per la sua grande disponibilità. Grazie anche al mio correlatore Michele Pini per la sua preziosa disponibilità nello spiegarmi la logica degli interminabili codici Fortran usati nella tesi. Se non fosse per lui, oggi sarei ancora davanti al computer, lamentandomi poco pacificamente sul perchè i dati non vengano prodotti correttamente.

Ringrazio tutta la mia famiglia, che mi sostiene e mi vuole bene da sempre. Grazie a voi, il ritorno a casa nei week-end dopo settimane passate a Bologna, diventava letteralmente una vacanza rilassante e rigenerante, facendomi dimenticare tutti i problemi e ricaricandomi per affrontare una nuova settimana impegnativa tra studio e lezioni. A mamma, con la tua forza, determinazione e dedizione verso tutto ciò che fai, tu che metti sempre me e tutti gli altri prima di te stessa. Tornare stanca domenica dopo pranzo dal lavoro e, come se nulla fosse, preparare accuratamente tutte le cose da portare via prima di prendere il treno ne è solo un minuscolo esempio. A babbo, tu che mi hai trasmesso solo un quarto di tutta la tua allegria e simpatia (e per fortuna, aggiungerei), è anche grazie a te se ho raggiunto questo traguardo con l'importante consapevolezza che nella vita non c'è solo serietà e lavoro. So che preferiresti avere indietro i soldi che hai speso per mantenermi e, anche se continui con tutte le tue battutine, sai bene che non posso darteli, ma posso darti la certezza che sei un grande padre che non ha mai fatto mancare nè ha imposto nulla al proprio figlio, e per questo ti voglio e ti vorrò sempre bene. A Elisa, sorella maggiore e seconda mamma, una donna forte e coraggiosa che non ha paura di dirti in faccia le cose come stanno. Mi hai fatto capire che nella vita bisogna sempre stare con i piedi per terra, ma soprattutto che non siamo invincibili e che da soli non si va lontano. Inoltre, un ringraziamento speciale per i consigli sul bellissimo

vestito che indosso oggi mi sembra d'obbligo. A Matteo, fratello maggiore di cui ho una immensa stima, sei sempre stato per me un modello di vita da emulare: da un lato una persona seria, intelligente e competente in quello che fa, dall'altro sai goderti la vita tra viaggi, sport, amici e, perchè no, anche qualche bevuta. Non è un caso se anche tu sei circondato da persone meravigliose, come Federica e i miei splendidi nipotini Lorenzo e Pietro. Alla Pali, la zia che mi ha viziato come solo lei sa fare ed a cui voglio un bene dell'anima; i pranzi domenicali da te sono una tappa fondamentale dei week-end a casa. A Neno, che oggi purtroppo non è potuto essere qui, ma mi guarda da qualche parte lassù con felicità e orgoglio e festeggia con noi questo mio traguardo.

Ringrazio i miei amici, per tutti i momenti di spensieratezza, divertimento e sfogo. Ad Alex, Benni, Borgo, Greg, Livi, Lollo, Mancio, Matt, Richi, Tommi, Tonno, meglio noti come NONMELOPOSSO, per essere la mia seconda famiglia (almeno così posso giustificarmi dicendo che uno gli amici se li sceglie, mentre la famiglia no!). Scherzi a parte, ci conosciamo ormai da una vita e ne abbiamo passate tante insieme, siete e sarete sempre un tassello fondamentale, persone su cui si può sempre contare anche se si è separati da una grande distanza o da un lockdown mondiale. Quando sono con voi ho la possibilità di mettere in modalità riposo il cervello senza alcun senso di colpa: per quanto possa sembrare una banalità, non avete idea di quanto questo sia importante per me. A Pietro, il coinquilino che mi ha insegnato a vivere (almeno questo è quello che gli lascio credere); ammetto di non aver mai aver conosciuto una persona come te, e non è solo quella voce nasale poco piacevole che spesso mi faceva da sveglia al mattino o tutti gli acquisti inutili che fatti in modo compulsivo, ma quel carisma e quella naturalezza che ti fanno dire subito dopo averti conosciuto «questa è una persona vera, a cui puoi dire tutto, una persona che puoi considerare un vero amico». Nonostante ciò, ammetto che in alcuni momenti è stata davvero dura, vista anche la mia scarsa pazienza, ma fortunatamente non ero l'unico a doverti sopportare: a tal proposito ringrazio anche te, Ilaria. A Fabio, il coinquilino gestionale con cui ho condiviso la camera; ammetto che i primi anni è stata dura studiare mentre tu di fianco a me te la godevi giocando alla playstation. A parte questo, sei sempre stato di una correttezza unica e trovare una persona come te con cui puoi trovarti a tuo agio in camera come se fosse un fratello non è sicuramente cosa da tutti i giorni. Ad Ale, Andre, Chiara, Gek, Giorgio, Laura, Mati P., Mati V., Matti, Nico, Piero, Sandro, Sara, Tommi, i colleghi di corso che hanno reso questo percorso, triennale o magistrale che sia, molto più piacevole e meno pesante, tra problemi da affrontare insime, caffè in pausa pranzo e serate varie. Siete stati fondamentali per raggiungere questo traguardo e spero che potremmo festeggiare nuovamente tutti insieme in futuro.

Ringrazio Monica, ragazza, amica e compagna di vita, per il suo continuo e infallibile amore, supporto e comprensione in tutti questi anni. La maggior parte dei momenti bellissimi passati in questo lungo periodo li devo a te: le gite fuori porta, le cenette, gli apertivi, le visite, gli eventi culturali, ma anche i week-end passati in relax a casa a cercare un film che non ti facesse addormentare, un'impresa tutt'oggi impossibile; spero di vivere ancora tanti momenti così insieme a te (o meglio, da

buoni ossessivi-compulsivi, spero di spuntare ancora tante caselle nelle tue fantastiche liste di cose da fare). So che stare con una persona come me a volte non è affatto facile, ma tu non ti sei mai persa d'animo ed ogni volta riesci a tirare fuori la mia parte più emotiva, nascosta da una corazza che in pochi sono capaci di penetrare. La tua determinazione, organizzazione e diligenza sono e saranno sempre d'esempio per me; posso dire con orgoglio di avere una ragazza incredibile al mio fianco, e spero che tu sia fiera di me almeno metà di quanto lo sono io di te.

Oggi si conclude un capitolo durato 5 anni, pieno di gioia, risate, ma anche di ostacoli, momenti difficili e demotivanti. Penso sia giusto dedicare questo traguardo anche a me stesso, ai miei sacrifici e alla mia tenacia che mi hanno permesso di arrivare fin qui. Tuttavia, ammetto che quest'ultimo anno è stato un periodo difficile, in cui ho dovuto combattere una battaglia interna contro me stesso che mai avrei pensato di dover affrontare. Da questa, ho finalmente capito che nella vita, prima o poi, tutti abbiamo bisogno di aiuto e, tutti voi, siete stati e spero sarete sempre la mano che ti rialza quando cadi.